AD-A106 481 DOUGLAS AIRCRAFT CO LONG BEACH CA F/G 18/3
NUCLEAR BLAST RESPONSE COMPUTER PROGRAM. VOLUME II. DOUBLET-LAT--ETC(U)
AUG 81 J P GIESING, T P KALMAN, W P RODDEN DNA001-75-C-0216
UNCLASSIFIED AFWL-TR-81-32-VOL-2 NL

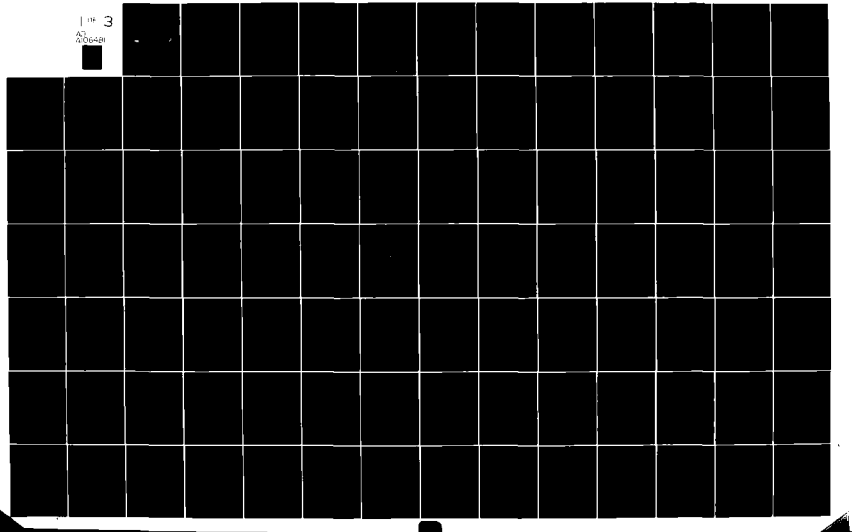

(2) LEVEL III

AFWL-TR-81-32, Vol. II

AFWL-TR-
81-32
Vol. II

AD A106481

NUCLEAR BLAST RESPONSE COMPUTER PROGRAM

Volume II of III
Doublet-Lattice and Piston Theory Aerodynamics

J. A. McGrew, et al.

Douglas Aircraft Company
3855 Lakewood Blvd.
Long Beach, CA 90846

August 1981

Final Report

Approved for public release; distribution unlimited.

THIS RESEARCH WAS SPONSORED BY THE DEFENSE NUCLEAR AGENCY UNDER SUBTASK N99AXAE500, WORK UNIT 04, WORK UNIT TITLE: NUCLEAR BLAST RESPONSE COMPUTER PROGRAM.

AIR FORCE WEAPONS LABORATORY
Air Force Systems Command
Kirtland Air Force Base, NM 87117

AFWL-TR-81-32

This final report was prepared by the Douglas Aircraft Company, Long Beach, California under Contracts DNA 001-75-C-0216 and DNA 001-76-C-0346, Job Order 88090340 with the Air Force Weapons Laboratory, Kirtland Air Force Base, New Mexico. Mr. Alfred L. Sharp (NTYV) was the Laboratory Project Officer-in-Charge.

When Government drawings, specifications, or other data are used for any purpose other than in connection with a definitely Government-related procurement, the United States Government incurs no responsibility or any obligation whatsoever. The fact that the Government may have formulated or in any way supplied the said drawings, specifications, or other data, is not to be regarded by implication, or otherwise in any manner construed, as licensing the holder, or any other person or corporation; or conveying any rights or permission to manufacture, use, or sell any patented invention that may in any way be related thereto.

This report has been authored by a contractor of the United States Government. Accordingly, the United States Government retains a nonexclusive, royalty-free license to publish or reproduce the material contained herein, or allow others to do so, for the United States Government purposes.

The Public Affairs Office has reviewed this report, and it is releasable to the National Technical Information Service, where it will be available to the general public, including foreign nationals.

If your address has changed, if you wish to be removed from our mailing list, or if your organization no longer employs the addressee, pleasy notify AFWL/NTYV, Kirtland AFB, NM 87117 to help us maintain a current mailing list.

This report has been reviewed and is approved for publication.

ALFRED L. SHARP
Project Officer

FOR THE COMMANDER

KENNEDY B. WILSON
Lt Colonel, USAF
Chief, Environment & Effects Branch

NORMAN K. BLOCKER
Colonel, USAF
Chief, Applied Physics Division

DO NOT RETURN COPIES OF THIS REPORT UNLESS CONTRACTUAL OBLIGATIONS OR NOTICE ON A SPECIFIC DOCUMENT REQUIRES THAT IT BE RETURNED.

UNCLASSIFIED

SECURITY CLASSIFICATION OF THIS PAGE (When Data Entered)

REPORT DOCUMENTATION PAGE

READ INSTRUCTIONS BEFORE COMPLETING FORM

1. REPORT NUMBER: AFWL-TR-81-32, Vol. II of III	2. GOVT ACCESSION NO.: AD-A106 481
3. RECIPIENT'S CATALOG NUMBER	
4. TITLE (and Subtitle): NUCLEAR BLAST RESPONSE COMPUTER PROGRAM. Volume II. Doublet-Lattice and Piston Theory Aerodynamics.	5. TYPE OF REPORT & PERIOD COVERED: Final Report
	6. PERFORMING ORG. REPORT NUMBER
7. AUTHOR(s): J. P. Giesing, T. P. Kalman, W. P. Rodden, H. H. Croxen, J. A. McGrew	8. CONTRACT OR GRANT NUMBER(s): DNA 001-75-C-0216, DNA 001-76-C-0346
9. PERFORMING ORGANIZATION NAME AND ADDRESS: Douglas Aircraft Company, 3855 Lakewood Blvd., Long Beach, CA 90801	10. PROGRAM ELEMENT, PROJECT, TASK AREA & WORK UNIT NUMBERS: 62601F/88090340
11. CONTROLLING OFFICE NAME AND ADDRESS: Air Force Weapons Laboratory (NTYV), Kirtland Air Force Base, NM 87117	12. REPORT DATE: Aug 1981
	13. NUMBER OF PAGES: 200
14. MONITORING AGENCY NAME & ADDRESS (if different from Controlling Office): Director, Defense Nuclear Agency, Washington, D.C. 20305	15. SECURITY CLASS. (of this report): Unclassified
	15a. DECLASSIFICATION DOWNGRADING SCHEDULE

16. DISTRIBUTION STATEMENT (of this Report)

Approved for public release; distribution unlimited.

17. DISTRIBUTION STATEMENT (of the abstract entered in Block 20, if different from Report)

18. SUPPLEMENTARY NOTES

This research was sponsored by the Defense Nuclear Agency under Subtask N99AXAE500, Work Unit 04, Work Unit Title: Nuclear Blast Response Computer Program.

(over)

19. KEY WORDS (Continue on reverse side if necessary and identify by block number)

Aircraft Structural Response
Mass Modeling
Aerodynamic Modeling
Digital Computer Program
Gust Response
Blast
Nuclear Vulnerability
Dynamic Loads

20. ABSTRACT (Continue on reverse side if necessary and identify by block number)

The VIBRA-6 computer program is a digital computer program developed to deter the response of aircraft to nuclear explosions when flying at subsonic speeds. It is similar to the VIBRA-4 program but uses the latest Doublet-Lattice Method for obtaining subsonic aerodynamic forces for arbitrary lifting surface-body configurations. The Double-Lattice procedure has been extended to account for the moving blast wave by considering it as a traveling gust. The nuclear blast representation remains the same as that used in the

DD FORM 1 JAN 73 1473

UNCLASSIFIED

SECURITY CLASSIFICATION OF THIS PAGE (When Data Entered)

18. SUPPLEMENTARY NOTES (Continued)

This report is divided into three volumes: Volume I of this report contains the overall program descriptions and method of analysis, the input and output data descriptions, the program operation and a sample problem. Volume II details the unsteady aerodynamic procedure and Volume III contains the program listings.

20. ABSTRACT (Continued)

VIBRA-4 program but the method of solution of the equations of motion has been changed from that of numerical integration of quasi-steady equations of motion to a Fourier transform procedure to move from frequency domain solutions to time history solutions. The concept of dynamic core has been introduced to the program thus removing any restrictions on the size of the aircraft idealization which can be analyzed.

PREFACE

This report was prepared by the Douglas Aircraft Company, Long Beach, California, under Contract DNA 001-75-C-0216 and documents the subsonic unsteady aerodynamic module development for the revised VIBRA-6 Nuclear Blast Response Computer Program. This work was performed under Program Element NWE D 62704H, Project N99QAXA, Task Area B500, Work Unit 04 and was funded by the Defense Nuclear Agency under: RDT & E RMSS Code B342075464N99QAXAE50004H2590D. Funding of this effort was also supported by the Air Force Weapons Laboratory under: Program Element 62601F, Project 8809, Task 03, Work Unit 40.

Inclusive dates of research and development as documented herein were May 1975 through June 1977.

Volume I of this report documents the overall program descriptions and the method of analysis, the input and output data descriptions, the program operation and a sample problem. Volume III contains the Fortran listing of the program.

J. A. McGrew was the program technical director for this task. The technical development was performed by J. P. Giesing and T. P. Kálmán with the assistance of Dr. W. P. Rodden. The programming effort was carried out by T. P. Kálmán and H. H. Croxen.

CONTENTS

ILLUSTRATIONS

Illustrations

Illustrations

TABLES

SECTION I

INTRODUCTION

The VIBRA-4 digital computer program (Ref. 1) analyzes the gross structural response (bending moments and accelerations) of an aircraft exposed to a nuclear blast. For aircraft flying at supersonic speeds, the aerodynamic loads are determined in VIBRA-4 by a lifting surface method that utilizes the indicial aerodynamic influence coefficient (AIC) approach which is an extension of the well-known Mach box method that has been used in supersonic flutter analyses for many years. For subsonic speeds, however, VIBRA-4 has used an indicial strip theory based on two-dimensional theory or empirical results derived from shock-tube measurements. The subsonic Doublet-Lattice Method (DLM, Refs. 2 and 3) has received wide acceptance since its appearance in 1968 for subsonic flutter analysis because of its generality regarding configurations. Current extensions (Refs. 3, 4 and 5) account for wing-body interference

---

1. Hobbs, N.P., Zartarian, G., and Walsh, J.P., *A Digital Computer Program for Calculating the Blast Response of Aircraft to Nuclear Explosions*, Air Force Weapons Laboratory, Report No. AFWL-TR-70-140, Vol. I, April 1971.

2. Albano, E., and Rodden, W.P., "*A Doublet-Lattice Method for Calculating Lift Distributions on Oscillating Surfaces in Subsonic Flows*," AIAA J., Vol. 7, No. 2, pp. 279-285, and No. 11, p. 2192, 1969.

3. Giesing, J.P., Kalman, T.P., and Rodden, W.P., *Subsonic Unsteady Aerodynamics for General Configurations; Part I - Direct Application of the Nonplanar Doublet-Lattice Method*, Air Force Flight Dynamics Labortory, Report No. AFFDL-TR-71-5, Part I, November 1971.

4. Giesing, J.P., Kalman, T.P., and Rodden, W.P., *Subsonic Unsteady Aerodynamics for General Configurations; Part II - Application of the Doublet-Lattice Method and the Method of Images to Lifting-Surface/Body Interference*, Air Force Flight Dynamics Laboratory, Report No. AFFDL-TR-71-5, Part II, April 1972.

5. Giesing, J.P., Kalman, T.P., and Rodden, W.P.,"*Subsonic Steady and Oscillatory Aerodynamics for Multiple Interfering Wings and Bodies*," J. Aircraft, Vol. 9, No. 10, pp. 693-702, 1972

and permit the determination of the aerodynamic loading on an entire aircraft in oscillatory motion or in a harmonic gust field (Ref. 6). The generality of the DLM makes it a desirable replacement for the present subsonic capability of VIBRA-4. The calculation of transient airloads from an oscillatory theory can only be made by the use of Fourier transform methods; however, the feasibility of calculating the transient blast loads by the DLM and Fourier techniques has already been demonstrated by Zartarian (Ref. 7), although it is necessary to add Piston Theory (Ref. 8) to supplement the DLM calculations at high reduced frequency as was pointed out by Zartarian.

The VIBRA-6 computer program, documented here, is an extension of earlier versions of VIBRA. The purpose of this report is to document the modifications to adapt the Doublet-Lattice Method and Piston Theory to the requirements of the new VIBRA-6 computer program. Only the modifications are described here since the documentation for the DLM and Method of Images and for Piston Theory is quite extensive. A brief summary, however, is presented in Volume I of this report. The modifications include addition of a travelling gust field, improvements in the aerodynamic influence coefficients, a compressible Slender Body Theory, and changes in the aerodynamic load output. This Volume also serves as a User's Manual since sections are included that 1) discuss considerations for modelling the entire aircraft, 2) provide the program input and 3) present an example problem. This Volume also presents a description of subroutines used in the aerodynamic module.

---

6. Giesing, J.P., Rodden,W.P., and Stahl, B., "*Sears Function and Lifting Surface Theory for Harmonic Gust Fields*",J. Aircraft, Vol.7, No. 3, pp. 252-255, 1970.

7. Zartarian, G., *Application of the Doublet-Lattice Method for Determination of Blast Loads on Lifting Surfaces at Subsonic Speeds*, Air Force Weapons Laboratory, Report No. AFWL-TR-72-207, January 1973.

8. Ashley, H., and Zartarian, G., "*Piston Theory - A new Aerodynamic Tool for the Aeroelastician*",J. Aero.Sci.,Vol. 23,No. 12, pp. 1109-1118, 1956.

SECTION II

THEORETICAL DEVELOPMENT

1. DOWNWASH BOUNDARY CONDITIONS

The loads imposed on a vehicle flying through an atmospheric gust or a blast wave arise from three sources. The first source is the aerodynamic angle of attack induced by the gust or blast wave, the second source is the angle of attack induced by the response motion, and the third is the impulsive diffraction loads induced as the pressure wave sweeps across the structure. It is generally assumed that the gust field or blast wave is known and is independent of the response, and that the additional aerodynamic loads induced by the motion must be determined by solution of the aeroelastic equations of motion. The aerodynamic loads are not known in general for arbitrary time-dependent downwash distributions (from motion or the gust) but only for harmonic time dependence of the downwash. The response problem is therefore easily formulated in the frequency domain and the time history of response follows from an inverse Fourier transformation. The specific intermediate problems are: 1) the determination of the harmonic downwash caused by a blast wave from an arbitrary burst orientation, and 2) the harmonic downwash caused by motion of the rigid body or vibration modes of the vehicle.

2. DOWNWASH INDUCED BY A TRAVELLING HARMONIC GUST

An important feature of the travelling gust is that the aerodynamic loads do not depend simply on the relative velocity between the gust and the vehicle. The downwash is, however, determined by the relative velocity but the basic analysis (Doublet-Lattice formulation) depends only on the

velocity U of the vehicle through the atmosphere (assumed to be fixed). A blast wave is a special case of a travelling gust. A travelling gust is usually considered to have a transverse velocity profile that is perpendicular to the direction of travel. In the analysis to follow, the gust velocity G is the material velocity of the fluid and is in the direction of travel of the blast wave, and the velocity V_g is the velocity of propagation of the pressure wave.

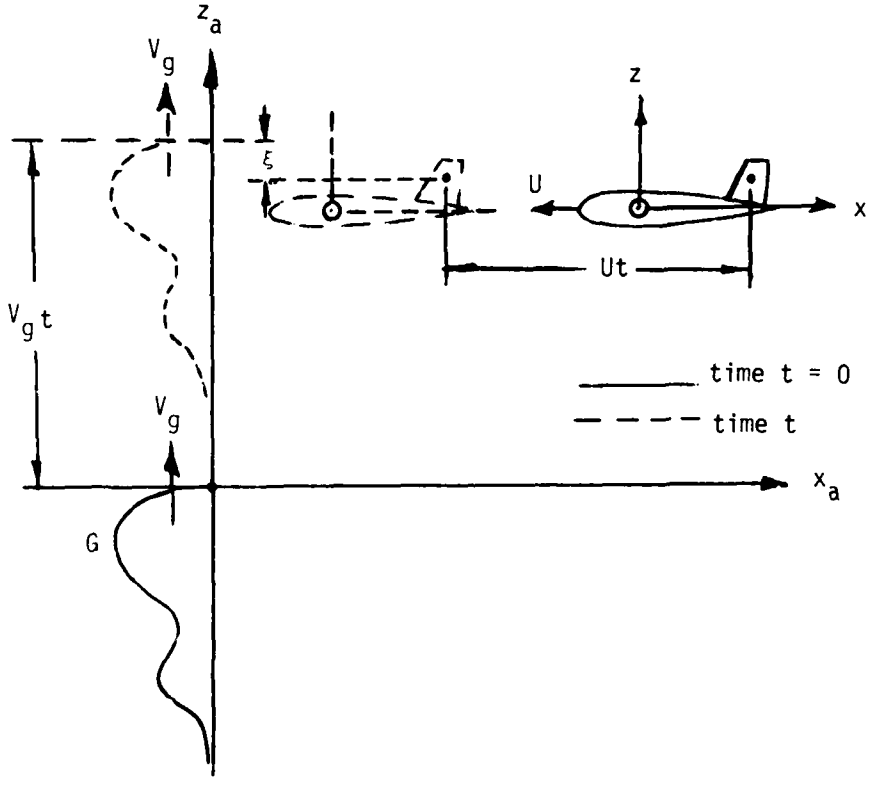

Figure 1. Vertical Gust Penetration

For introductory purposes we consider the simplest case of a vertical blast wave encountering a horizontally moving aircraft. We denote the gust velocity by $G(\xi)$ where ξ denotes the penetration distance into the

gust; i.e., the distance normal to the gust wave front. Figure 1 shows the initial positions of the gust field and the aircraft and the positions at a time t after penetration. From Figure 1 we find the penetration distance is

$$\xi = V_g t - (z + z_a) \tag{1}$$

where z_a is the coordinate of the aircraft reference point in the global $x_a - z_a$ coordinate system, and z is the coordinate of the point of interest relative to the reference point in the local x-z coordinate system.

In this elementary case, the penetration distance is independent of the aircraft velocity. As discussed in the Introduction, the oscillatory aerodynamic lifting surface analysis requires a harmonic downwash amplitude which may be determined from a harmonic gust profile with wave length λ. Letting

$$G(\xi) = G_o \cos 2\pi\xi/\lambda \tag{2a}$$

$$= \text{Re}\,[\bar{w}(x,y,z)\exp(i\omega t)] \tag{2b}$$

we find the frequency is

$$\omega = 2\pi V_g/\lambda \tag{3}$$

and the complex downwash amplitude is

$$\bar{w}(x,y,z) = G_o \exp\,[\,-i2\pi(z + z_a)/\lambda\,] \tag{4}$$

Introducing the reduced frequency

$$k_r = \omega\bar{c}/2U \tag{5}$$

and eliminating the wave length, we obtain

$$\bar{w}(x,y,z) = G_o \exp\,[\,-i2k_r(z + z_a)R/\bar{c}\,] \tag{6}$$

where

$$R = U/V_g \tag{7}$$

We next consider the general three-dimensional problem. If, at a particular point in space, the gust field velocity is again $G(\xi)$, and the velocity vector of the gust front is $\vec{V}_g$, then the gust vector G is

$$\vec{G} = (\vec{V}_g/|\vec{V}_g|)G(\xi) \tag{8}$$

where $|\vec{V}_g|$ is the magnitude of $\vec{V}_g$. In terms of the direction cosines of the gust velocity vector, the unit gust velocity vector is

$$\vec{v}_g = \vec{V}_g/\left|\vec{V}_g\right| \tag{9a}$$

$$= \vec{i}\cos\alpha + \vec{j}\cos\beta + \vec{k}\cos\gamma \tag{9b}$$

If the unit normal vector to a lifting surface is given by $\vec{n}$, then the component of the gust vector normal to the surface, i.e, the normalwash is

$$w_g = \vec{n} \cdot \vec{G} \tag{10a}$$

$$= (\vec{n} \cdot \vec{v}_g)G(\xi) \tag{10b}$$

$$= \theta\, G\,(\xi) \tag{10c}$$

where $\theta = \vec{n} \cdot \vec{v}_g$ is a parameter that depends only on the aircraft geometry and the relative angles between the blast and the aircraft.

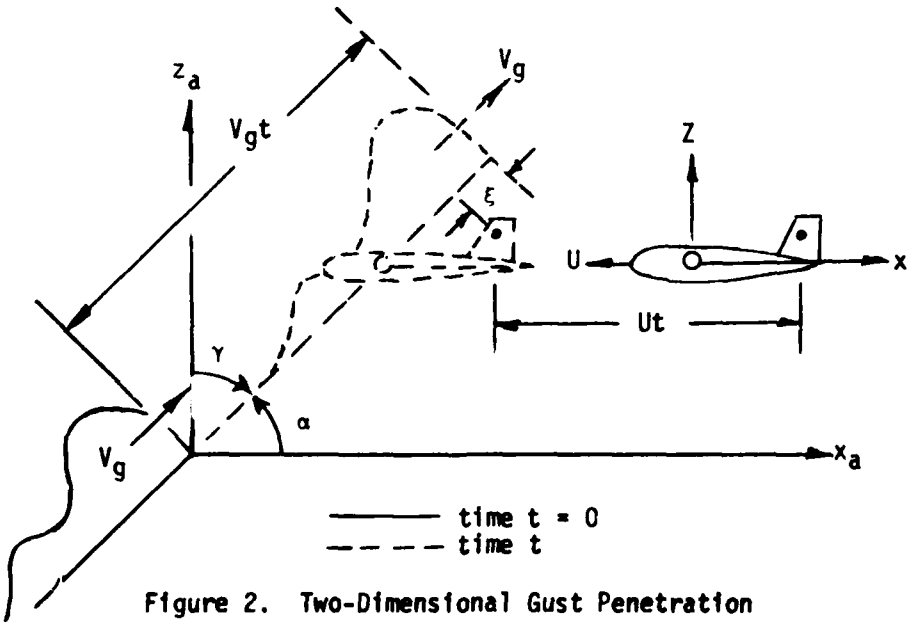

Figure 2. Two-Dimensional Gust Penetration

A two-dimensional variation of Figure 1 is shown in Figure 2. In the three-dimensional case, the penetration distance is found as follows. Let the initial vector from the blast origin to an arbitrary point on the aircraft be

$$\vec{r} = \vec{i}(x + x_a) + \vec{j}(y + y_a) + \vec{k}(z + z_a) \tag{11}$$

and the velocity vector of the aircraft be

$$\vec{U} = - \vec{i}U \tag{12}$$

Then the penetration distance is given by

$$\xi = V_g t - (\vec{U}t + \vec{r}) \cdot \vec{v}_g \tag{13a}$$

$$= (V_g + U \cos\alpha)t - (x + x_a)\cos\alpha - (y + y_a)\cos\beta - (z + z_a)\cos\gamma \tag{13b}$$

In two-dimensions $\beta = 90°$ and $\gamma = 90° - \alpha$, and Equation (13b) leads to the result shown in Figure 2.

For the harmonic case we again assume the forms in Equation (2). From Equations (2) and (13b), we find the frequency to be

$$\omega = 2\pi (V_g + U \cos\alpha)/\lambda \tag{14}$$

and the complex normalwash amplitude to be

$$\bar{w}(x,y,z) = G_0 \theta \exp [-i 2\pi \ell(x,y,z)/\lambda] \tag{15}$$

where

$$\ell(x,y,z) = (x + x_a) \cos\alpha + (y + y_a) \cos\beta + (z + z_a) \cos\gamma \tag{16}$$

Again, we may introduce the reduced frequency k_r and eliminate the wave length, and we obtain

$$\bar{w}(x,y,z) = G_0 \theta \exp (- i 2 k_r \ell R/\bar{c}) \tag{17}$$

where

$$R = U/(V_g + U \cos\alpha) \tag{18}$$

3. DOWNWASH INDUCED BY VIBRATIONAL MOTION

The normalwash induced by motion is found from a substantial derivative of the deflection normal to the surface

$$w(x,y,z,t) = U\frac{\partial h}{\partial x} + \frac{\partial h}{\partial t} \tag{19}$$

For harmonic motion

$$h(x,y,z,t) = \text{Re}\,[\bar{h}(x,y,z)\exp(i\omega t)] \tag{20}$$

$$w(x,y,z,t) = \text{Re}\,[\bar{w}(x,y,z)\exp(i\omega t)] \tag{21}$$

so that the complex amplitudes of the normalwash and deflection are related by

$$\bar{w}(x,y,z) = U\frac{\partial \bar{h}}{\partial x} + i\omega\bar{h} \tag{22a}$$

$$= U\left(\frac{\partial \bar{h}}{\partial x} + i2k_r\frac{\bar{h}}{\bar{c}}\right) \tag{22b}$$

Equation (22b) may be generalized for all points in the matrix equation

$$\{\bar{w}\} = \left(U\left\{\frac{\partial \bar{h}}{\partial x}\right\} + i2\frac{k_r}{\bar{c}}\{\bar{h}\}\right) \tag{23}$$

In Equations (19) through (23), the deflection h (and $\bar{h}$) is required at the collocation points appropriate to the aerodynamic theory, in the case of the Doublet-Lattice Method at the three-quarter chord location of each aerodynamic box, and in the case of Piston Theory, at the midchord of each box. This requirement sets a further requirement for interpolation from the structural grid points. The structural deflections are given in the form of rigid body modes and vibration modes since modal methods are usually employed to reduce the number of degrees of freedom in a response analysis. The deflections of the structural grid points, Δ, are determined from a series of rigid body and vibration modes ϕ_n as

$$\Delta(x,y,z) = \sum_n q_n \phi_n(x,y,z) \tag{24}$$

where the q_n are the amplitudes of the vibration modes. In matrix form we have

$$\{\Delta\} = [\phi]\ \{q\} \tag{25}$$

The deflections at the aerodynamic collocation points are found by interpolating among the structural grid points. If the interpolation function is $I(x_j,y_j,z_j;\ x_k,y_k,z_k)$ then the deflections of the aerodynamic points are

$$h(x_j,y_j,z_j) = \sum_k I(x_j,y_j,z_j;x_k,y_k,z_k)\Delta(x_k,y_k,z_k) \tag{26a}$$

$$= \sum_n q_n \sum_k I(x_j,y_j,z_j;x_k,y_k,z_k)\ \phi_n(x_k,y_k,z_k) \tag{26b}$$

or, in matrix form

$$\{h\} = [I_{jk}]\{\Delta\} \tag{27a}$$

$$= [I_{jk}][\phi]\ \{q\} \tag{27b}$$

The downwash follows by substituting Equation (26b) into Equation (22b) and noting that the streamwise differentiation only involves the aerodynamic coordinates (the j-set) and not the structural coordinates (the k-set). The downwash at point j becomes

$$\bar{w}_j = U \sum_n q_n \sum_k \left(\frac{\partial I_{jk}}{\partial x_j} + \frac{i2k_r I_{jk}}{\bar{c}}\right) \phi_{nk} \tag{28}$$

or, in general,

$$\{\bar{w}\} = U\left\{\left[\frac{\partial I}{\partial x_j}jk\right] + \frac{i2k_r}{\bar{c}}\ [I_{jk}]\right\}\ [\phi]\ \{q\} \tag{29}$$

It remains to discuss the form of a suitable interpolation function.

A linear spline, which is based on the small deflection equation of an infinite uniform beam, has been quite useful for one-dimensional interpolation. A variety of two-dimensional schemes have been proposed over many years all of which have had one shortcoming or another. An

ingenious resolution of this classical problem in Aeroelasticity is the surface spline of Harder and Desmarais (Ref. 9). It is based on the small deflection equation of an infinite uniform plate. The main advantages of the surface spline are that the coordinates of the known points need not be located in a rectangular array and the function may be differentiated analytically to find slopes.

A variation of the linear spline, which can be used for interpolation along an elastic axis is developed later. It utilizes the elastic axis degrees of freedom; i.e., the normal deflection, twist about the axis, and the bending slope of the axis, in order to interpolate for the aerodynamic downwashes in the streamwise coordinate system. However, we will develop the surface spline equations first.

The surface spline relates the deflections Δ_k at the structural grid points to the structural loads F_ℓ at all of the same points.

$$\Delta_k = a_o + a_1 x_k + a_2 y_k + \sum_{\ell=1}^{N} F_\ell \, R_{k\ell} \tag{30}$$

where

$$R_{k\ell} = r_{k\ell}^2 \, \ell n \, r_{k\ell}^2 \tag{31}$$

and

$$r_{k\ell}^2 = (x_k - x_\ell)^2 + (y_k - y_\ell)^2 \tag{32}$$

where k and ℓ range over the structural deflection points. The three additional equations to determine the N + 3 unknowns are the static equilibrium equations.

---

9. Harder, R.L., and Desmarais, R.N., "*Interpolation Using Surface Splines*" J. Aircr., Vol. 9, No. 2, pp. 189-919, 1972.

$$\Sigma F_\ell = 0 \tag{33}$$

$$\Sigma x_\ell F_\ell = 0 \tag{34}$$

$$\Sigma y_\ell F_\ell = 0 \tag{35}$$

In matrix form, Equation (30) and Equations (33) through (35) may be written as

$$\{\Delta\} = [P_k]\{a\} + [R_{k\ell}]\{F\} \tag{36}$$

and

$$[P_k]^T \{F\} = 0 \tag{37}$$

where $[P_k]$ denotes the planar coefficient matrix

$$[P_k] = [\, I \vdots x_k \vdots y_k] \tag{38}$$

We add a rigid body displacement term to Equation (37) so it now reads

$$[B]\{a\} + [P_k]^T \{F\} = 0 \tag{39}$$

The matrix [B] normally should be zero, except in the case where y_k is constant, as for a fuselage, an external store, or an elastic axis beam; in this case the nonzero value of [B] chosen as

$$[B] = \begin{bmatrix} 0 & 0 & 0 \\ 0 & 0 & 0 \\ 0 & 0 & 1 \end{bmatrix} \tag{40}$$

avoids a singular solution, and results in a quasi-linear spline interpolation.*

Solving Equations (36) and (39) simultaneously yields

$$\{a\} = -([B] - [P_k]^T [R_{k\ell}]^{-1} [P_k])^{-1} [P_k]^T [R_{k\ell}]^{-1} \{\Delta\} \tag{41a}$$

$$= [I_{a\Delta}]\{\Delta\} \tag{41b}$$

$$\{F\} = [R_{k\ell}]^{-1} (\{\Delta\} - [P_k]\{a\}) \tag{42a}$$

$$= [R_{k\ell}]^{-1} (\lceil I \rfloor - [P_k][I_{a\Delta}])\{\Delta\} \tag{42b}$$

$$= [I_{F\Delta}]\{\Delta\} \tag{42c}$$

*The usual linear-spline is a series of continuous cubics and differs from the degenerate case of the surface-spline. Either provides an acceptable interpolation function.

The deflections at the aerodynamic points are obtained by rewriting Equation (36) as

$$\{h\} = [P_j]\{a\} + [R_{j\ell}]\{F\} \tag{43}$$

where P_j are the planar coefficients for the aerodynamic points

$$[P_j] = [\, I \vdots x_j \vdots y_j \,] \tag{44}$$

and

$$R_{j\ell} = r_{j\ell}^2 \ell n\, r_{j\ell}^2 \tag{45}$$

where

$$r_{j\ell}^2 = (x_j - x_\ell)^2 + (y_j - y\ell)^2 \tag{46}$$

where "j" ranges over the aerodynamic box points and "ℓ" ranges over the structural points.

Substituting Equations (41b) and (42c) into Equation (43) and identifying the result with Equation (27a) leads to the desired interpolation matrix.

$$[I_{jk}] = [P_j]\,[I_{a\Delta}] + [R_{j\ell}]\,[I_{F\Delta}] \tag{47}$$

The derivative of Equation (47) is also needed in Equation (29). It is

$$\left[\frac{\partial I_{jk}}{\partial x_j}\right] = \left[\frac{\partial P_j}{\partial x_j}\right]\left[I_{a\Delta}\right] + \left[\frac{\partial R_{j\ell}}{\partial x_j}\right]\left[I_{F\Delta}\right] \tag{48}$$

where

$$\left[\frac{\partial P_j}{\partial x_j}\right] = [0 \vdots I \vdots 0] \tag{49}$$

and

$$\left[\frac{\partial R_{j\ell}}{\partial x_j}\right] = [2(x_j - x_\ell)(1 + \ell n\, r_{j\ell}^2)] \tag{50}$$

4. AERODYNAMIC INFLUENCE COEFFICIENT MODIFICATIONS

An analysis of the blast onset pressure field is presented in Appendix A. The gust or velocity field and the overpressure field are different

aspects of the blast wave and are not independent. To be completely accurate, the lift induced by the onset pressure field, however small it is, should be added to the lift induced by the gust field. Presently, the aerodynamics module calculates only the loadings induced by the gust field. When it becomes desirable to include the additional effects of the overpressure, the equations of Appendix A can be added to the aerodynamics module.

The matter of lifting- or side-forces on bodies with elliptical cross sections has also been the subject of futher investigation since the publication of Reference 4. The control parameter IBFS determined which of two methods could be used to integrate the body loads. Experience with the option IBFS=0 has not led to generally satisfactory results, so the option IBFS=1 for circular bodies has been chosen for present applications with a modification for elliptical bodies based on slender body theory. The modification for elliptical bodies uses the circular body formula for lift, but for side-force, multiplies the lift by the square of the cross sectional aspect ratio (AR = height/width), i.e., F_z is found from the formula in Reference 4 for IBFS = 1, and $F_y = (AR)^2 F_z$. The effect of compressibility has also been considered in a modification of Slender Body Theory using the technique of Miles (Ref. 10,p. 165). Miles' basic equation for the running load $\partial(F/q)/\partial x$, in the direction of the upwash w (see Figure 3), is

---

10. Miles, J.W., *The Potential Theory of Unsteady Supersonic Flow*, Cambridge: At the University Press, 1959.

$$\partial(F/q)/\partial x = 2\frac{D\tilde{M}}{Dt} \tag{51}$$

$$\frac{D\tilde{M}}{Dt} = \frac{\partial \tilde{M}}{\partial x} + i\frac{\omega}{U}\tilde{M} \tag{52}$$

$$\tilde{M} = \oint_C \Phi a \cos\phi \, d\phi \tag{53}$$

where Φ is the two-dimensional potential due to the crossflow w and is obtained from either the incompressible or compressible crossflow differential equations. Usually the incompressible equation is used for subsonic flow; however, at high frequency the compressible form should be used. The compressible result is:

$$\Phi = aw\, S_1(p) \cos\phi \tag{54}$$

$$p = 2k_r M_\infty a/\bar{c} \tag{55}$$

$$S_1(p) = \frac{1}{1 + pS} \tag{56}$$

$$S = H_0^{(2)}(p)/H_1(2)(p) \tag{57a}$$

$$= \{J_0(p) - iY_0(p)\}/\{J_1(p) - iY_1(p)\} \tag{57b}$$

in which "a" is the local body radius. Placing Φ into the expression for $\tilde{M}$ gives

$$\tilde{M} = a^2 w\, S_1(p) \oint \cos^2\phi \, d\phi \tag{58a}$$

$$= \pi a^2 w\, S_1(p) \tag{58b}$$

Then substituting $\tilde{M}$ into the expression for the running load gives

$$\frac{\partial(F/q)}{\partial x} = 2\pi \frac{D}{Dt}\left\{\frac{w}{U} a^2 S_1(p)\right\} \tag{59a}$$

$$= S_1(p) \frac{2\pi D\,(a^2 w/U)}{Dt} + 2\pi\frac{w}{U}\frac{\partial p}{\partial x}\frac{\partial S_1}{\partial p} a^2 \tag{59b}$$

in which

$$\frac{\partial S_1}{\partial p} = -\{1 - S^2 - S/p\} \tag{60a}$$

$$\frac{\partial p}{\partial x} = \frac{2\, k_r M_\infty}{\bar{c}}\frac{da}{dx} \tag{60b}$$

The first term (with $S_1 = 1$) is the same as that given by the incompressible theory, the second term and the coefficient S_1 are the compressibility corrections.

First order piston theory for motion (Ref. 8) results in a lifting pressure coefficient on a box given by

$$\Delta C_p = \frac{4}{M_\infty} \frac{\bar{w}}{U} \tag{61}$$

where the downwash $\bar{w}$ is taken as the value at the midpoint of the box centerline. The box lift is assumed to act at the same midpoint. This assumption has sufficient accuracy because at high frequency the downwash comes primarily from the plunging motion which is relatively constant over the small box area. However, at high frequencies there is substantial variation of the gust downwash over the box so it is necessary to evaluate the lift by integration over the box area. The assumption is still made that the lift acts at the box center and is justified because the net lift is small at high frequencies. The average pressure is then found by dividing the integrated lift by the box area. The geometry of a typical box is shown in Figure 4.

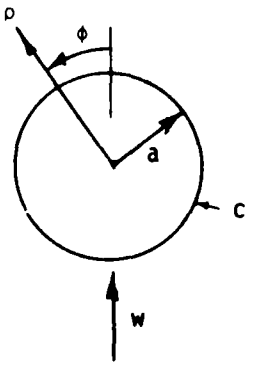

Figure 3. Cross Flow to a Body Cross Section

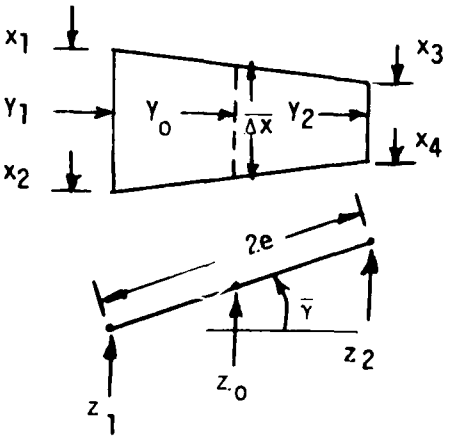

Figure 4. Lifting Surface Box Geometry

$$\Delta C_p = \frac{1}{2e\,\overline{\Delta x}} \int \frac{4}{M_\infty} \frac{\bar{w}_g}{U} \, dA \tag{62}$$

where

$$\bar{w}_g = G_0\theta \exp(-i2\, k_r \ell\, R/\bar{c}) \tag{63}$$

and the integration is performed over the box area. Carrying out the integration of Equation (62) leads to the following expression for the pressure coefficient.

$$\begin{aligned}\Delta C_p = \frac{4}{M} \frac{G_0\theta}{\overline{\Delta x}\,\tau\cos\alpha} \{&(A_{31}\cos\tau\ell_1 - B_{31}\sin\tau\ell_1 \\ &-A_{42}\cos\tau\ell_2 + B_{42}\sin\tau\ell_2) \\ &+ i\,(-B_{31}\cos\tau\ell_1 - A_{31}\sin\tau\ell_1 \\ &+ B_{42}\cos\tau\ell_2 + A_{42}\sin\tau\ell_2)\}\end{aligned} \tag{64}$$

where

$\overline{\Delta x}$ is the average box chord as shown in Figure 4,

$$\tau = 2k_r R/\bar{c} \tag{65}$$

$$\ell_m = x_m \cos\alpha + (y_0 - e\cos\bar{\gamma})\cos\beta + (z_0 - e\sin\bar{\gamma})\cos\gamma \tag{66}$$

$$A_{mn} = (\cos\tau\Delta\ell_{mn} - 1)/\tau\Delta\ell_{mn} \tag{67}$$

$$B_{mn} = (\sin\tau\Delta\ell_{mn})/\tau\Delta\ell_{mn} \tag{68}$$

and

$$\Delta\ell_{mn} = (x_m - x_n)\cos\alpha + 2e\,(\cos\bar{\gamma}\cos\beta + \sin\bar{\gamma}\cos\gamma) \tag{69}$$

and where $\theta = \vec{n} \cdot \vec{v}_g$; i.e., the component of the gust normal to the element.

The case of $\alpha = 90°$ ($\cos\alpha = 0.0$) requires special consideration. The limiting value of ΔC_p is

$$C_p = \frac{4G_0\theta}{M_\infty} e^{-i\lambda_0} \left| Q + i\left(\frac{x_1 - x_2 - x_3 + x_4}{x_1 - x_2 + x_3 - x_4}\right)\left(\frac{\cos\tau eg - Q}{\tau eg}\right)\right| \tag{70}$$

where

$$\lambda_0 = \tau(y_0 \cos\beta + z_0 \cos\gamma) \tag{71}$$

$$g = \cos\beta \cos\bar{\gamma} + \cos\gamma \sin\bar{\gamma} \tag{72}$$

$$Q = \frac{\sin \tau eg}{\tau eg} \tag{73}$$

These "average" pressures are used for the generalized force integration calculation. However, in some special cases actual pressures are required. When this is the case a "point" pressure formula is used.

$$\Delta C_p = \theta \frac{4}{M_\infty} \exp(-i2k_r R\ell/\bar{c}) \tag{74}$$

A "piston theory" may be obtained for slender bodies from the compressible slender body theory by a frequency expansion in the parameter p ($p = 2kM_\infty a/\bar{c}$) at high frequencies. Expanding Equation (59b) for large p gives

$$\frac{\partial(F/q)}{\partial x} = \frac{2\pi a}{ip}\left|\frac{w}{U}\left(i\frac{p}{M_\infty} + \frac{da}{dx} - \frac{1}{2M_\infty}\right) + \frac{a}{U}\frac{\partial w}{\partial x}\right| \tag{75}$$

For the loads caused by motion, the downwash is

$$-\frac{w}{U} = \frac{dh}{dx} + \frac{ip}{aM_\infty} h \tag{76}$$

Substituting this into Equation (75) and retaining terms of orders p and unity leads to

$$\frac{\partial(F/q)}{\partial x} = -\frac{2\pi}{M_\infty}\left|\left(\frac{da}{dx} - \frac{1}{2M_\infty}\right) h + 2a\frac{dh}{dx} + \frac{i2k_r a}{\bar{c}} h\right| \tag{77}$$

For the loads induced by a harmonic gust, the downwash is given by

$$\frac{w}{U} = w_g \theta \exp(-i2k_r R\ell/\bar{c}) \tag{78}$$

and

$$\frac{1}{U}\frac{\partial w}{\partial x} = \frac{-i2k_r R \cos\alpha}{\bar{c}}\frac{w}{U} \tag{79}$$

Substituting these expressions into Equation (75) gives

$$\frac{\partial(F/q)}{\partial x} = 2\pi a \frac{w}{U}\left|\frac{1}{M_\infty}(1-R\cos\alpha) - i\frac{\bar{c}}{2k_r a M_\infty}\left(\frac{da}{dx} - \frac{1}{2M_\infty}\right)\right| \tag{80}$$

This expression gives the loading at a particular body station. Because of the variation in downwash at high frequency along a body lifting element, it is necessary to integrate over the length of the element to obtain the total load to be used in the generalized force calculation. For a slender body it can be assumed that "a" and da/dx are constant along the element and the average values are taken at the element midchord point. Then the integrated force on the element of length Δx and centered at x_0 is

$$\Delta F/q = L\int_{-\Delta x/2}^{\Delta x/2} \frac{w}{U}\, d\bar{x} \tag{81}$$

where

$$L = 2a\pi\left|\frac{1}{M_\infty}(1-R\cos\alpha) - i\frac{\bar{c}}{2k_r a M_\infty}\left(\frac{da}{dx} - \frac{1}{2M_\infty}\right)\right| \tag{82}$$

and

$$\bar{x} = x - x_0 \tag{83}$$

The integrated force becomes

$$\frac{\Delta F/q}{\Delta x} = 2\pi a \frac{w}{U}(x = x_0)\ \frac{\sin\bar{\tau}}{\bar{\tau}}\ \left|\frac{1}{M_\infty}(1-R\cos\alpha) - i\frac{\bar{c}}{2k_r a M_\infty}\left(\frac{da}{dx} - \frac{1}{2M_\infty}\right)\right| \tag{84}$$

where

$$\bar{\tau} = \Delta x\, k_r R\cos\alpha/\bar{c}. \tag{85}$$

When "point" running loads are needed, we simply set $(\sin\tau)/\tau$ equal to unity in this formula.

In general, an arbitrary burst location results in an asymmetric loading of the flight vehicle. Since any asymmetric condition can be

found as a linear combination of a symmetric and an antisymmetrical condition (assuming linear systems, as we are), both the symmetric and antisymmetric aerodynamic analyses need to be performed. In Reference 4, either is optional to the user, but for the present applications, the modifications always to generate both have been added. If the gust normalwash on the right side is $w_g\ (x,y,z,\bar{\gamma})$ and on the left side is $w_g\ (x,-y,z,-\bar{\gamma})$, then the symmetrical normalwash is

$$w_{gs} = \frac{1}{2}\left[w_g(x,y,z,\bar{\gamma}) + w_g(x,-y,z,-\bar{\gamma})\right] \tag{86}$$

and the antisymmetrical normalwash is

$$w_{ga} = \frac{1}{2}\left[w_g(x,y,z,\bar{\gamma}) - w_g(x,-y,z,-\bar{\gamma})\right] \tag{87}$$

5. AERODYNAMIC DATA REQUIRED FOR VIBRA-6

The aerodynamic data required from Reference 4 for the blast response analysis consist of generalized aerodynamic forces for symmetric and antisymmetric modes of vibration and for symmetric and antisymmetric harmonic gust fields having a number of orientations. The orientations depend on the burst locations. The thirteen burst locations are shown in Figure 5 and the standard orientations are specified by the direction cosines tabulated in Table 1; arbitrary oritentations must be specified separately by the user. The generalized forces are required at a sufficient number of reduced frequencies that interpolation will lead to accurate values at intermediate frequencies.

The aerodynamic geometry is also required in order to perform the integrations that lead to the structural responses. That is, the structural responses are required in the form of shears, moments and torques at selected critical stations. A separate stress transformation matrix must be input to

VIBRA-6, for the determination of bending and shear stresses and margins of safety.

6. AERODYNAMIC MONITORING DATA

The computer program of Reference 4 generates aerodynamic coefficients and load distributions as a matter of course for each mode as a means of checking the input data. This is necessary since generalized forces do not have enough physical significance to assist the user in detecting mistakes in input data. This monitor output has been retained in the present application for any two modes selected by the user; e.g., symmetric pitching and antisymmetric yawing. The monitor output for the lifting surfaces includes the pressure distributions, spanwise distributions of lift coefficient, moment coefficient, center of pressure, and loading ($c_\ell c/\bar{c}$), and total lift and moment coefficients. The monitor output for bodies includes the running loads (vertical and lateral) and the total force coefficients. Finally, the total force and moment coefficients are given for the entire aircraft. The specific definitions of aerodynamic coefficients are presented in the sample output.

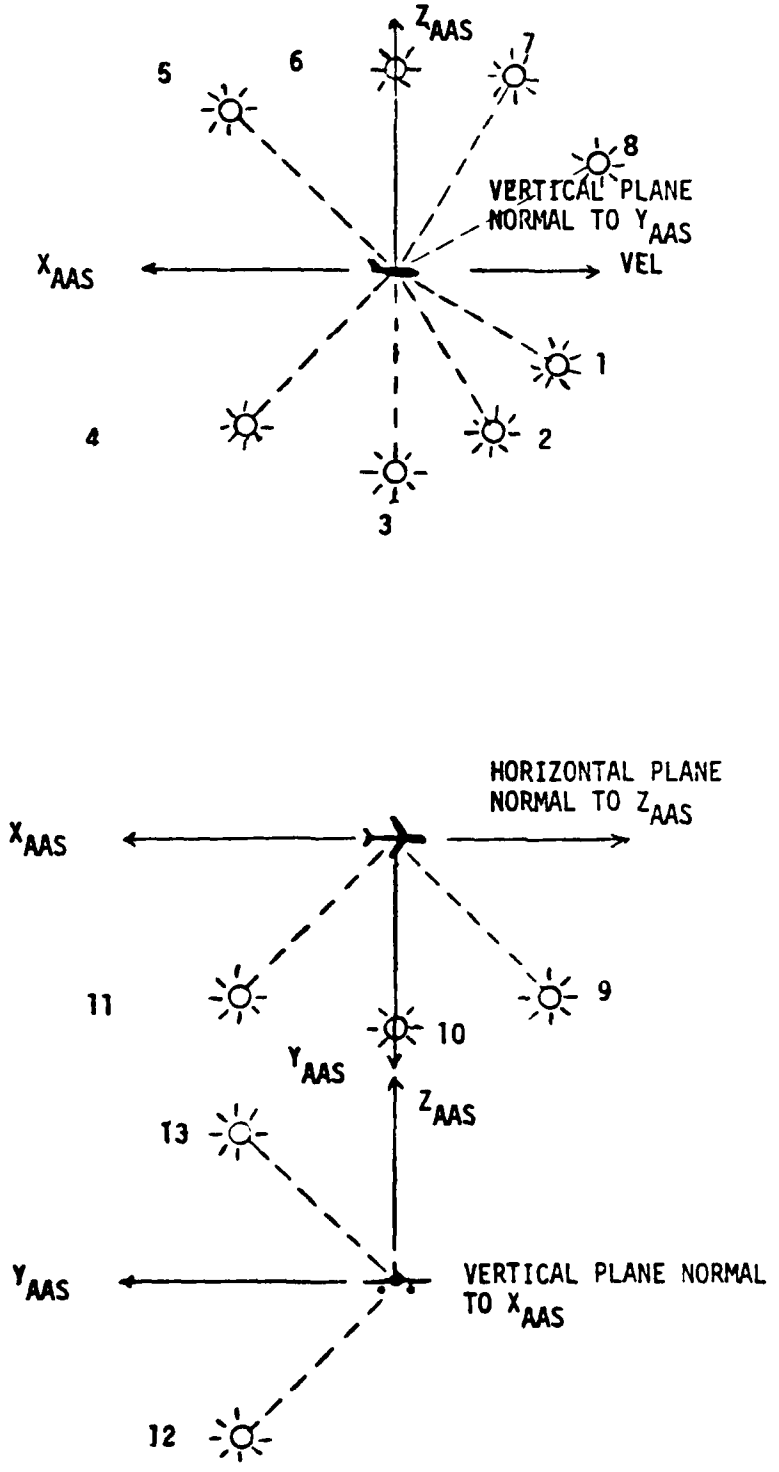

Figure 5. Blast Orientations for Aero Module.

TABLE 1

DIRECTION COSINES FOR STANDARD ORIENTATIONS

ORIENTATION NUMBER	γ_x	γ_y	γ_z
1	0.8660254	0.0	0.50
2	0.50	0.0	0.8660254
3	0	0.0	1.0
4	-0.7071068	0.0	0.7071068
5	-0.7071068	0.0	-0.7071068
6	0	0.0	-1.0
7	0.50	0.0	-0.8660254
8	0.8660254	0.0	-0.50
9	0.7071068	-0.7071068	0.0
10	0	-1.0	0.0
11	-0.7071068	-0.7071068	0.0
12	0.0	-0.7071068	0.7071068
13	0.0	-0.7071068	-0.7071068

SECTION III

AIRCRAFT IDEALIZATION

Finite element methods in aerodynamics (as in structures) require a compromise between accuracy and computing time. A sufficient number of elements must be used to obtain acceptable accuracy but not so many as to result in exorbitant computational costs. Experience has been gained with the Doublet-Lattice/Image Method on advanced aircraft configurations in Reference 11 that suggests guidelines to achieve this compromise in applications to gust and blast response analyses.

The basic modelling elements include lifting surfaces, slender bodies, and interference surfaces. These are consistent with the assumptions of linearized aerodynamic theory. The idealization into these modelling elements results in an aircraft geometry that is much simpler than the actual geometry. However, the essential features are retained such as surface planforms and body volume distribution, although some secondary features are neglected such as thickness effects of the lifting surfaces. The aerodynamic coordinate system is shown in Figure 6.

1. LIFTING SURFACES

Lifting surfaces are idealized as plane panels; as such they have no thickness, camber or twist, but do have dihedral. The effects of camber or twist and angle of attack are accounted for in the linearized small disturbance boundary condition of tangential flow at the surface; i.e., the so-called normalwash boundary condition. The idealization of each lifting surface consists of small trapezoidal elements (boxes) arranged in strips parallel to the freestream (see Figs. 7 and 8) such that

---

11. Giesing, J.P., and Kalman, T.P., *Aerodynamic Loads on Advanced Fighter Aircraft*, Air Force Flight Dynamics Laboratory, Report No. AFFDL-TR-73-45, October 1973.

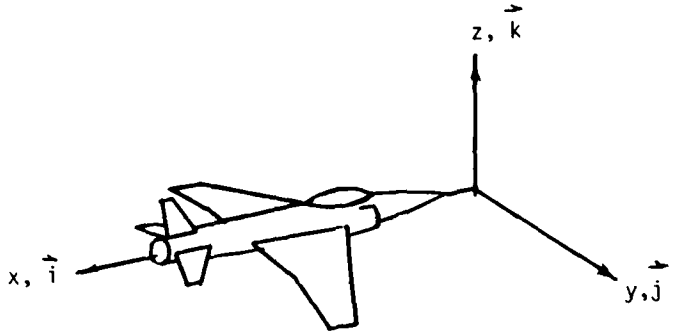

Figure 6. Aerodynamic Coordinate System

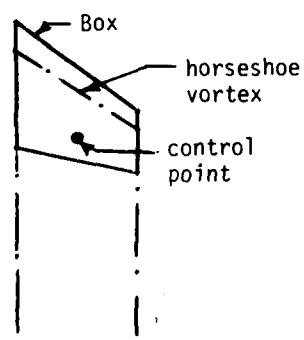

Figure 7. Surface Lifting Element (Box)

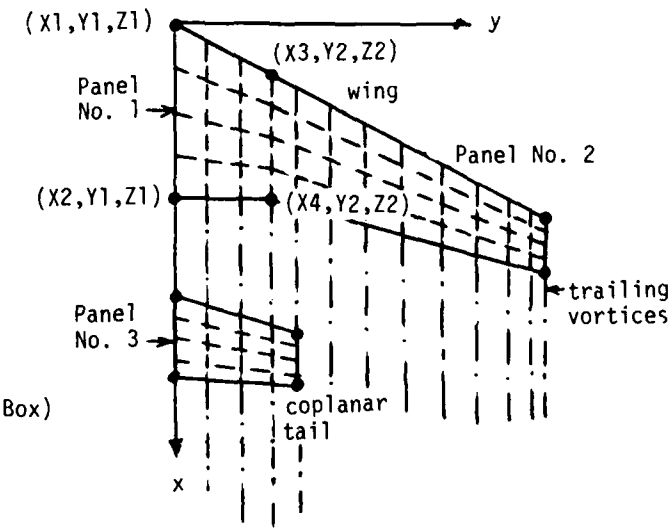

Figure 8. Idealization of Lifting Surface

box boundaries lie on surface edges, fold lines, and control surface edges. The lift on each box is represented by an unsteady horseshoe vortex having its bound leg located on the box quarter-chord and its trailers extending downstream, and is determined by satisfying the normalwash boundary condition at a control point at the three-quarter chord location along the centerline of each box (Fig. 7). For coplanar or near-coplanar surfaces, the boxes must be aligned in the streamwise direction so that the control points are centered between the trailing vortices (Fig. 8). For non-coplanar surfaces, the strips need not be aligned; sufficient perpendicular separation is one strip width. For intersecting surfaces, the intersections must also be located at box edges as in the case of a wing pylon.

The lifting surface can be idealized into a single panel if there are no planform (or dihedral) discontinuities; otherwise, the planform discontinuities determine the subset of trapezoidal panels. A panel is then described by the coordinates of its inboard chord, X1, X2, Y1, and Z1, and the coordinates of its outboard chord, X3, X4, Y2, and Z2; see wing panel #1 in Fig. 8. The panel then has a dihedral $\gamma = \arctan\left[(Z2-Z1)/(Y2-Y1)\right]$, and its normal vector is $\vec{n} = -\vec{j}\sin\gamma + \vec{k}\cos\gamma$, where $\vec{j}$ and $\vec{k}$ are the unit vectors in the y and z directions, respectively. The panels provide the means of generating the boxes within the computer; the boxes are generated from the additional input information of the spanwise fractional divisions τ_n (n = 1, NS) and the chordwise fractional divisions θ_i (i = 1, NC). The panel should be subdivided so that there are a sufficient number of boxes per wave length; i.e., the box chords should be approximately less than $\bar{c}/6k_r$. This rule was relaxed somewhat for test configuration shown on page 53 to reduce cost. Actually, 14 boxes should be used on the root strip and 5 boxes on the tip strip with a uniform variation in between. This corresponds to a maximum k_r, used for the DLM, of 2.0 based on $\bar{c}$ = m.a.c. The minimum number of boxes on a chord is four. The number

of strips spanwise should be chosen so the box aspect ratios are of order unity; i.e., less than three and greater than one-third.

2. SLENDER BODIES

The idealization of fuselage, nacelles, or external stores as slender bodies does not require geometric similarity to the actual body. The slender body idealization is only used to construct the boundary conditions. It is recommended that the best elliptical representation of the body cross sectional area be used independent of the interference body geometry; this idealization is permitted to pass through lifting surfaces. The elliptical cross section is specified by its width and aspect ratio (ratio of height to width). The cross section should be centered on a straight line along the planform centerline of the body; the centerline coordinates are at YC and ZC as shown in Figure 9. The (small) displacements of the body during motion are accounted for in the upwash and sidewash boundary conditions.

Slender Body Theory is used to calculate the axial doublet strength and the cross-flow forces. Hence, the maximum loading occurs where the cross-sectional area has its greatest rate of change. All bodies, including jet engines, must be idealized as having pointed noses. This is an essential assumption of Slender Body Theory. However, a body need not be closed at its downstream end and a suitable base area may be selected to approximate viscous or flow separation effects.

In addition to the idealization of the body cross sections, the body length is divided into segments. The segment is described by its length and its cross-sectional area at each end. The cross-flow force is assumed

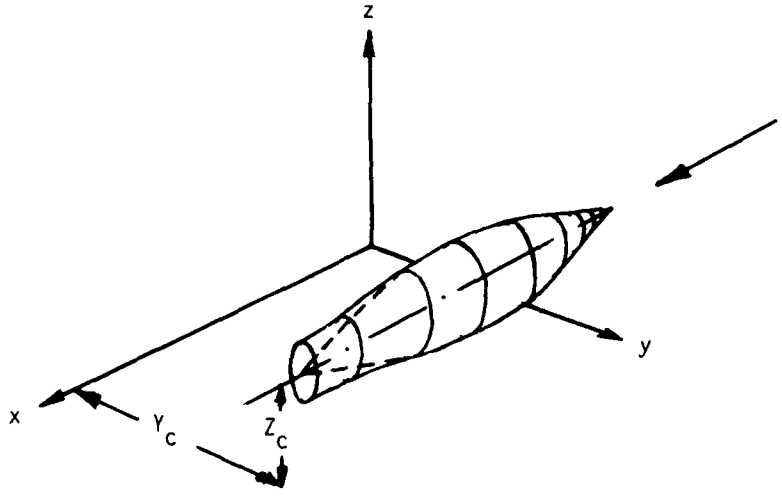

Figure 9. Slender Body Geometry

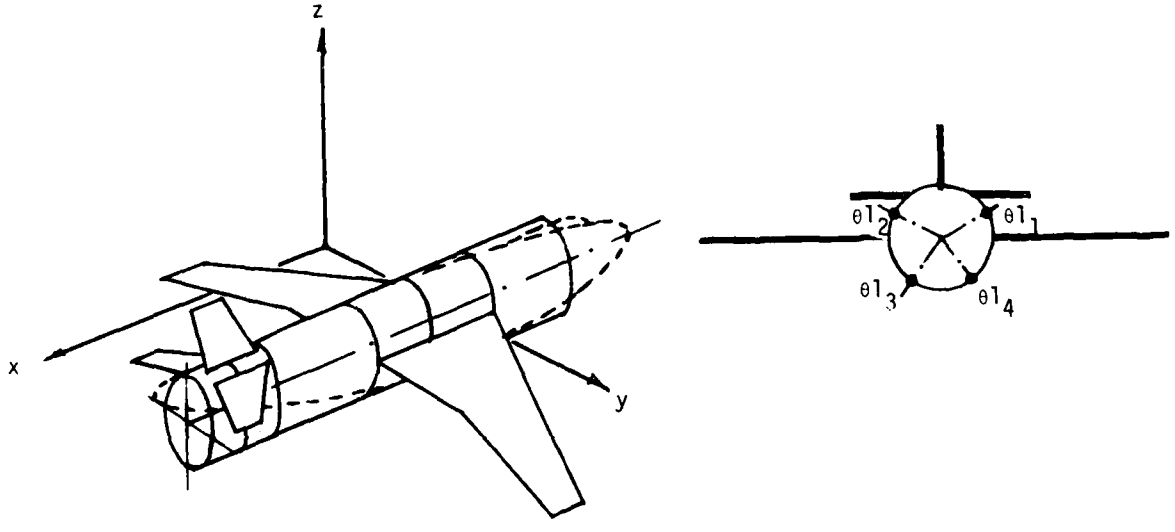

Figure 10. Idealization of Aircraft into Lifting-Surfaces, a Slender Body, and Interference Bodies

to act at the center of the segment length. The segment lengths are chosen from considerations of streamwise changes in geometry. Smaller lengths are chosen where the body cross section is changing rapidly and in regions of maximum interference with lifting surfaces as near the wing root or at a nacelle-pylon intersection.

3. INTERFERENCE BODIES AND IMAGE SYSTEMS

A cylindrical tube with an elliptical cross section is used to generate images. All attached lifting surfaces are connected to this tube. Within this tube is placed an image system of oscillatory horseshoe vortices. This image system approximately negates the flow field at the body surface induced by lifting surfaces. The images of lifting surface strips which lie close to the interference tube are of prime importance, since the end-plating effect of the interference tube has the greatest effect on these. However, those that lie further than two interferance tube radii can usually be neglected in the interest of computational efficiency. However, there should be at least two adjacent lifting surface strips imaged within the tube. For this reason a term called SCALER, which is a "non-dimensional image radius" is an input. This number, when multiplied by the tube radius, gives a radius (from the tube center line) within which lie all the lifting surface strips which possess an image within the tube. Strips whose centerlines lie outside of this radius will not have an image within the tube in question.

The nondimensional image radius is not input per body but is the same for all bodies. Even though the nondimensional image radius (SCALER), is the same for all bodies the actual dimensional image radius, a_I is different for each body since, as mentioned above, a_I is the result of

multiplying the term SCALER times the tube radius in question. Thus the following equation holds:

$$a_I = \text{SCALER } a$$

Thus the nondimensional image radius (SCALER) must be selected such that at least two strips of the adjacent lifting surfaces be imaged for each body/surface combination. If this is not a problem then use the usual value to 2.0.

The image system primarily negates the effects of the trailing vortex system; an additional slender body term must also be included to cancel the residual effects arising primarily from the bound vortex system. The interference tube is segmented into elements by means of angular divisions θ1 around its circumference and streamwise divisions along its length as shown in Figure 10. The angular positions must not be located at lifting surface/body intersections, and there must be at least two positions; four is a preferred number of positions, although six or more will improve the accuracy of the average upwash and sidewash calculations but will result in excessive computational cost. Since the interference elements increase the computational cost, their number should be limited. They need only be used near lifting-surface/body intersections and only upstream and downstream within a short-length of the lifting surface. In situations in which high accuracy is not required; eg., for external stores, the number of interference elements might be severely reduced.

After the upwash and sidewash have been averaged around the interference body circumference, they constitute boundary conditions which are applied to the actual slender body surface. The slender body cross-sectional properties must be input (again) at the interference

body element end points. This input is called the interference body radius (or width for elliptic cross sections) distribution. Once the cross flow forces on the slender-body/interference-body combination are calculated, they are integrated together as concentrated forces at the slender body element control points located at the streamwise midpoint of each segment.

4. ASSEMBLAGE OF BASIC MODELLING ELEMENTS INTO AN AIRCRAFT IDEALIZATION

The following outline summarizes the steps necessary to idealize a complete aircraft into a configuration of lifting surfaces, slender bodies, and interference bodies.

Step 1. The aircraft is replaced by a series of lifting surface panels, for the wings, empennage and pylons, and interference tubes of constant cross section, for the fuselage, nacelles and stores. An example is shown in Figure 11. The wing is made up of three panels. The first panel is inboard of the pylon, the second is between the pylon and the aileron, and the third includes the aileron. The pylon is a single panel intersecting the wing between the wing first and second panels. (Note: it is not necessary that a pylon intersection be between wing panels, but only at a strip edge.) The horizontal and vertical stabilizers are each a single panel attached to the fuselage interference tube.

Some liberty must be taken with the actual configuration in order

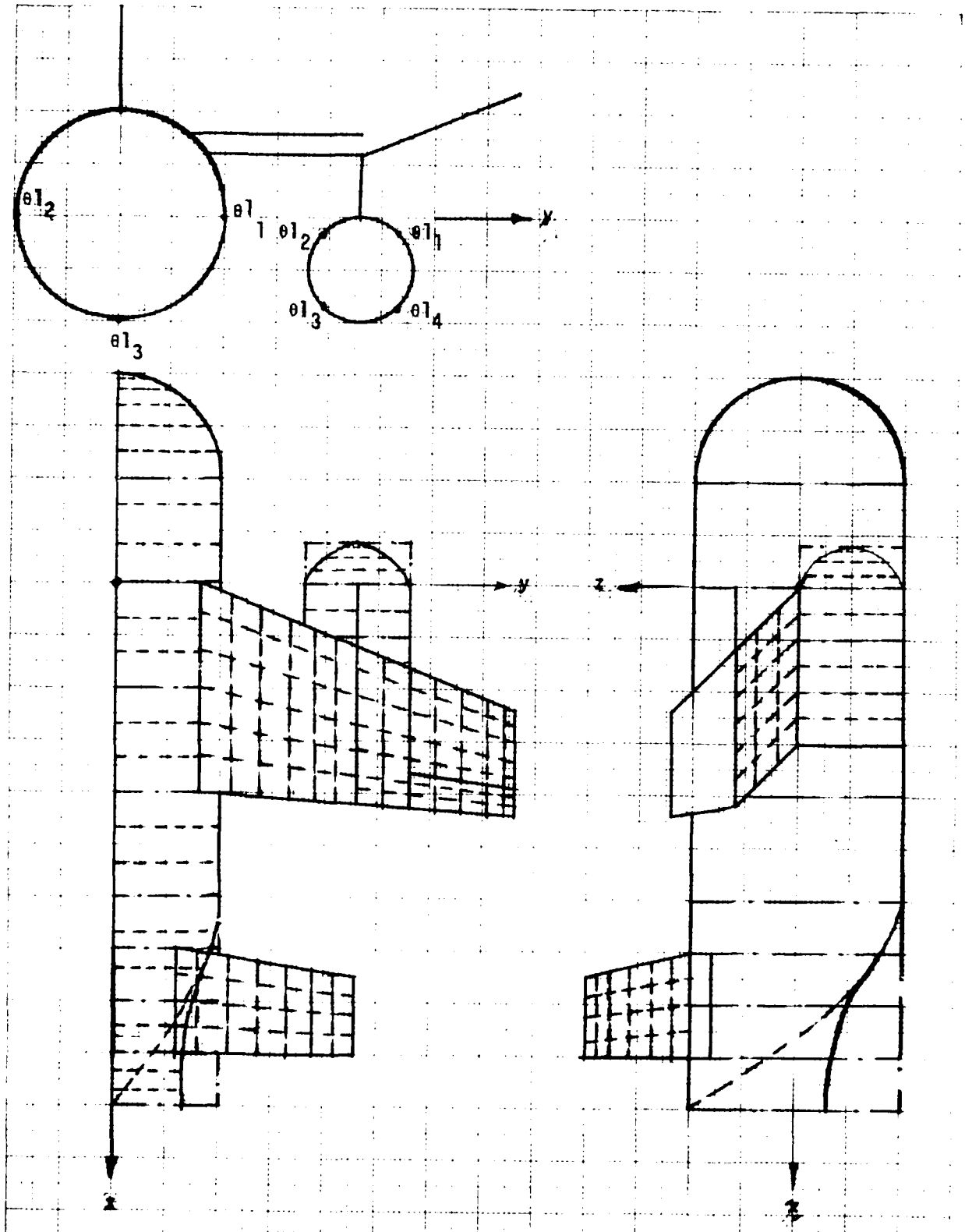

Figure 11. Idealization of Aircraft

to accomplish these replacements. For example, the horizontal tail root is moved from the contour that fits the aft fuselage to a streamwise position that fits the fuselage interference tube. This may actually result in moving the tail outboard. It is important that gaps or overlaps are not inadvertantly permitted between adjacent connected components.

The nacelle in Figure 11 is shown pointed at the nose and open at its base. Bodies should be idealized with pointed noses even if an open engine nacelle is being represented; this simulates the crosswise flow at the intake. Bodies need not be closed at their bases and an open base can be used to simulate flow separation.

For irregularly shaped bodies, the cross sections should be approximated by ellipses having the same cross sectional area. The slender body idealization is described in terms of the body width and aspect ratio (the constant ratio of height to width of the ellipse). For elliptic cross sections the parameter θl is no longer the angle at which the pickup points are located. It is a parameter such that the pickup point locations are given as

$$y = a \cos\theta l$$
$$z = a\, AR \sin\theta l$$

Step 2. Next, the surface panels are divided into boxes. Figure 11 also shows these subdivisions. Four to six chordwise boxes are recommended but if a panel contains a control surface seven to twelve are advised. If the reduced frequency is high, a box chord less than $\bar{c}/6\ k_r$ is necessary for accuracy. On a high aspect ratio surface 10 to 15 spanwise strips are recommended. For low aspect ratio tail surfaces at least 8 strips are

desirable. One or two strips are usually sufficient for pylons depending on the aspect ratio. In general, the aspect ratio of boxes should be of order unity; e.g., box $0.33 < AR < 3.0$ is suggested.

At surface intersections, e.g., on a T-tail, the leading and trailing edges of boxes should coincide. However, it has not been found necessary to align box end points on adjacent coplanar panels, although it probably is desirable. It is also desirable to tailor the spanwise strip widths to the anticipated spanwise load distribution; narrower strips should be used in regions of rapid changes in loading, e.g., near the tips. Figure 11 shows the horizontal tail divided into strips aligned with the wing strips. This is a requirement for a coplanar or near-coplanar tail surface so that the normalwash collocation points on the tail are centered between all trailing vortices. If vertical separation between the tail surface and the wing wake is greater than a strip width, the alignment of tail strips with those of the wing is not necessary.

Step 3. The last step divides the bodies into slender-body elements and interference-body elements. Each body is idealized with a pointed nose and an open or closed base and with an elliptical cross section. The elliptical cross section has a variable area along the length of the body which is equal to the cross sectional area of the actual body but with a constant aspect ratio (height to width ratio). The length of the body is divided into segments with shorter segments in regions of maximum rate of change of cross sectional area and in regions of a lifting-surface/body intersection. A sufficient number of elements are required to describe accurately the body cross sectional area distribution. However, even in regions where the cross section is not changing, a number of elements

should be placed to establish the points at which the body force distribution is calculated. Figure 11 shows a number of elements on parts of the fuselage and parts of the nacelle where the cross sections are constant.

The interference tube is usually divided into four or five elements for each lifting-surface/body intersection. Figure 11 shows these divisions by a dot-dash line. There are four near the wing and four near the tail. These elements compensate for the residual wing-body interference not accounted for by the image system in cancelling the flow through the fuselage surface, so they only have to be used near a lifting-surface/body intersection. In cases where high accuracy is not required, the interference element system can be severely reduced, and a cost savings will result. The eight interference elements around the fuselage (four for the wing and four for the tail) are divided around the circumference at three points. Only three are selected so that the computing cost is reduced. The three angular positions around the tube, θl_1, θl_2 and θl_3, are spaced such that both the horizontal y-velocity and vertical z-velocity can be determined; i.e., θl_1 and θl_2 give the horizontal component and θl_3 gives the vertical velocity. If there were no vertical fin $\theta l_4 = 90°$ would be added to obtain a more accurate average vertical velocity. The angular positions must be chosen away from lifting-surface intersections because the trailing vortices at these locations result in a singular calculation of crossflow velocity.

The slender body radius (or width) distribution approximates the body whereas the interference tube has a constant cross section. The slender body radius distribution may therefore lie within the tube as shown in

Figure 11 or it may pass outside the tube (not shown), and it may even pass through lifting-surfaces. A total of 27 slender body elements on the fuselage and 10 on the nacelle are shown in Figure 11.

5. INTERPOLATION OF MODAL DATA

The surface-spline technique described in Section II, Part 3, is used to interpolate for the aerodynamic normalwash distribution. In addition to the specification of aerodynamic control points, which has been discussed previously, the node points at which the modal deflections are given (called aerodynamic nodal points) must also be specified. Figure 12 shows a set of nodal points for the configuration of Figure 11. The surface-spline fitting through the deflections at the nodes to obtain deflections and slopes of the aerodynamic boxes is illustrated in Figure 13. It should be emphasized that the surface-spline is very accurate for interpolation, but loses accuracy rapidly as extrapolation distances increase; extrapolation should be avoided whenever possible.

The sign convention for positive deflections on bodies is upward (+z-direction) and outboard on the starboard wing (+y-direction). On lifting surfaces, a positive deflection is normal to the surface where the positive normal direction is

$$+\vec{n} = -\vec{j}\sin\gamma + \vec{k}\cos\gamma$$

in which the positive dihedral γ is given in Section III, Part 1.

A separate surface-spline is fit over various specified areas; the surface fit does not extend beyond the boundaries of these areas. These

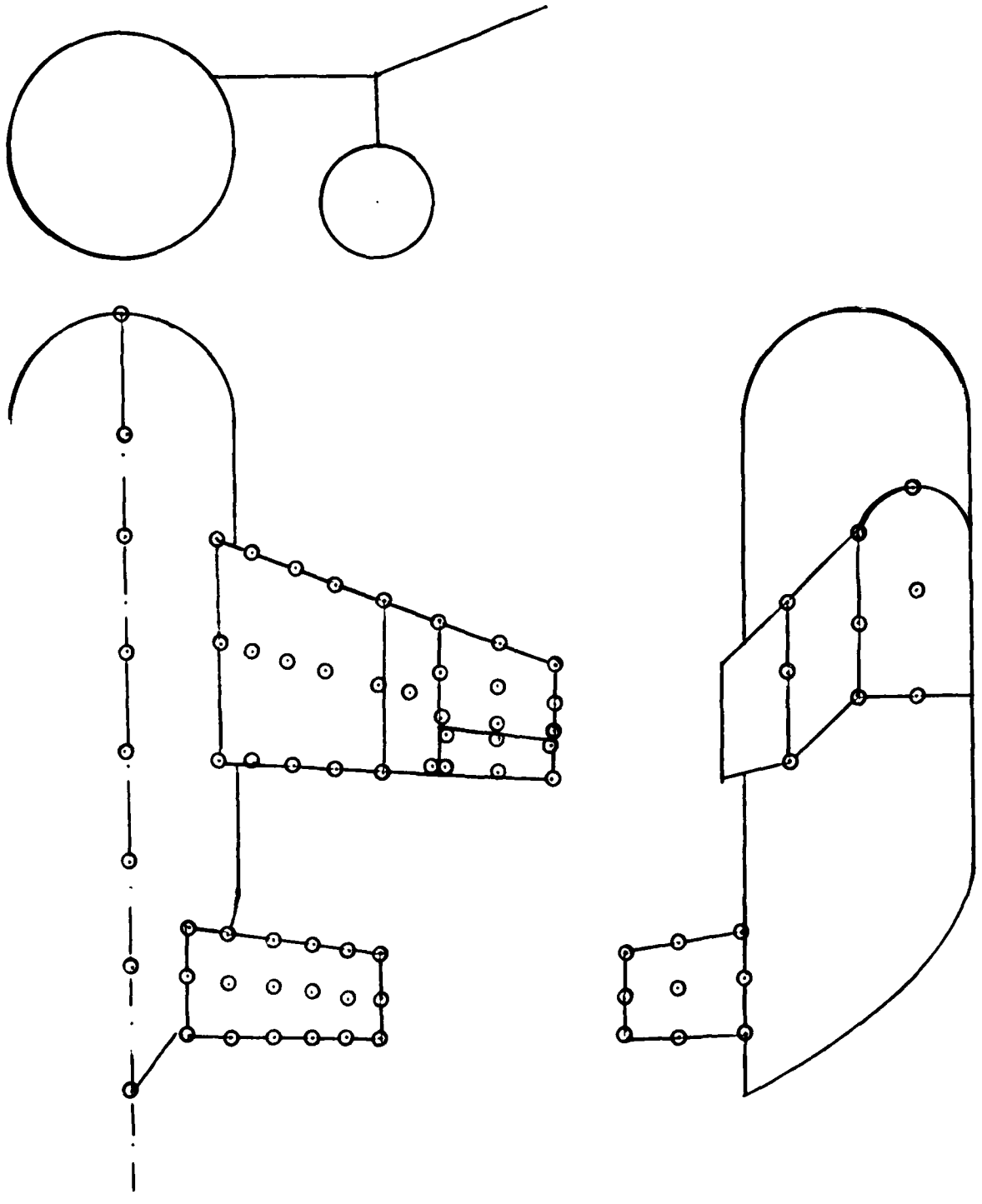

Figure 12. Aerodynamic Nodal Points for Surface-Splines

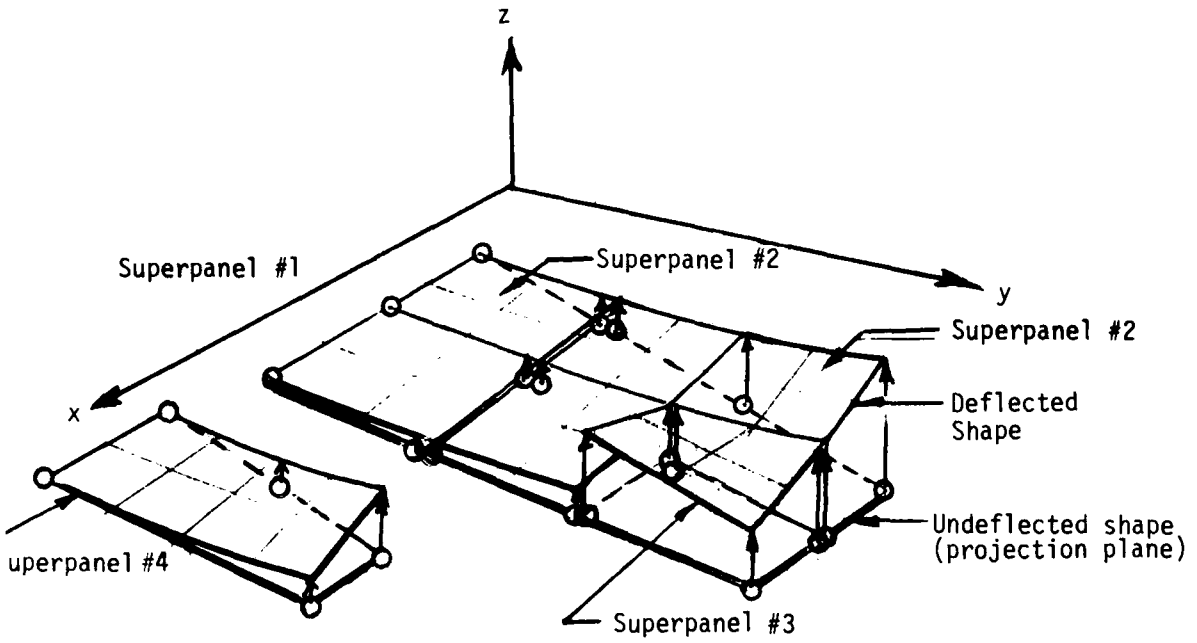

Figure 13. Deflection of Surface-Splines

specified areas on lifting surfaces are referred to as "superpanels"; on bodies they are called "superbodies". See Figure 13. In Figure 12, Panels No. 2 and 3 comprise one superpanel. Dihedral of wing panels does affect the interpolation function for rigid body modes. Thus, panels of dissimilar dihedral angles are not combined into the same superpanel. For panels with less than 45° dihedral, the surface-spline is based on the horizontal (x, y) coordinates of the vertically projected nodal points; for panels with greater than 45° dihedral, the spline is based on the (x, z) coordinates of the horizontally projected nodal points. A control surface, Panel No. 4 in Figure 13, must always be a separate superpanel since it can have discontinuities in spanwise deflections and streamwise slopes. If continuity in deflections between superpanel edges is required, the common nodal points must be specified twice, once on each superpanel. An example is the control surface hinged at its leading edge (see Fig. 13); the nodal points on the hinge-line must be specified once on the wing superpanel and again on the control surface superpanel. A second example is the common side edge between superpanels #1 and #2.

A second type of interpolation procedure for superpanels is obtained using the elastic axis degrees of freedom, h, the normal bending deflection of the elastic axis, α, the twist about the axis, and θ, the bending slope of the axis. These degrees of freedom are illustrated in Figure 14. These elastic deflections are given at nodal points along the elastic axis, but not at the end points (XA, YA, ZA) and (XB, YB, ZB).

As with the spline interpolation, control surfaces must be defined as separate superpanels. If absolute (rather than relative) control surface

deflections are used, the wing and control surface superpanels are mutually exclusive as before. However, if relative control surface deflections are used, the control surface superpanel is superimposed on the wing superpanel. In this case, the aerodynamic boxes on the control surface lie on both superpanels. In the input procedure a selection is made among the degrees of freedom (h, α, and/or θ) that are to be used; e.g., if relative coordinates are used for a control surface, then only α might be used. The nodal points along the elastic axis are normally the mass reference points. However, for control surfaces, the computer program automatically calculates nodal points when the superpanel is flagged as "associated" with another superpanel since there are no mass reference points on the control surfaces.

Figure 14 gives a graphical illustration of how the control surface nodes are determined. Lines are drawn normally to the elastic axis of the associated superpanel and not along radial lines. The points at which they intersect the control surface superpanel elastic axis are the generated nodes.

Each superpanel, whether it be a wing, control surface, tail, etc., is divided into "sections". A "section" is an area of a superpanel in which a specific way of generating the wing surface deflection and slope (in the x-direction) is employed. Usually, the deflection of the superpanel is given by line generators normal to the elastic axis (see Figure 14, superpanel section #2). However, special provision has been made for the root and tip areas. In these areas a radial or fan type of line generator is used so that the line generator lies parallel to the inboard and outboard chords of the "section" with a monotonic variation in between. Figure 14 illustrates the radial line generators in superpanel sections #1

and #3. In this case the outboard chord of section #1 is normal to the elastic axis as is the inboard chord of section #3. However, this is not necessary.

In order to find the deflection and slope at all points on the surface, an interpolation procedure must be applied to h, α, and θ along the elastic axis. A modified one-dimensional spline is used for this purpose. This type of curve-fitting function is not adequate for extrapolation. To overcome this difficulty, a linear extrapolation from the first two and last two nodes is made to obtain the deflection at the elastic axis end points. If {h} is the set of N bending deflections at the nodes, excluding the elastic axis end points, then the set of (N + 2) nodal deflections $\{\bar{h}\}$ which include the end points may be written

$$\{\bar{h}\} = [T]\{h\} \tag{88}$$

where the transformation matrix [T] appear as

$$[T] = \begin{bmatrix} \bar{a} & b & 0 & \cdots & 0 & \bar{0} \\ 1 & 0 & 0 & \cdots & 0 & 0 \\ 0 & 1 & 0 & \cdots & 0 & 0 \\ 0 & 0 & 1 & \cdots & 0 & 0 \\ \vdots & & & & & \vdots \\ 0 & 0 & 0 & \cdots & 0 & 1 \\ \underline{0} & 0 & 0 & \cdots & c & \underline{d} \end{bmatrix} \tag{89}$$

in which

$$a = 1 - b \tag{90}$$

$$c = 1 - d \tag{91}$$

$$b = (\tau_1 - \tau_2)/(\tau_3 - \tau_2) \tag{92}$$

$$c = (\tau_{N+2} - \tau_N)/(\tau_{N+1} - \tau_N) \tag{93}$$

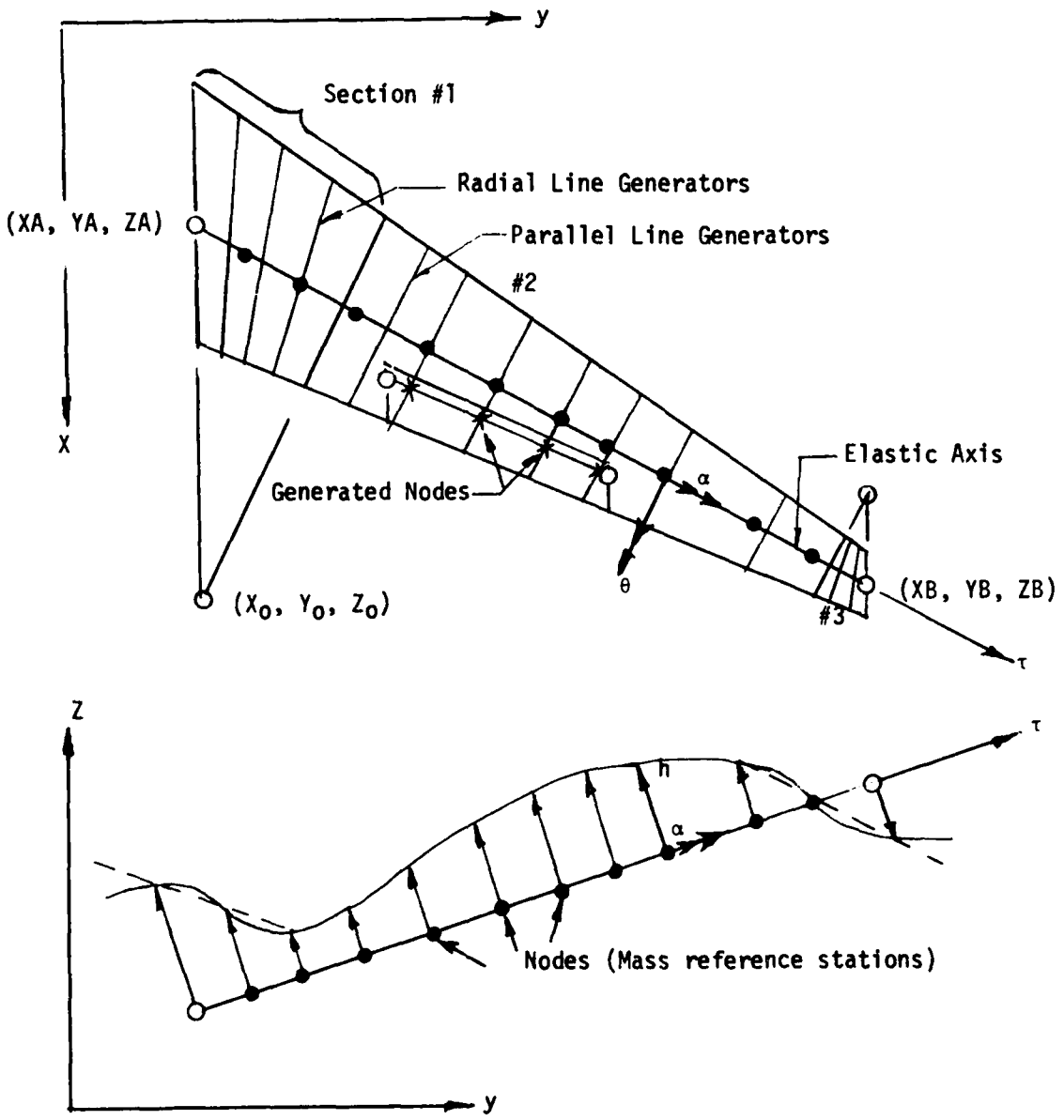

Figure 14. Graphical Description of Elastic Axis Representation

where the τ_j are the nodal coordinates, including the end points as measured along the elastic axis from XA, YA, ZA (see Figure 14); i.e., $\tau_1 = 0$. The same transformation applies to obtain the slopes, $\{\bar{\alpha}\}$ from $\{\alpha\}$, and $\{\bar{\theta}\}$ from $\{\theta\}$, so we write

$$\{\bar{\alpha}\} = [T]\{\alpha\} \tag{94}$$

$$\{\bar{\theta}\} = [T]\{\theta\} \tag{95}$$

Separate one-dimensional splines are then fit through the values of h, α, and θ at all of the node points and the end points of the elastic axis, as illustrated in Figure 14. From the variation of h, α, and θ along the elastic axis, which we denote as $h(\tau)$, $\alpha(\tau)$, and $\theta(\tau)$, we may find the deflection H of any point on the superpanel surface and its streamwise slope dH/dx. There are two cases depending on whether the point is on a parallel line generator normal to the elastic axis or on a radial line generator. For points on the parallel line generators, the deflection is

$$H = h(\tau) + \tilde{y}\sin\Lambda - (\tilde{x}-XA)\cos\Lambda\,\alpha(\tau) \tag{96}$$

where $\tilde{x}$ and $\tilde{y}$ are given in Equations 103 and 104.

The streamwise slope is

$$\frac{dH}{dx} = -\theta(\tau)\sin\Lambda - \alpha(\tau)\cos\Lambda + \frac{d\alpha}{d\tau}\sin\Lambda\,(\tilde{y}\sin\Lambda - (\tilde{x} - xA)\cos\Lambda) \tag{97}$$

where Λ is the sweep angle of the elastic axis in the plane of the surface and τ is the distance along the axis from the origin at (XA, YA, ZA).

For points with radial line generators from an origin at (XO, YO, ZO), the deflection is

$$H = h(\tau) - (\rho - \rho_b)\cos(\Lambda + \phi)\,[\alpha(\tau) + \theta(\tau)\tan(\Lambda + \phi)] \tag{98}$$

and the streamwise slope is

$$\frac{dH}{dx} = -\theta(\tau)\sin\Lambda - \alpha(\tau)\cos\Lambda + \frac{\rho_b}{\rho}(\rho - \rho_b)\sin\phi\left[\frac{d\alpha}{d\tau} + \frac{d\theta}{d\tau}\tan(\Lambda + \phi)\right] \tag{99}$$

where

$$\rho = \sqrt{(\tilde{x} - \tilde{X0})^2 + (\tilde{y} - \tilde{Y0})^2} \tag{100}$$

$$\phi = \arctan\left(\frac{\tilde{y} - \tilde{Y0}}{\tilde{x} - \tilde{X0}}\right) \tag{101}$$

$$\rho_b = \rho_o \frac{\cos(\phi_o + \Lambda)}{\cos(\phi + \Lambda)} \tag{102}$$

and

$$\tilde{x} = x \tag{103}$$

$$\tilde{y} = (y - YA)\cos\bar{\gamma} + (z - ZA)\sin\bar{\gamma} \tag{104}$$

$$\tilde{X0} = X0 \tag{105}$$

$$\tilde{Y0} = (Y0 - YA)\cos\bar{\gamma} + (Z0 - ZA)\sin\bar{\gamma} \tag{106}$$

$$\rho_o = \sqrt{(\tilde{XA} - \tilde{X0})^2 - (\tilde{YA} - \tilde{Y0})^2} \tag{107}$$

$$\phi_o = \arctan\left(\frac{\tilde{YA} - \tilde{Y0}}{\tilde{XA} - \tilde{X0}}\right) \tag{108}$$

in which $\bar{\gamma}$ is the dihedral angle of the plane containing the elastic axis and

$$\tilde{XA} = XA \tag{109}$$

$$\tilde{YA} = 0 \tag{110}$$

SECTION IV

APPLICATIONS TO RIGID AIPCRAFT

A number of applications have been made to a two-dimensional airfoil and to a typical large twin-engine transport that is assumed to be rigid. The applications are intended to exhibit the convergence characteristics of the Fourier transformation and the effects of the transition from the Doublet-Lattice Method (DLM) to Piston Theory (PT).

The number of calculated aerodynamic solutions depends on the blast orientation. An estimate of the required reduced frequency spacing is

$$\Delta k_r = \pi(1+M_\infty \cos\alpha)/(\mu_1 M_\infty \bar{\ell}/\bar{c}) \qquad (111)$$

where $\bar{\ell}$ is the slant distance from the pressure point in question to the blast plane as it passes through the aircraft origin. To render all pressure solutions accurate, the maximum value of $\bar{\ell}$ is usually used in this formula. Also, μ_1 is the number of solutions per cycle, recommended in the range of 6 to 8. The maximum frequency that must be considered is

$$k_{r_{max}} = \mu_2 \pi\left(\frac{1 + M_\infty \cos\alpha}{M_\infty \bar{c}/U_\infty}\right) \text{ or } k_{r_{max}} = \mu_2\pi\left(\frac{1 + M\cos\alpha}{M_\infty}\right) \qquad (112)$$

where μ_2 is recommended as 2 or 3.

The transition gap between the two aerodynamic theories results in differing frequency response curves. The smaller the gap, the more pronounced is the difference between the frequency responses and the larger are the ripples in the time domain.

Calculated results are shown in Figures 15 through 31. Each solution is based on a step function escitation frequency response because the step function is a good approximation to the frequency response of a blast wave (see Figure 19) and the time histories will approach steadystate values that are known.

Figures 15 through 17 show results for a two-dimensional airfoil. Figure 15 shows the convergence of the DLM to the PT for pitching, plunging, and gusts at 45^{o} and 90^{o} angle of attack in the frequency domain.

The term f_{max}, in many of the figures to follow, is the frequency, in cps or Hz, at which the frequency response is terminated. Such a termination leads to a small error originating in the inverse Fourier Transformation. This error becomes smaller as f_{max} is increased. Figure 16(a) compares the transient lift (with effectively infinite f_{max} in the PT) to results obtained by Lomax, etal. (Ref. 12). The calculations followed Zartarian's suggestion (Ref. 7) of obtaining the PT contribution analytically and the contribution from the difference between the DLM and PT from the numerical Fourier transform. Figure 16(b) shows the pressure at two points near the leading and trailing edges induced by a 45^{o} gust. The irregularities in the curves show the effects of the DLM-PT transition at $k_r = 5.0$. The agreement with PT is seen at the appropriate intercept times for each point. Figure 17 presents a convergency study as a function of maximum k_r with a vertical gust. The DLM-PT transition is at $k_r = 10.0$. Slow convergence is seen in this case at high subsonic Mach number ($M = 0.8$).

Figure 18 gives the idealization of a three-dimensional transport; the test case in Volume I, which is being used to gain insight and experience in the use of the aerodynamic aspects of VIBRA-6. Even though the idealization is crude, much valuable information has been gained. The dots shown on the transport idealization are the points at which pressures or running loads are calculated on the rigid vehicle. No problem has been found on the elastic vehicle once the aerodynamic frequency response has been well

---

12. Lomax, H., Heaslet, M.A., and Sluder, L., "*The Indicial Lift and Pitching Moment for a Sinking or Pitching Two-Dimensional Wing Flying at Subsonic or Supersonic Speeds*", NACA TN 2403, July 1951.

defined for the rigid vehicle. Notice the row of dots on the section located at Y/(b/2) = 0.71. This allows for the integration of a section c_ℓ at this spanwise station.

Figure 19 provides the basis for using the step function blast approximation. A typical blast wave does not differ significantly from the step function (notice that it approaches the step function very quickly; i.e., before f = 5.0 [k_r =0.42]) and the step function leads to known asymptotic steady-state values. The term $|g|$ is the modulus of the frequency response of a typical neuclear blast gust velocity.

Figure 20 shows the frequency response of a leading edge pressure from a vertical blast. The frequency response curve is obtained by fitting a spline curve through specific hard points (in frequency). The frequency hard points are shown as dots along the abscissa. The transition of this curve between the Doublet Lattice and Piston Theories is simply obtained by leaving a gap in hard point frequencies between the two and allowing the spline to fill this gap. Different curves will result for different gaps. Notice in Figure 20 the two different curves in the gap regions for the real part. Two separate curves are not noticeable for the imaginary part.

The effects of these gaps are seen in subsequent figures. In general, the smaller the gap is, the greater is the discontinuity in the frequency response, and the irregularities in the time history are more extensive.

The frequency response of a leading edge pressure is shown in Figure 21. At low frequency (f < 10 Hz), the original distribution of calculated points did not contain a sufficient number (see dots) to be able to predict the

peaks accurately by interpolation. Subsequently, three new DLM points were added signified by x's on the axis. In the PT region, the same problem is seen in that the interpolated curve is not a good sinusoid. No new points were added however since convergence of the inverse Fourier transformation occurred at f_{max} = 24 Hz and for this blast orientation piston theory is not needed. The effect of the insufficiency of calculated points is seen in later figures.

Figure 22 shows excellent results for a 60° blast. There is a sufficient number of calculated points and the DLM-PT transition has no significant discontinuities.

Results in Figure 23 show the lift time history for various f_{max} values; i.e., f_{max} = 24, 120 and 300 Hz. All curves lie on top of one another which shows the case of f_{max} = 24 Hz was converged. The precursor in the lift before blast interception at the section deserves further investigation. It may be a property of the numerical Fourier transform.

In Figure 24, we see another converged result for f_{max} = 120 for the case of a 60° head on step-blast gust. The transition frequency is at f = 24 Hz as in Figure 22.

Figure 25 presents another convergence study for a vertical blast. The figure shows that f_{max} is an important parameter for the vertical blast in determining the initial pressure rise. This is a general property of Fourier transforms; i.e., the high frequency behavior determines the initial response, and the low frequency behavior determines the approach to the steady-state response. This figure shows that the three-dimensional case

converges faster in f_{max} than does the two-dimensional case. This case has converged at f_{max} = 300 (k_r = 25) whereas the two-dimensional case of Figure 17 converges somewhere between k_r = 25 and 75.

Figures 26 through 31 show plots obtained with the computer printout. Figures 26 through 28 present pressures at three different points on the wing. Figures 29 and 30 give loadings at two fuselage stations, and Figure 31 shows pressures on the horizontal tail. Figure 26 shows pressure time histories for an outboard point forward of the midchord (x/c = 0.406, 2y/b = 0.71) for three blast orientations. The vertical line shows the intercept time for each blast to reach the point. The initial pressure rise can be compared to the Piston Theory value shown and the approach to the steady-state solution is seen at large values of time. The pressures are negative in Figure 26(a) because the blast is from overhead.

Figure 27 shows pressures at the same spanwise station but farther aft (x/c = 0.657, 2y/b = 0.71) for two blast orientations. Reasonable agreement with both Piston Theory and the steady state solution is observed. Figure 27(b) also shows the effect of increasing the number of DLM points in the frequency response plot (Figure 21). The three additional DLM solutions improve the time-history although more improvement is still needed.

Figure 28 shows pressures at the same outboard station but at a point near the trailing edge (x/c = 0.906, 2y/b = 0.71) for an overhead blast. The figure shows the effect of two transitions (gaps) between DLM and Piston Theory. The transition begins at 24 Hz in both cases but a gradual transition (large gap) reduces the irregularities over the abrupt transition (small gap).

Figure 29 shows the running load at the fuselage nose for three blast orientations. Figure 29(a) shows a large effect of gap size. A moderate gap reduces the variations in the time history.

Figure 30 gives the fuselage loading toward the aft end for one blast orientation. A similar effect of gap size is seen again.

Figure 31 shows the pressures at a point of the horizontal tail near the leading edge and tip ($x/c = 0.0625$, $2y/b = 0.888$) for three blast orientations. The curves in Figures 31(a) and (b) are seen to be well behaved. The pressures begin to increase to the steady state values for the isolated tail until the wing downwash reaches the tail at which time the pressures decrease to the steady state wing-tail interference value of approximately one-half the value for the isolated tail. The effect of adding three DLM points is shown in the solid curve in Figure 31(c). The general effect is to smooth the curve but the remaining irregularities are unexplained.

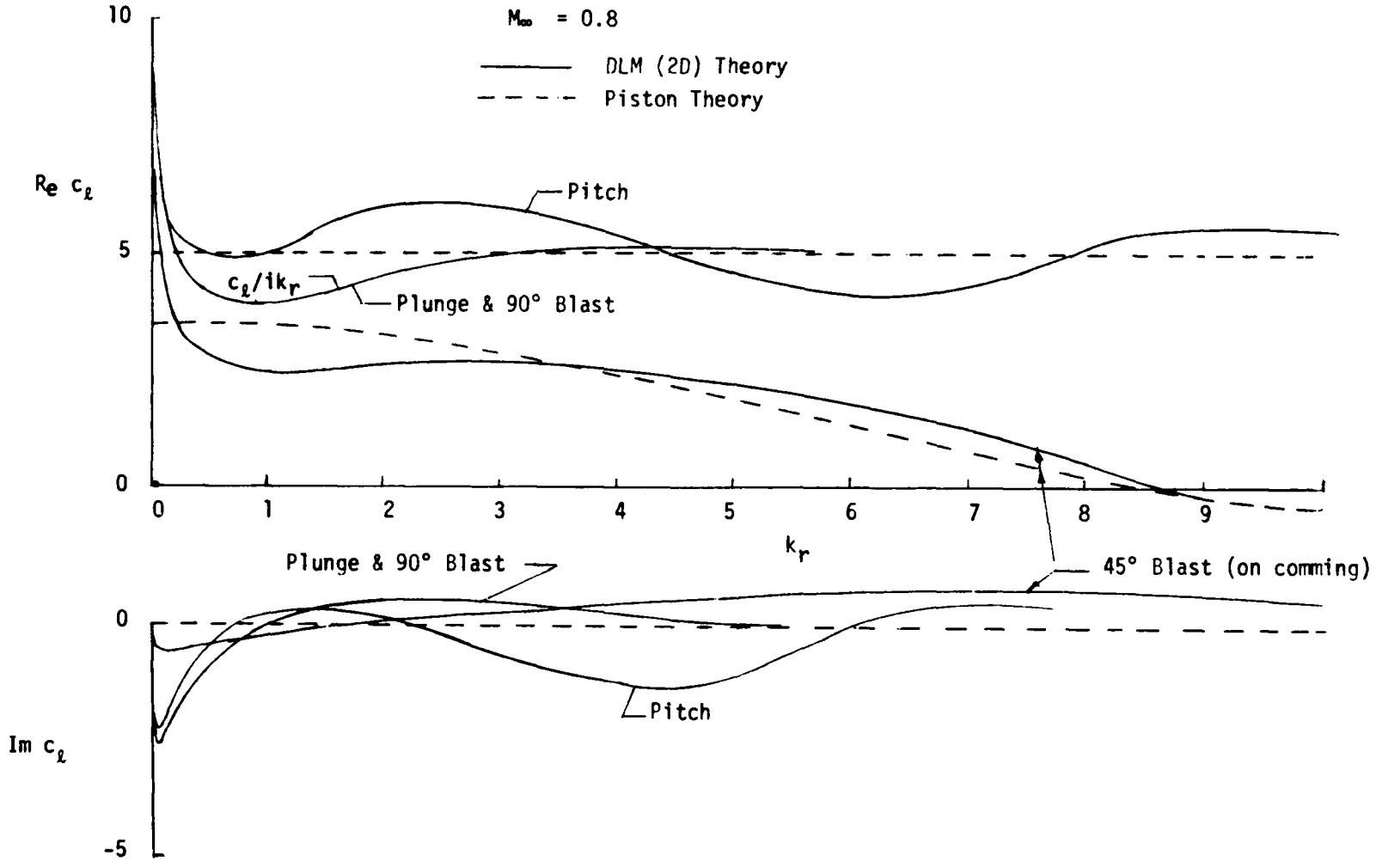

Figure 15. Frequency Response of a Two-Dimensional Airfoil in Pitch and Plunge, and in Two Blast Gust Fields

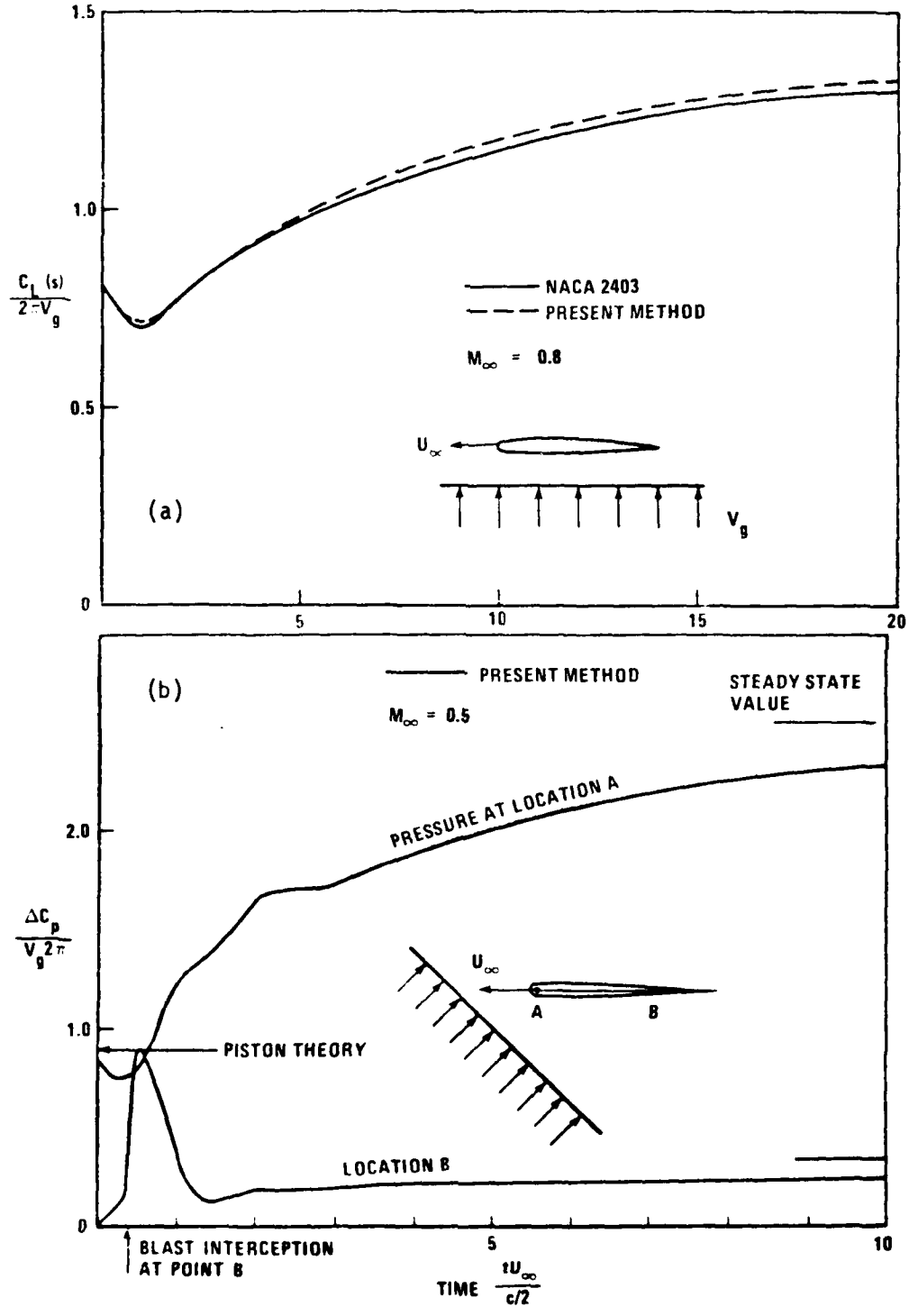

Figure 16. Time Histories of (a) Lift and (b) Pressures, Due to Airfoils Encountering Sharp Edge Gusts. (a) M_∞ = 0.8, α_g = 90 Deg and (b) M_∞ = 0.5, α_g = 45 Deg.

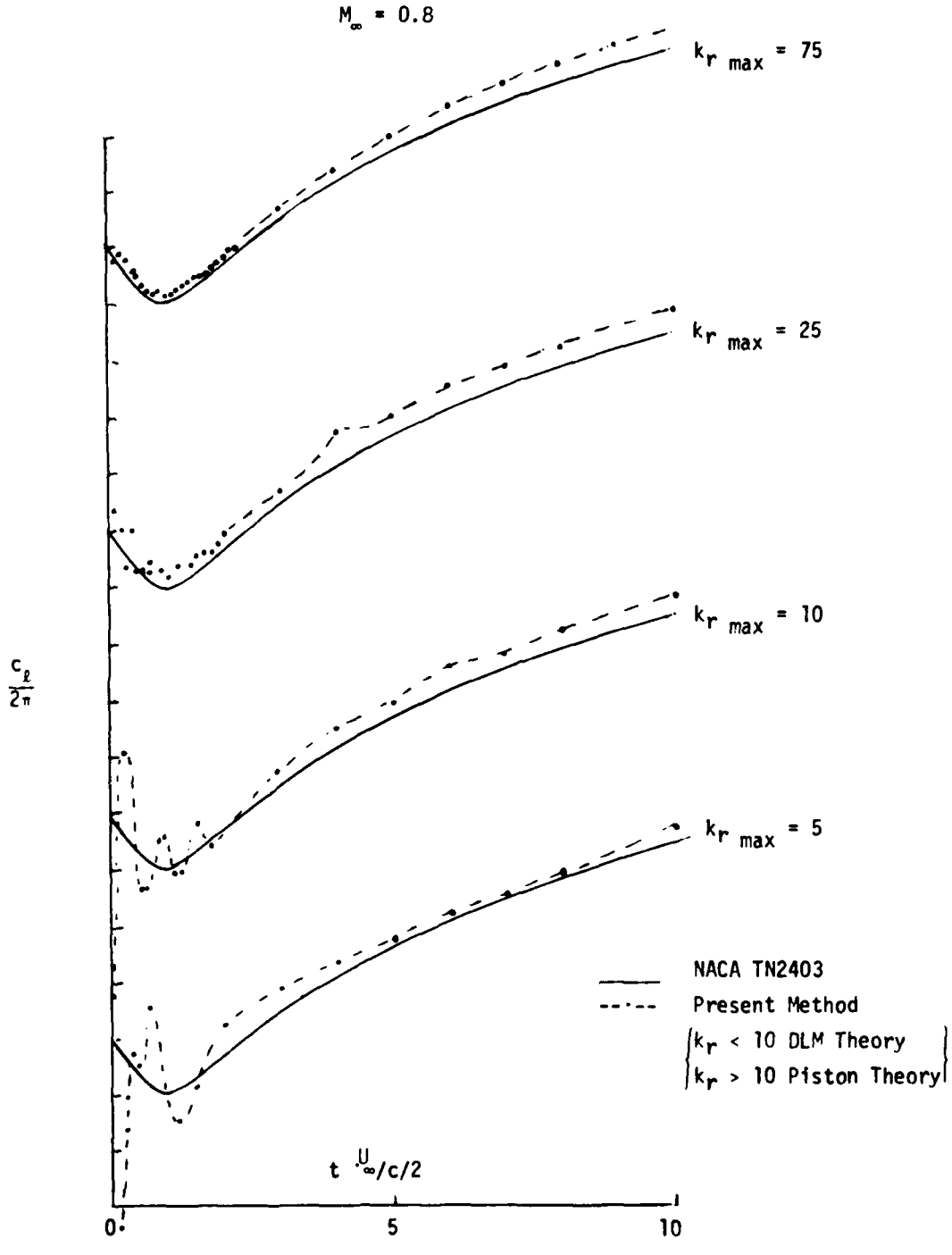

Figure 17. Time History of Lift Due to a Step-Function Blast Gust at 90°.

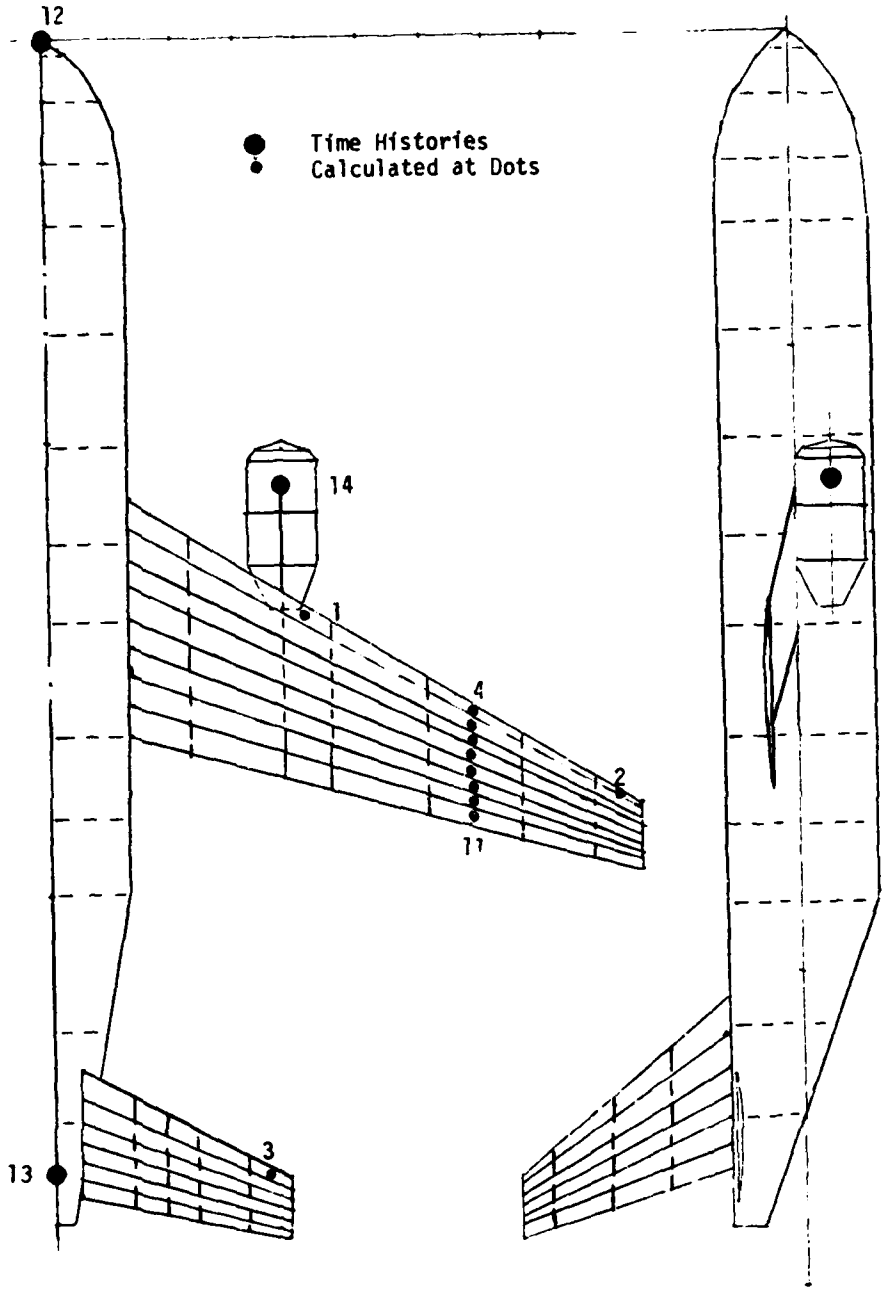

Figure 18. Doublet Lattice Method (DLM) Aerodynamic Idealization. Also Points at Which Time Histories are Given, are Illustrated.

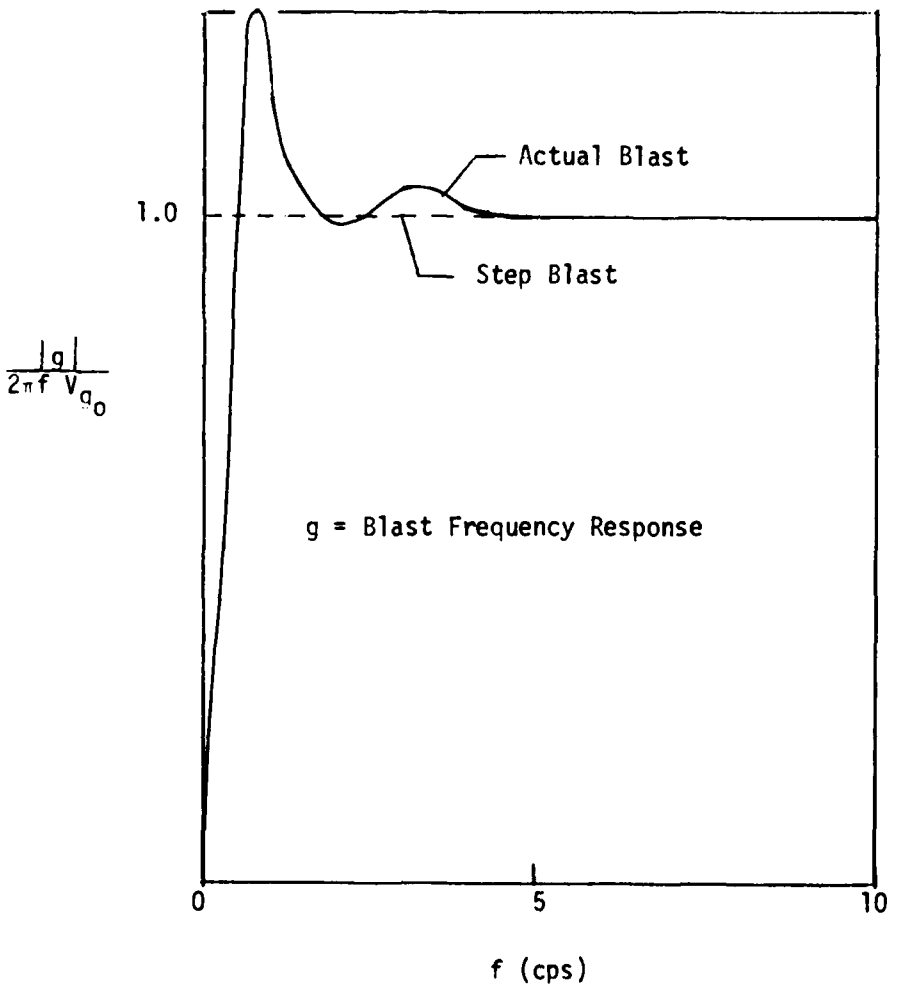

Figure 19. Frequence Response of a Nuclear Blast Gust Velocity Normalized by that Due to a Step-Function.

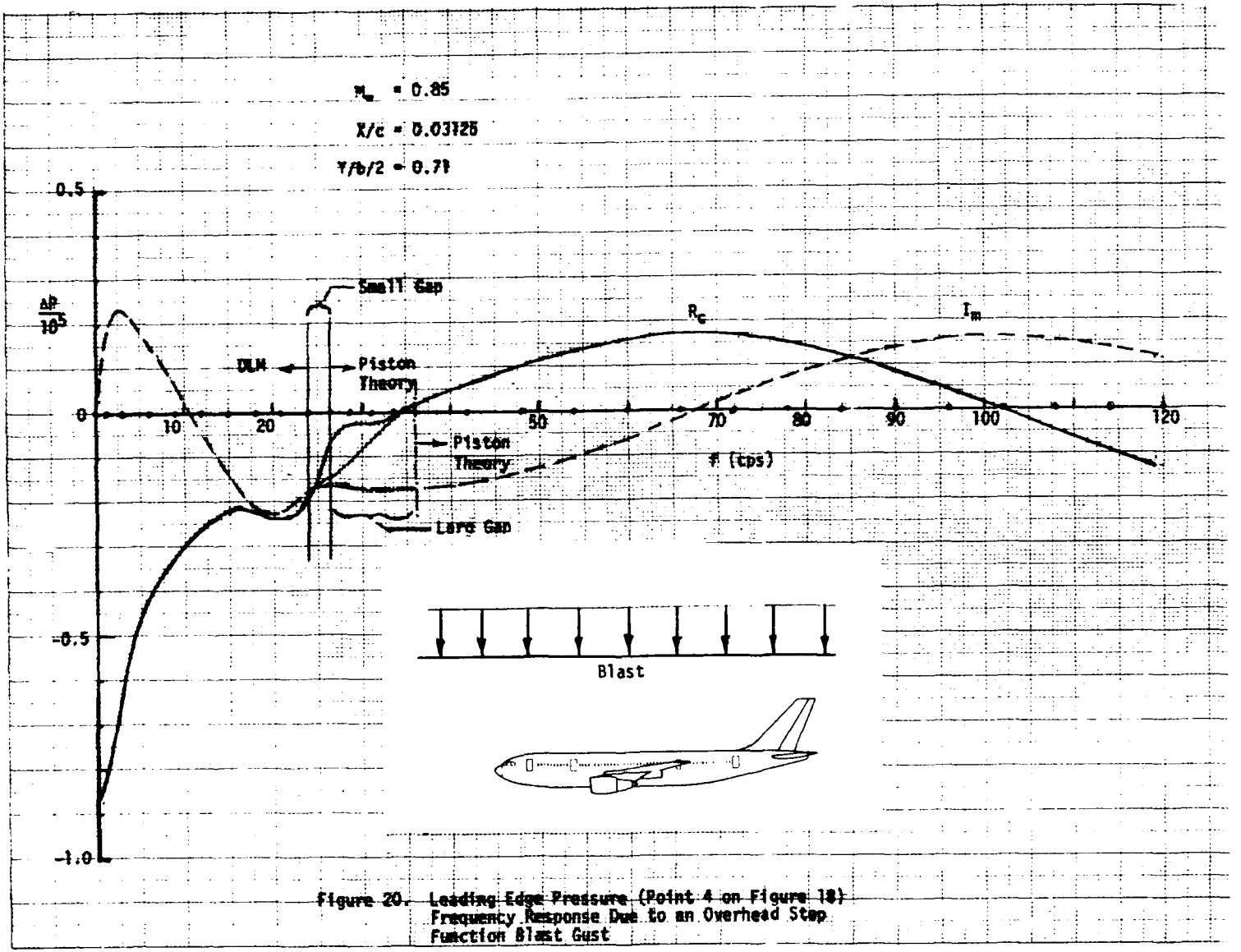

Figure 20. Leading Edge Pressure (Point 4 on Figure 18) Frequency Response Due to an Overhead Step Function Blast Gust

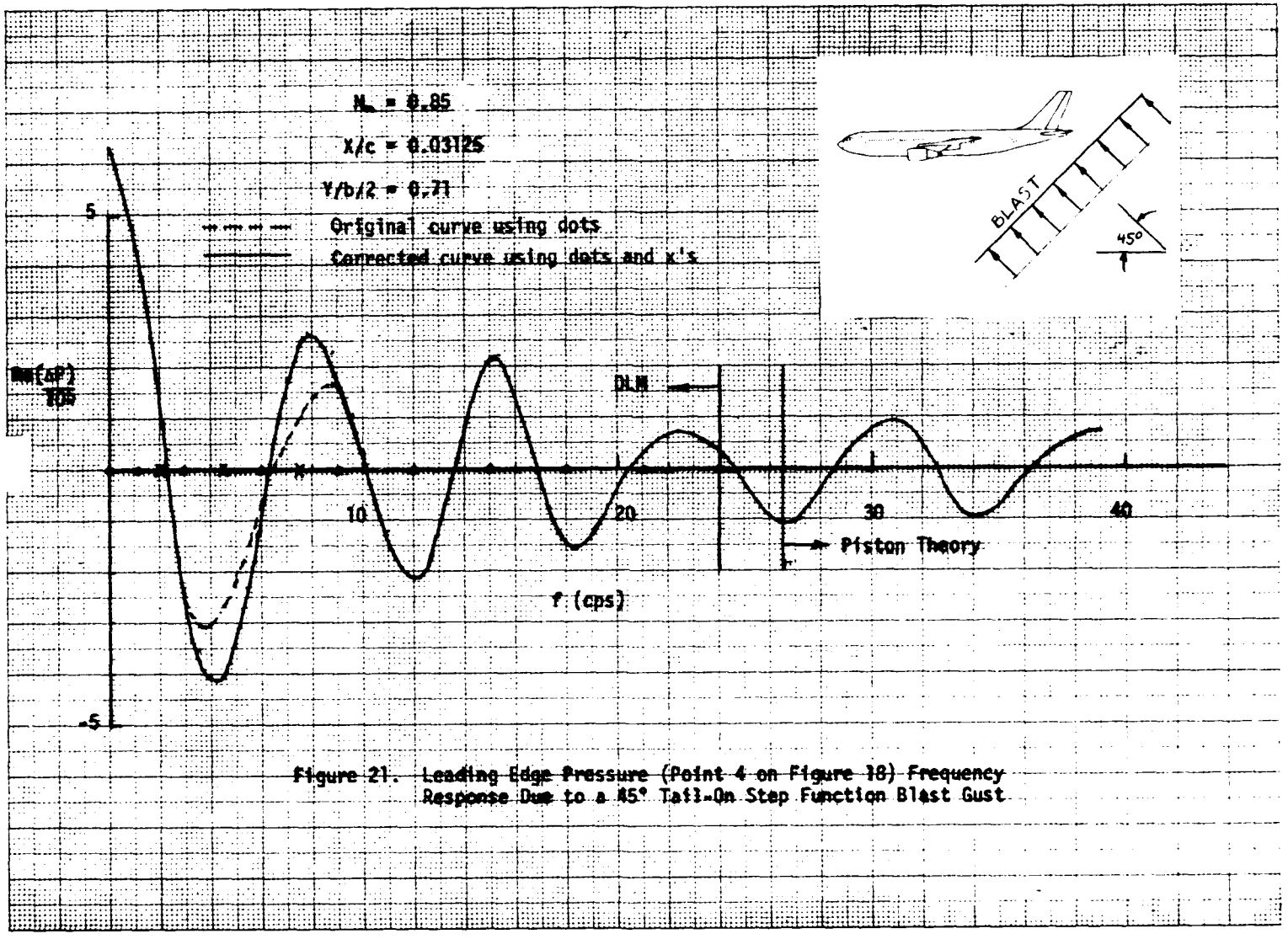

Figure 21. Leading Edge Pressure (Point 4 on Figure 18) Frequency Response Due to a 45° Tail-On Step Function Blast Gust

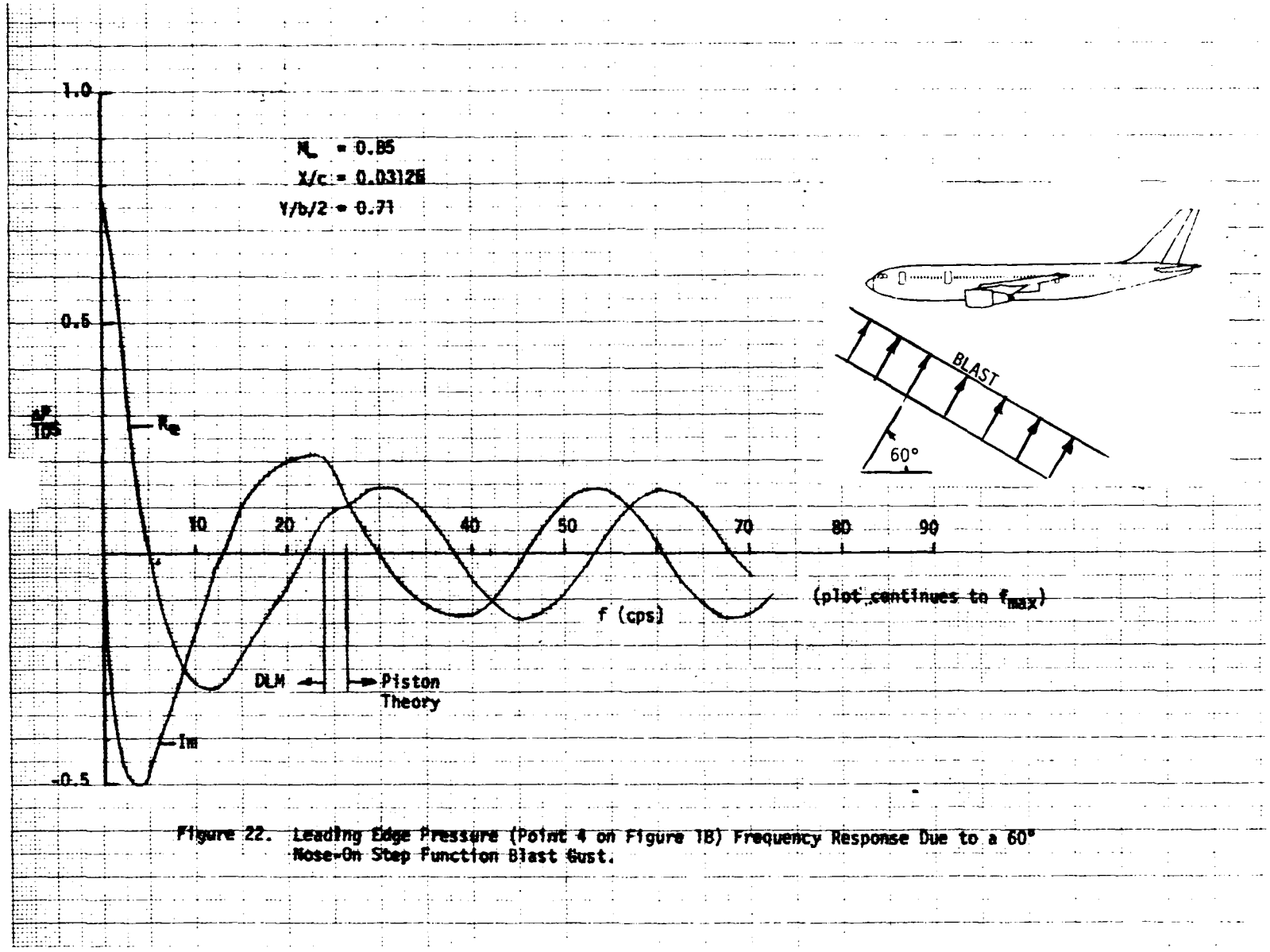

Figure 22. Leading Edge Pressure (Point 4 on Figure 1B) Frequency Response Due to a 60° Nose-On Step Function Blast Gust.

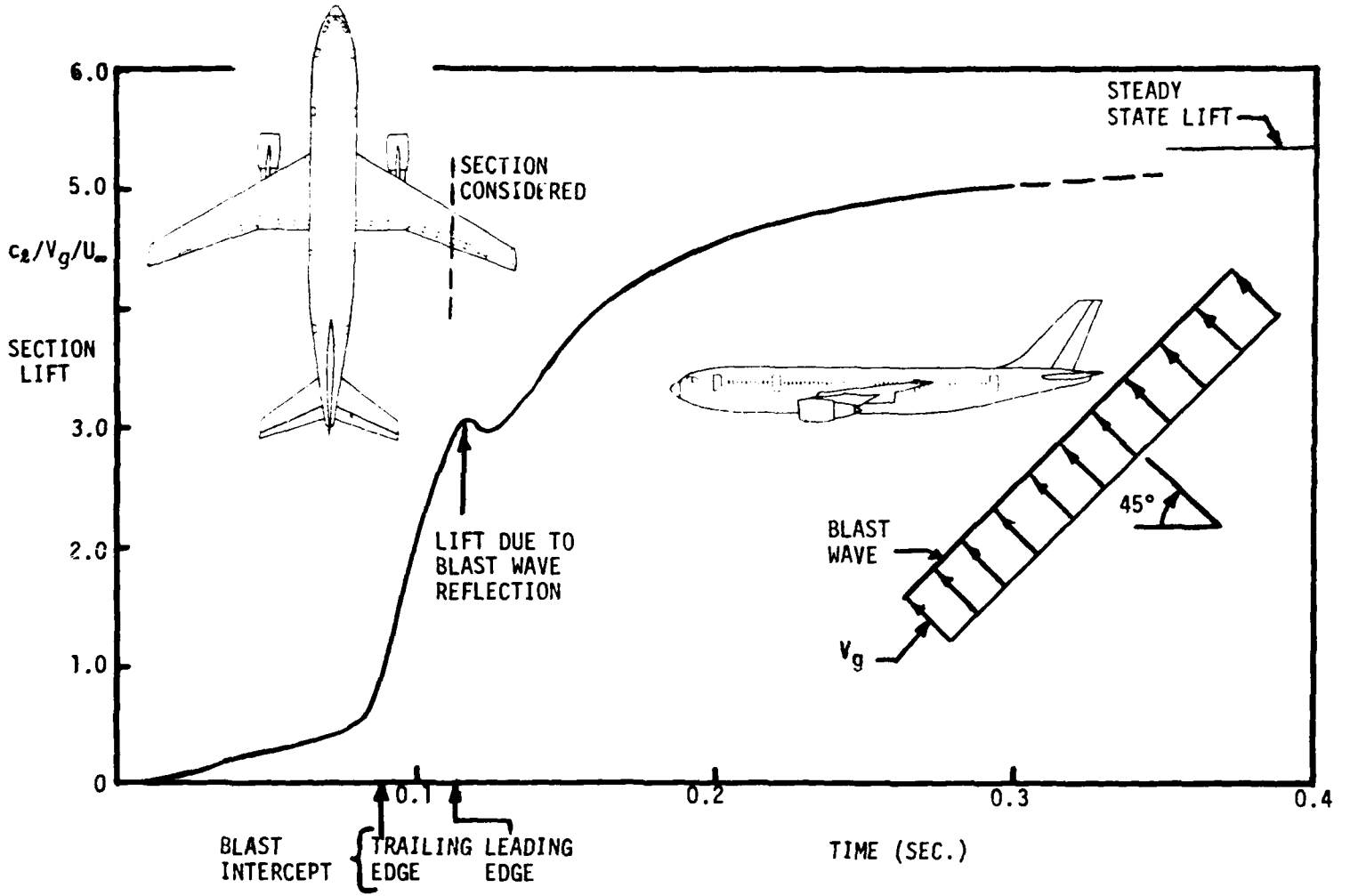

Figure 23. Section Lift Coefficient Time History Due to a 45° Tail-On Step Blast Gust

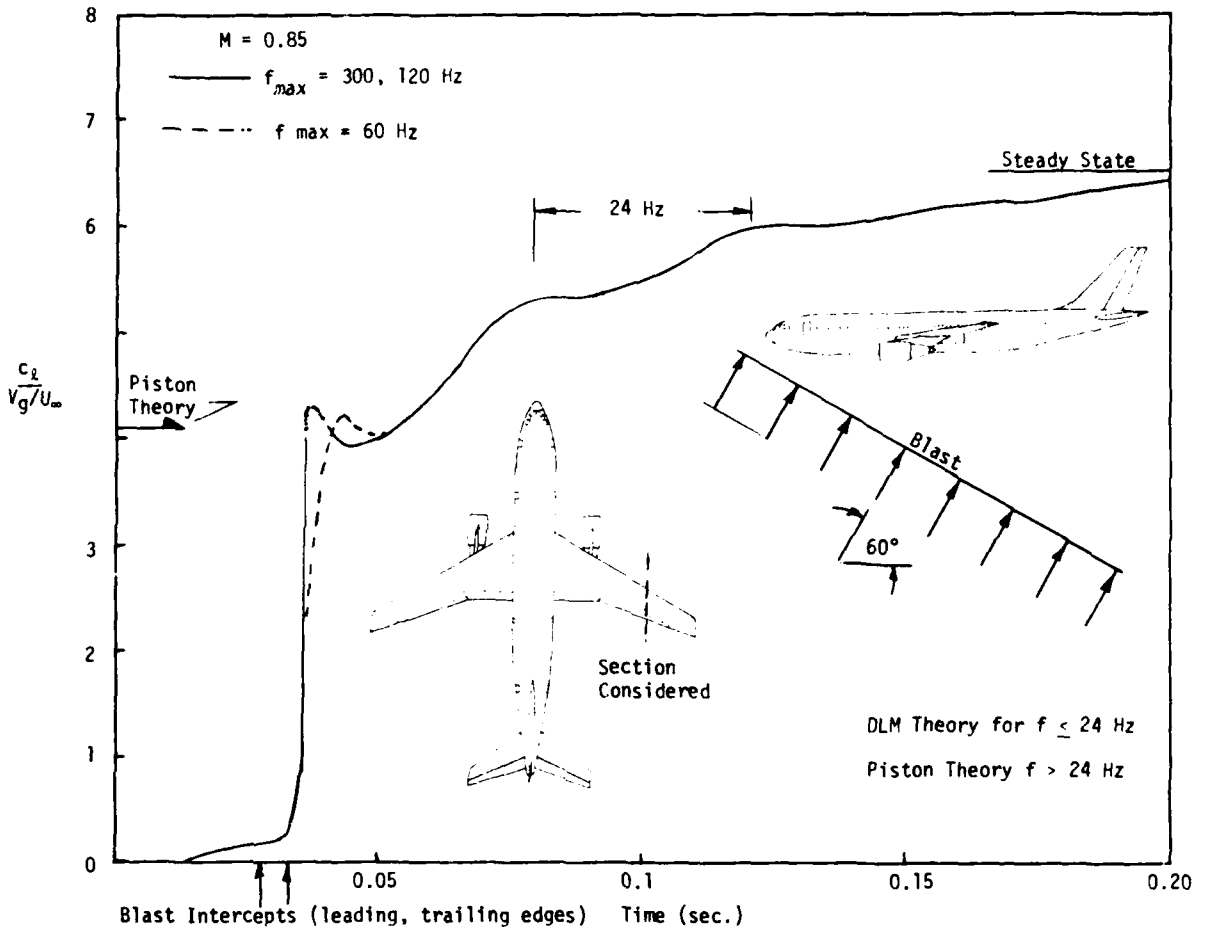

Figure 24. Section Lift Coefficient Time History Due to a 60° Nose-On Step Blast Gust

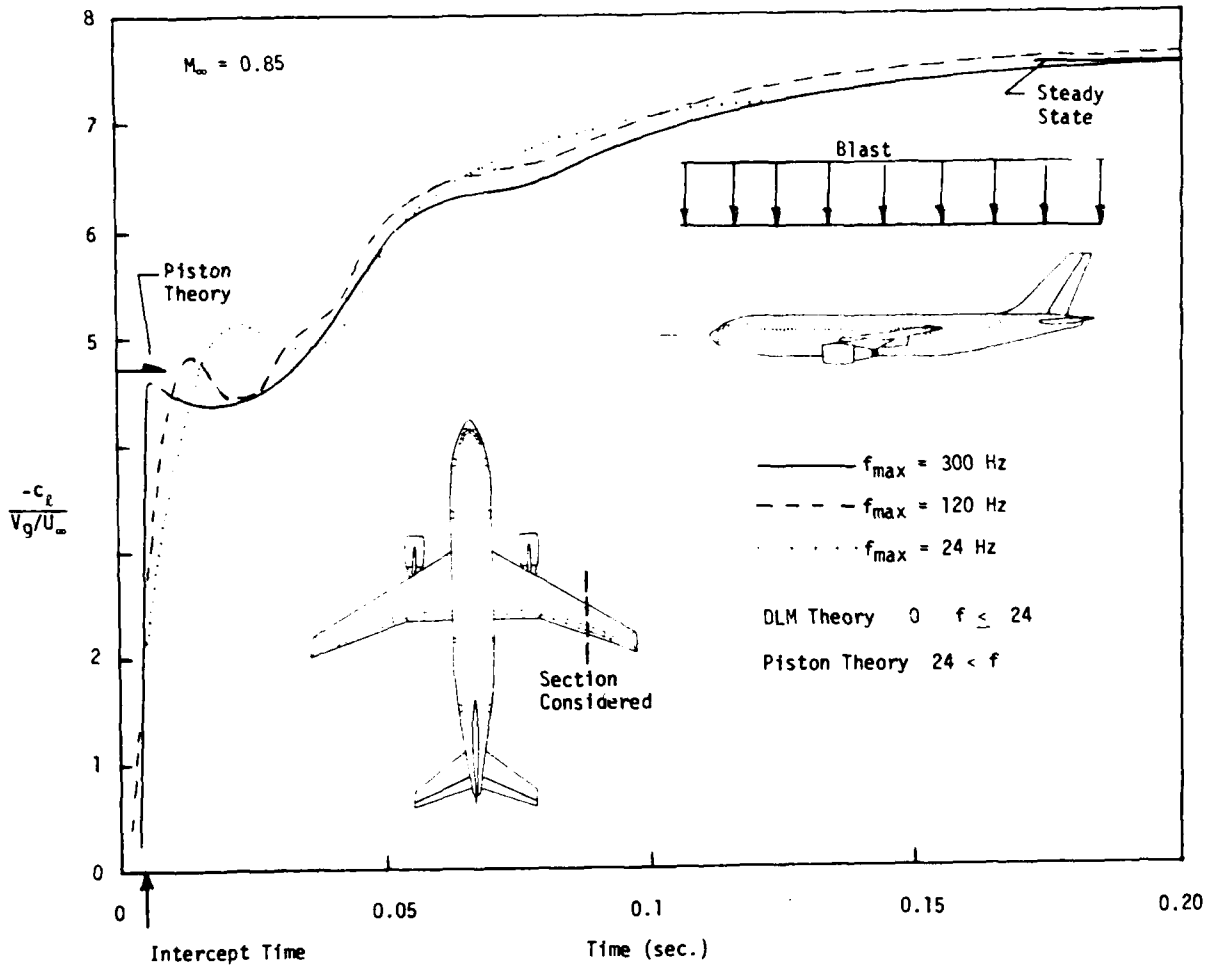

Figure 25. Section Lift Coefficient Time History Due to an Overhead Step Blast Gust

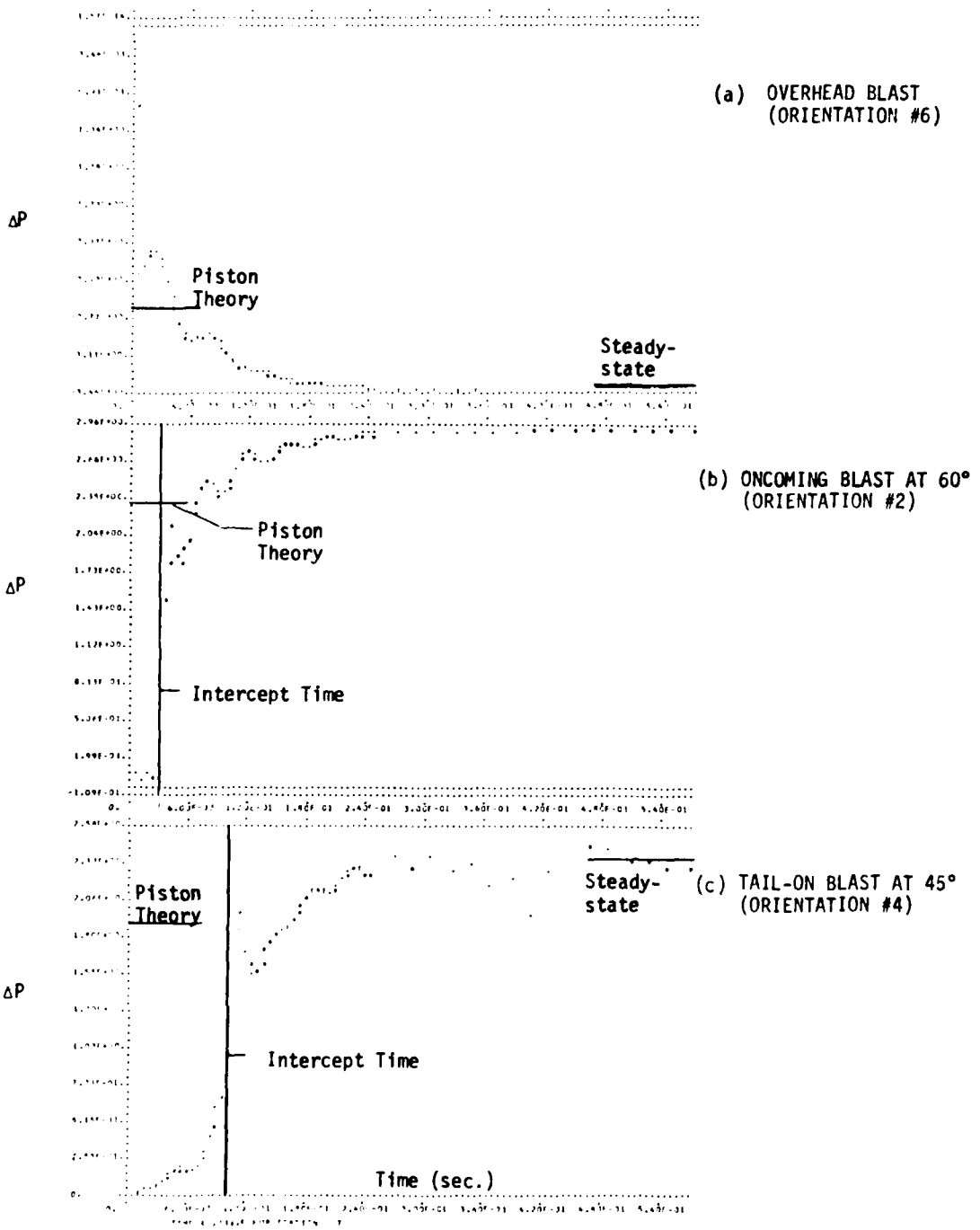

Figure 26. Pressure Time Histories for a Point Located on the Wing at $x/c = 0.406$ and $Y/(b/2) = 0.71$ (Station 7) for Various Blast Orientations. $M_\infty = 0.8$.

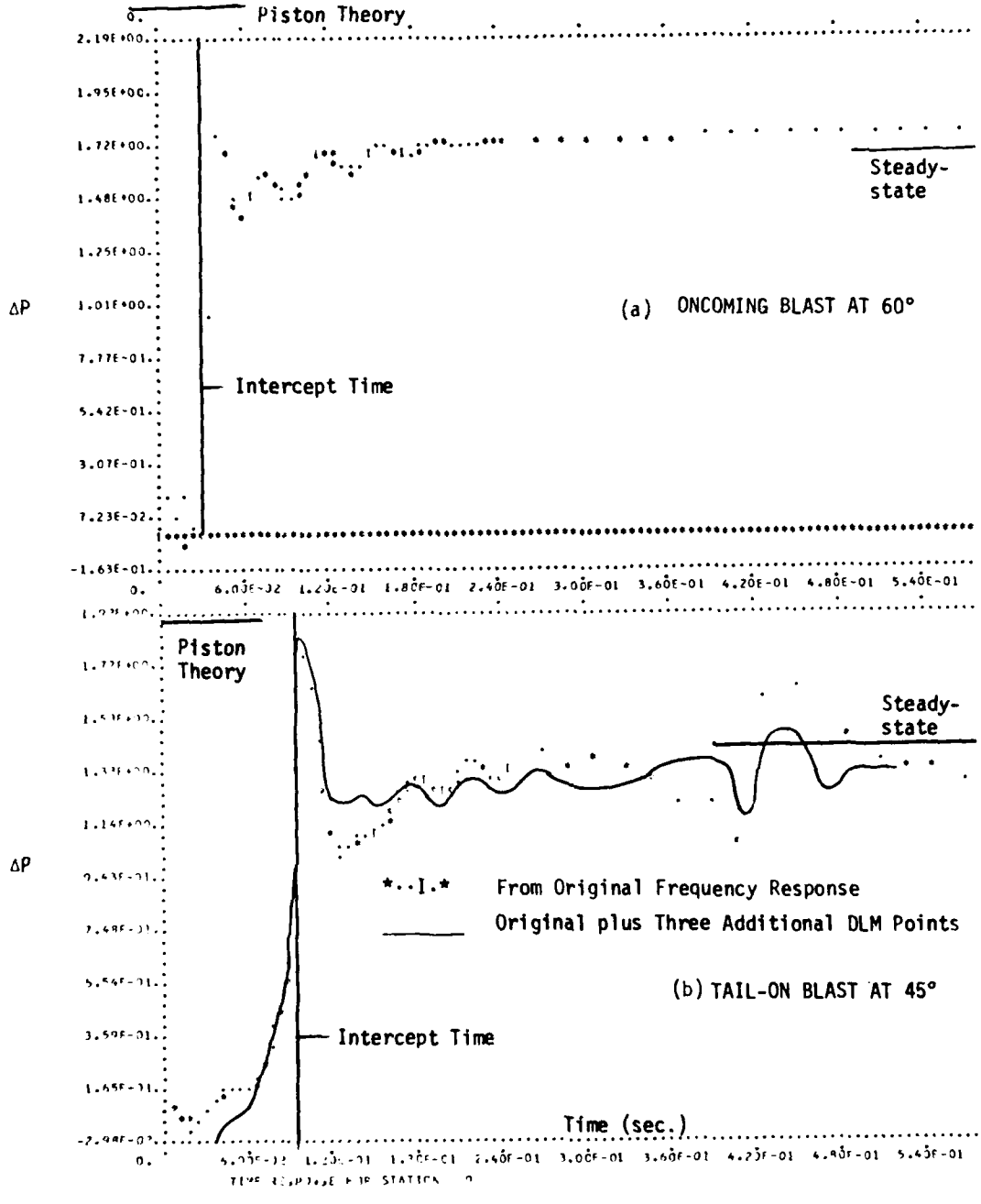

Figure 27. Pressure Time Histories for a Point Located on the Wing at x/c = 0.657 and Y/(b/2) = 0.71 (Station 9) for Various Blast Orientations. M_∞ = 0.8

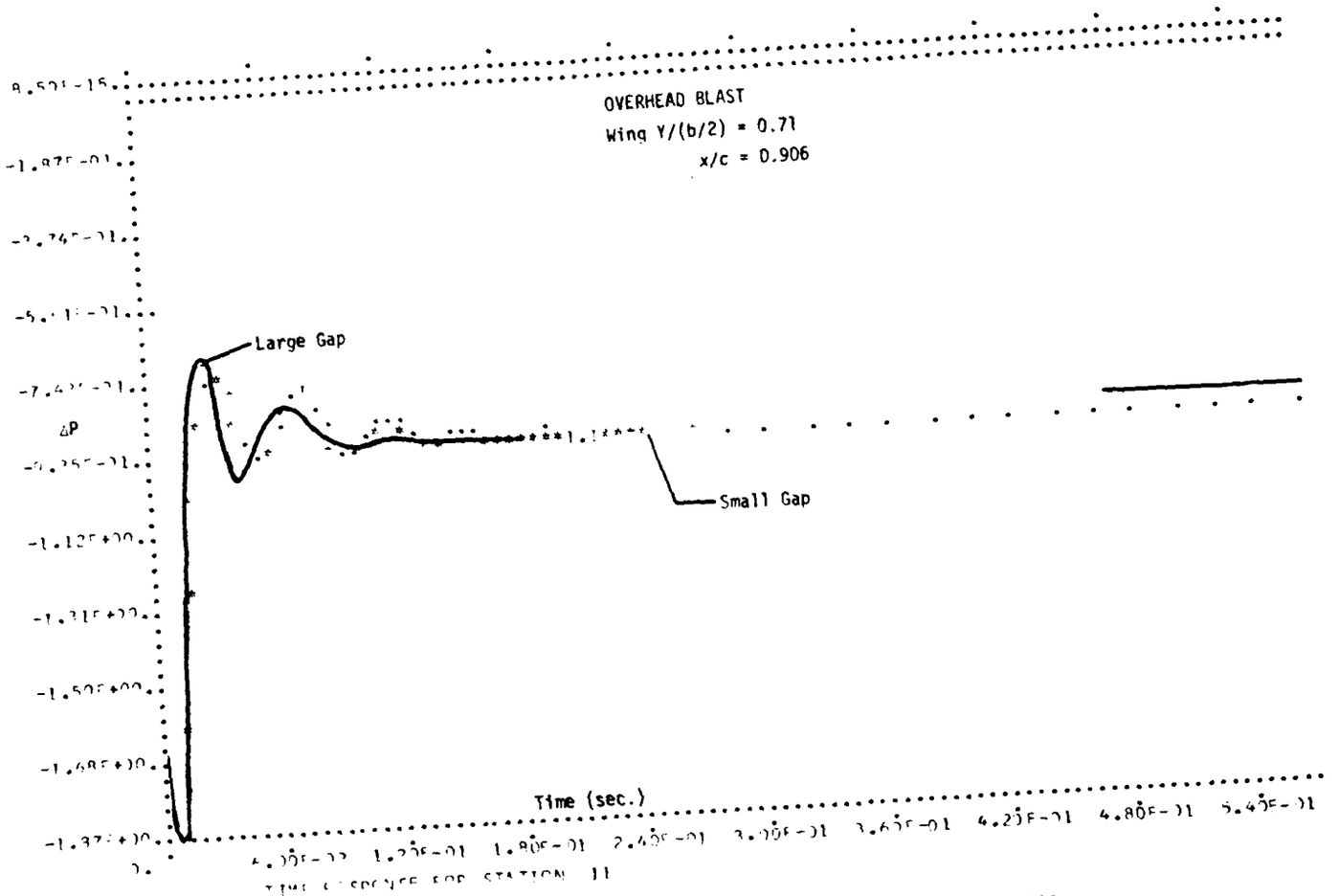

Figure 28. Pressure Time History for a Point Located on the Wing at x/c = 0.906 and Y/(b/2) = 0.71 (Station 11) for an Overhead Blast. M_∞ = 0.8

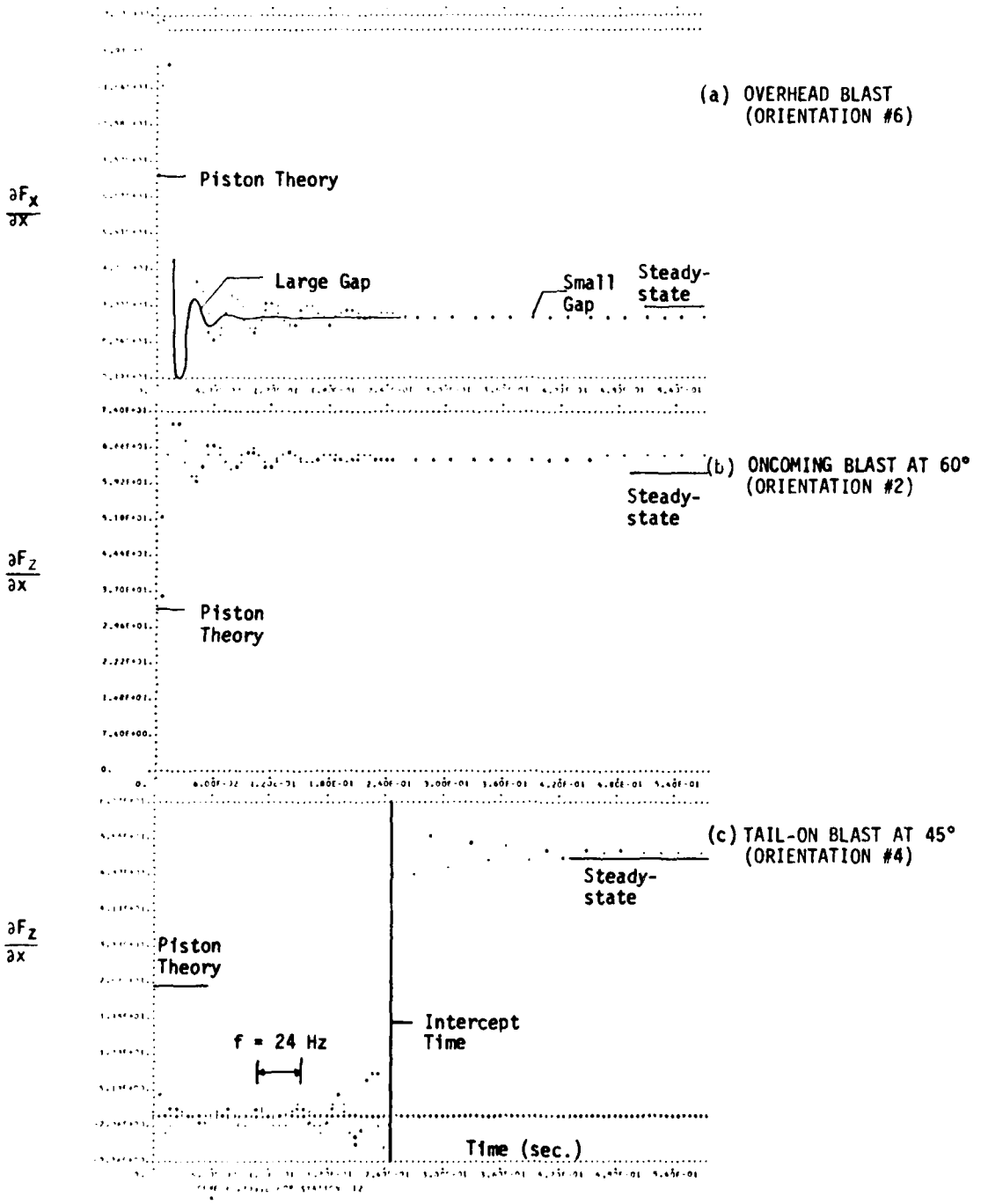

Figure 29. Time History of the Running Load at the Fuselage Nose (Station 12) for Various Blast Orientations. $M_\infty = 0.8$

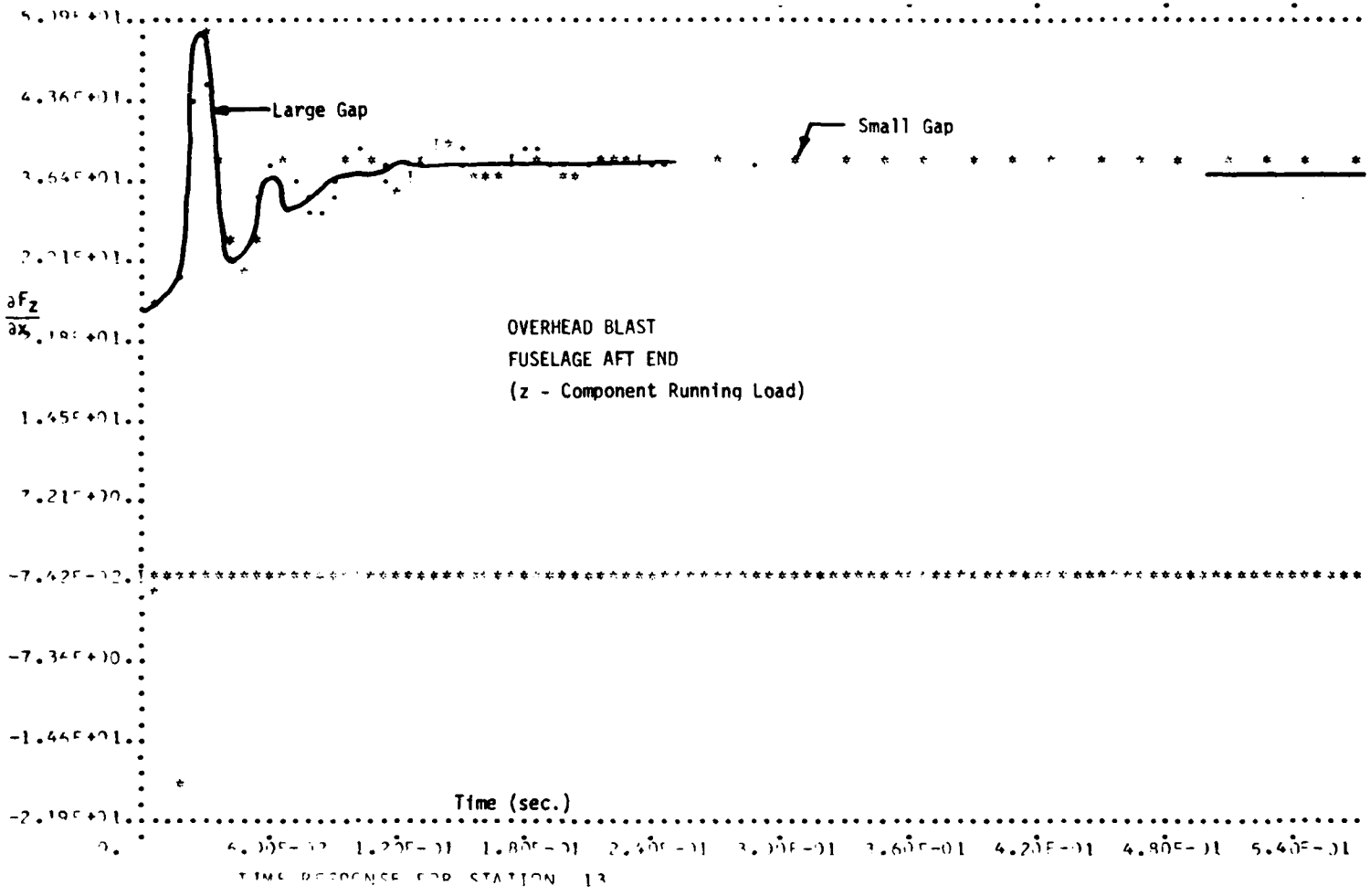

Figure 30. Time History of the Running Load at the Aft End of the Fuselage (Station 13) for an Overhead Blast. $M_\infty = 0.8$

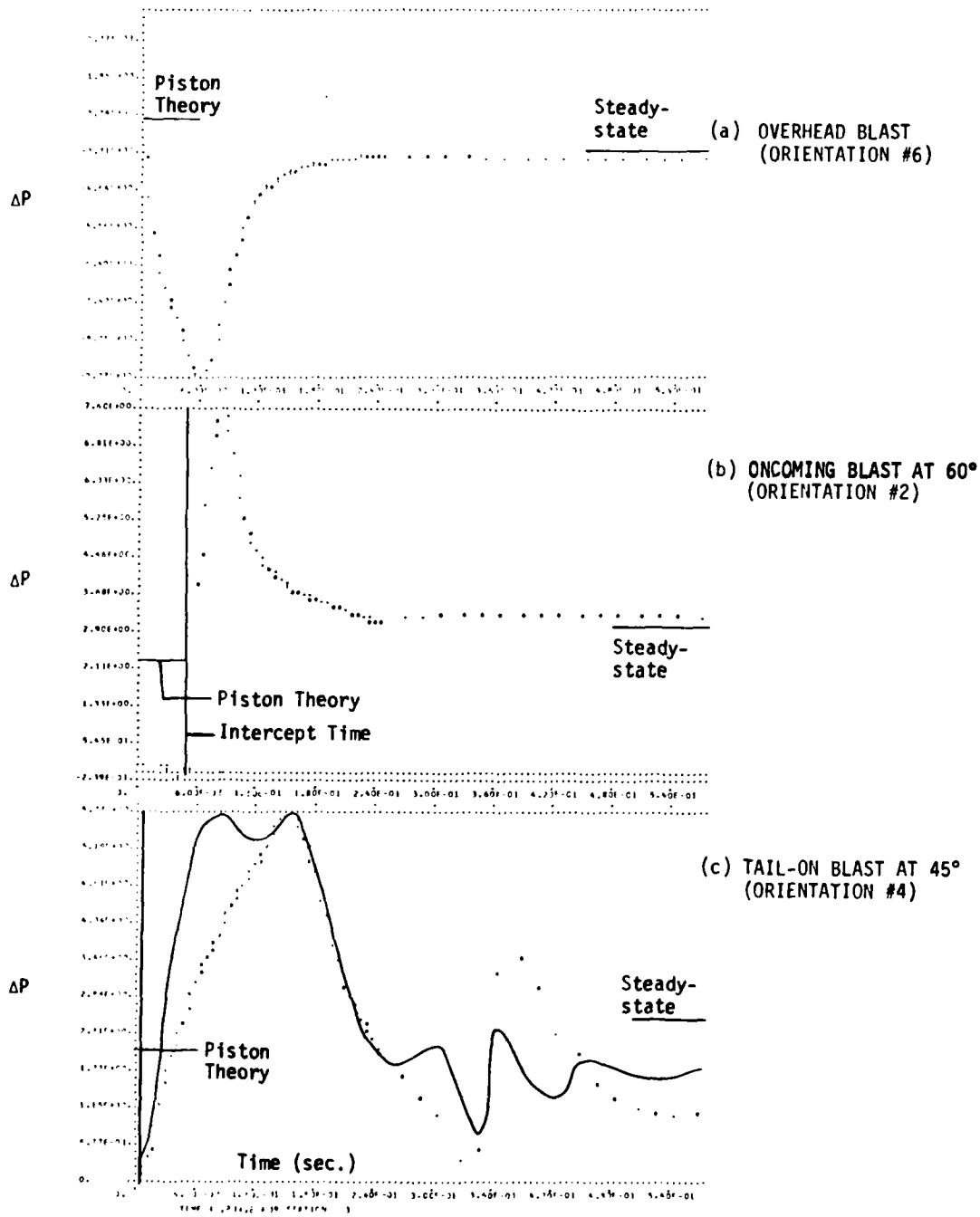

Figure 31. Pressure Time Histories for a Point Located on the Horizontal Tail (Station 3) for Various Blast Orientations. $M_\infty = 0.8$

SECTION V

PROGRAM INPUT

1. DESCRIPTION OF INPUT DATA

The program input consists of the following five groups of data: general data, panel data, body data, modal spline interpolation data, and gust data. The general data, panel data, and modal spline interpolation data must always be input, but the body data and gust data are optional as specified by flags in the general data.

The general data consist of flags for dimensioning and program control, locations of and deflections at the aerodynamic nodal points, and constants. The panel and body data consist of the input necessary to define completely each panel and body. The modal spline interpolation data consist of the data to relate the aerodynamic nodal points to the panel and body data. The gust data allow nonstandard blast orientations to be input for the gust calculations.

A detailed description of the input data is given in Volume I of this report.

2. TEST CASE INPUT DATA

The configuration discussed in Section III (Figure 11) is used as the basis for the test case presented here. In the interest of simplifying the input and saving space for the output this configuration has been reidealized with fewer lifting surface boxes, fewer body elements and the tail surfaces missing. Also fewer nodal points (at which modal deflections are given) are used. Figure 32 presents an illustration of this idealization. Table 2 tabulates the important quantities required for input while Table 3 presents the actual input data.

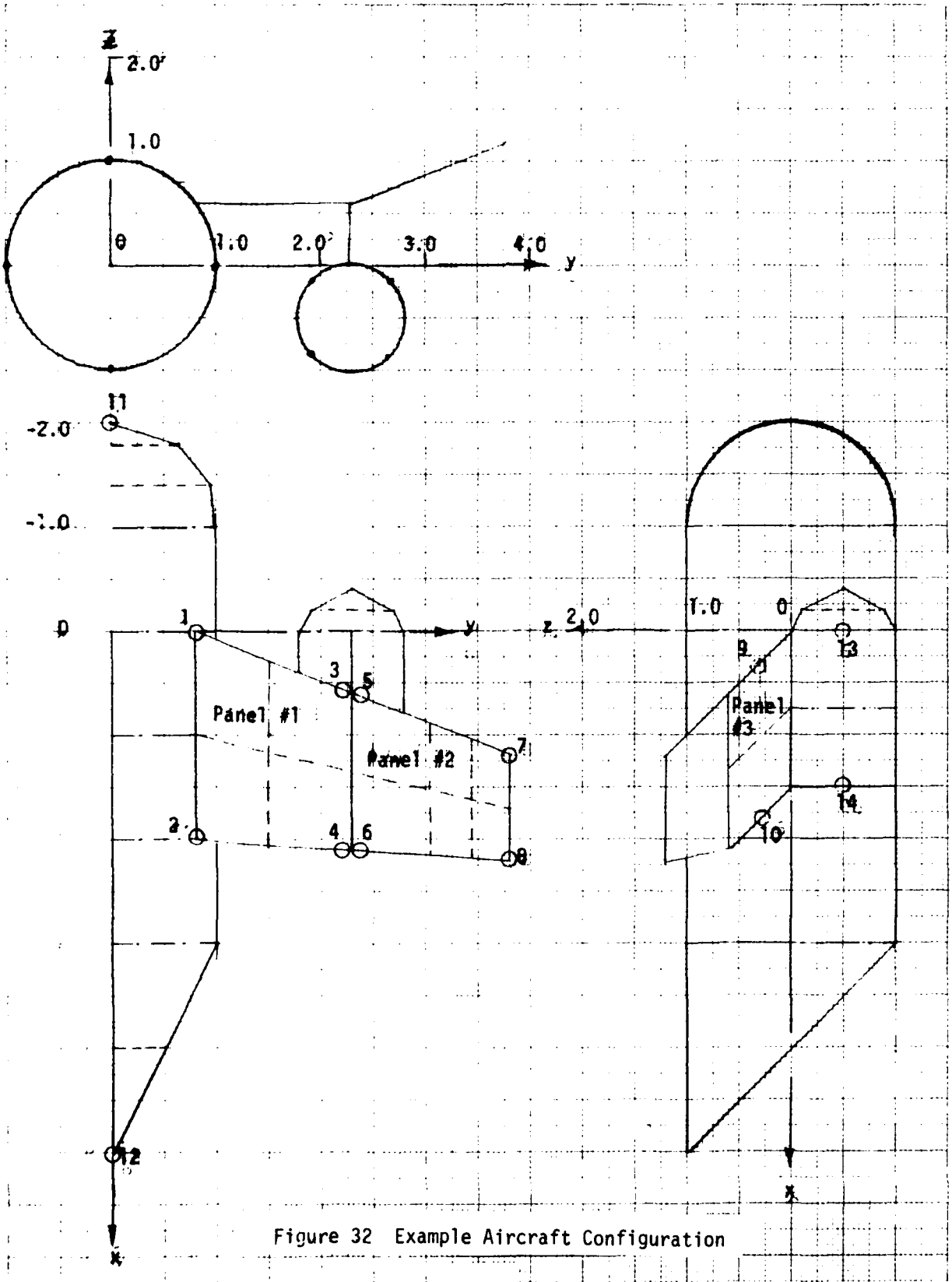

Figure 32 Example Aircraft Configuration

TABLE 2

TEST CASE DATA

General Data

Mach No. = 0.85

Ref. Chord $\bar{c}$ = 2.0

Ref. Area A = 9.0

Reduced Frequency k_r = 0.1

Ref. Semispan S = 3.8

Wing Data

Panel #1

leading edge inboard X1 = 0, Y1 = .8, Z1 = .6*

trailing edge inboard X2 = 2.0

leading edge outboard X3 = .6, Y2 = 2.3, Z2 = .6

trailing edge outboard X4 = 2.1

Chordwise divisions, in fractions of chord, θ = 0, 0.5, 1.0

Spanwise divisions in fractions of span, τ = 0, 0.45, 1.0

Panel #2

X1 = .6, X2 = 2.1, X3 = 1.2, X4 = 2.2

Y1 = 2.3, Y2 = 3.8, Z1 = .6, Z2 = 1.2

θ = 0, 0.5 1.0; τ = 0, 0.5, 0.75, 1.0

Panel #3

X1 = .6, X2 = 2.1, X3 = 0, X4 = 1.5

Y1 = 2.3, Y2 = 2.3, Z1 = .6, Z2 = 0

θ = 0, 0.5 1.0; τ = 0, 1.0

* Specific units not required; however they all must be consistent.

Body Data

Fuselage

fuselage center coordinates $Y_c = 0$, $Z_c = 0$, tube radius a = 1.0

slender body element endpoints XIS and radii RS and interference element endpoints XII and radii RI

XIS	RS	XII	RI
-2	0	-1	1.0
-1.8	.65	0	1.0
-1.4	.95	1	1.0
-1.0	1.0	2	1.0
0	1.0	3	1.0
1.0	1.0		
2.0	1.0		
3.0	1.0		
4.0	0.5		
5.0	0		

Angular flow field points $\theta 1 = 0^0, 90^0, 180^0, 270^0$

Aspect ratio of cross-section = 1.0

Nacelle $Y_c = 2.3$, $Z_c = -.5$, a = 0.5

XIS	RS	XII	RI
-.4	0	0	.5
-.2	.4	.75	.5
0	.5	1.5	.5
.75	.5		
1.5	.5		

$\theta 1 = 45^0, 135^0, 225^0, 315^0$

Aspect ratio of cross-section = 1.0

Mode Description

Aerodynamic Nodal Points

The x y z coordinates of the aerodynamic nodal points are

NO.	ELXIA	ELYIA	ELZIA
1	0	.8	.6
2	2.0	.8	.6
3	0.6	2.3	0.6
4	2.1	2.3	0.6
5	0.6	2.3	0.6
6	2.1	2.3	0.6
7	1.2	3.8	1.2
8	2.2	3.8	1.2
9	0.3	2.3	0.3
10	1.8	2.3	0.3
11	-2.0	0.0	0.0
12	5.0	0.0	0.0
13	0.0	2.3	-0.5
14	1.5	2.3	-0.5

Modal Deflections

Mode 1, Symmetric Nose Up Aircraft Pitch

ϕ_n (1, 2, 3, 4, 5, 6, 7, 8) = -x cos $\bar{\gamma}$, ϕ_n (9, 10) = 0.0

ϕ_z (11, 12, 13, 14) = -x

ϕ_y = 0.0

Mode 2, Symmetric Nose Left Nacelle-Pylon Yaw

ϕ_n (9, 10) = x

ϕ_z = 0.0

ϕ_y (13, 14) = x

Mode 3, Antisymmetric Nose Left Aircraft Yaw

ϕ_n (1, 2, 3, 4, 5, 6, 7, 8) = -x sin $\bar{\gamma}$, ϕ_n (9, 10) = x

ϕ_z = 0.0

ϕ_y (11, 12, 13, 14) = x

TABLE 3

TEST CASE INPUT DATA

GROUP NO. 1 General Data

ITEM NO. 1 Data Designator Card

AERO

ITEM NOS. 2-4 Dimensioning Data

14	2	1	1	3
3	6	3	2	12
2	13	6		

ITEM NO. 5 Aerodynamic nodal point coordinates x,y,z

0.0	0.8	0.6
2.0	0.8	0.6
0.6	2.3	0.6
2.1	2.3	0.6
0.6	2.3	0.6
2.1	2.3	0.6
1.2	3.8	1.2
2.2	3.8	1.2
0.3	2.3	0.3
1.8	2.3	0.3
-2.0	0.0	0.0
5.0	0.0	0.0
0.0	2.3	-0.5
1.5	2.3	-0.5

ITEM NO. 6 Modal Deflection data PHINA, PHIZA, PHIYA

Mode 1

0.0		
-2.0		
-0.6		
-2.1		
-0.5571		
-1.950		
-1.114		
-2.043		
0.0		
0.0		
	2.0	0.0
	-5.0	0.0
	0.0	0.0
	-1.5	0.0

Mode 2

0.0		
0.0		
0.0		
0.0		

```
 0.0
 0.0
 0.0
 0.0
 0.3
 1.8
              0.0          0.0
              0.0          0.0
              0.0          0.0
              0.0          1.5

                        Mode 3
 0.0
 0.0
 0.0
 0.0
-0.2228
-0.7799
-0.4456
-0.8170
 0.3
 1.8
              0.0         -2.0
              0.0          5.0
              0.0          0.0
              0.0          1.5

ITEM NOS. 7-8  Control Flags
            0            0            0            0
            1            0            0            0

ITEM NO. 9  Case Data, Mach number, A,S,C,XM,SCALER
 0.85        9.0          3.8          2.0          0.0          2.0

ITEM NO. 10  Reduced Frequencies
 0.1

GROUP NO. 2              Panel Data

ITEM NOS. 1-5  X1...Z2, NC, NS, IGRUP, Theta, Tau

                        Panel 1
 0.0          2.0          0.6          2.1
 0.8          2.3          0.6          0.6
            2            2            1
 0.0          0.5          1.0
 0.0          0.45         1.0

                        Panel 2
  .6          2.1          1.2          2.2
  .           3.8          0.6          1.2
            2            3            2
              0.5          1.0
              0.5          0.75         1.0
```

Panel 3

0.6	2.1	0.0	1.5
2.3	2.3	0.6	0.0

2	1	3

0.0	0.5	1.0
0.0	1.0	

GROUP NO. 3 Body Data

ITEM NOS. 1-7 ZC, YC, AR, NBE...NT1, XII, RI, TH1, XIS, RS

Body 1

0.0	0.0	1.0	1.0		
4		9	0	1	4
-1.0	0.0	1.0	2.0	3.0	
0.0	90.0	180.0	270.0		
-2.0	-1.8	-1.4	-1.0	0.0	1.0
2.0	3.0	4.0	5.0		
0.0	0.65	0.95	1.0	1.0	1.0
1.0	1.0	0.5	0.0		

Body 2

-0.5	2.3	0.5	1.0		
2		4	0	1	4
0.0	0.75	1.5			
45.0	135.0	225.0	315.0		
-0.4	-0.2	0.0	0.75	1.5	
0.0	0.4	0.5	0.5	0.5	

GROUP NO. 4 Modal Spline Interpolation Data

ITEM NO. 1 Control Data

2	3	25	1

ITEM NO. 2-4 Control data, bodies, nodes

Superbody 1

1	2	1	0	0
1				
11	12			

Superbody 2

1	2	1	0	0
2				
13	14			

ITEM NO. 2-4 Control data, panels, nodes

Superpanel 1

0	4	1	0
1			
1	2	3	4

Superpanel 2

0	4	1	0
2			
5	6	7	8

Superpanel 3

0	2	1	0
3			
9	10		

SECTION VI

MONITORING AND USE OF OUTPUT DATA

1. AERODYNAMIC DATA MONITOR AND TEST CASE OUTPUT

For any two pre-selected modes, e.g., symmetric pitch and antisymmetric yaw, a detailed set of aerodynamic parameters are printed so that the output aerodynamics can be properly monitored. The parameters and geometric data printed are outlined as follows:

(1) Lifting pressures plus the locations of pressure points. (XOC = x/c. Full pressures and forces are printed for the vertical fin and fuselage and not half values.)

(2) Spanwise distribution of load, lift coefficient, moment coefficient (1/4 chord), and center of pressure, versus spanwise location.

(3) Vertical and lateral running loads on bodies (force per unit length) are output versus longitudinal location on all bodies. Output given at slender body element center locations.

(4) Total force and moment coefficients for the entire aircraft and for lifting surfaces only.

Printed output for the test case described in Section V is given in Table 4. Mode 1 (rigid body pitch of wing surface (not nacelle) and mode 3 (rigid body yaw of pylon and nacelle) are monitored.

The following definitions are used in the calculation of the coefficients described above:

$$c_n = \frac{1}{c} \sum_j \Delta C_{p_j} \Delta X_j \tag{113}$$

$$Cm_{1/4} = -\frac{1}{c^2} \sum_j \Delta C_{p_j} (X_j - X_{1/4}) \Delta X_j \tag{114}$$

$$\text{Real C.P.} = \text{Re } Cm_{1/4}/\text{Re}C_{\ell} + X_{1/4}/c \tag{115}$$

$$\text{Imag. C.P.} = \text{Im } Cm_{1/4}/\text{Im}C_{\ell} + X_{1/4}/c \tag{116}$$

In the equations to follow the following constants are used:

A = reference total area

$\bar{c}$ = reference chord

c = local chord length

XM = moment axis longitudinal location

$2e$ = spanwise strip width

NB = number of bodies

NSTRIP = number of spanwise strips

$\xi 14$ = 1/4 chord point of a box

δ = symmetry flag = $\begin{cases} 1 \text{ symmetry} \\ -1 \text{ antisymmetry} \end{cases}$

$\left.\begin{matrix} y_j \\ z_y \end{matrix}\right\}$ = y- and z-coordinates of the centerline of strip 'j'

$\left.\begin{matrix} y_c^{(b)} \\ z_c^{(b)} \end{matrix}\right\}$ = y- and z-coordinates of the centerline of slender body 'b'

$$G_j = \begin{cases} 1/2 \text{ if } y_j = 0 \text{ and } \cos\gamma_j = 0 \text{ and } \delta \neq 0 \\ 1 \text{ otherwise} \end{cases}$$

and

$$g^{(b)} = \begin{cases} 1/2 \text{ if } y_c^{(b)} = 0 \\ 1 \text{ otherwise} \end{cases}$$

The total lift and moment coefficients, including body effect are defined as follows:

$$C_Z = (1 + \delta)\left\{\frac{1}{A}\sum_{j=1}^{NSTRIP} G_j 2e_j c_j c_{n_j} \cos\gamma_j + \sum_{b=1}^{NB} g^{(b)} C_Z^{(b)}\right\} \tag{117}$$

$$C_Y = (1 - \delta)\left\{\frac{1}{A}\sum_{j=1}^{NSTRIP} -G_j 2e_j c_j c_{n_j} \sin\gamma_j + \sum_{b=1}^{NB} g^{(b)} C_Y^{(b)}\right\} \tag{118}$$

$$C_M = (1 + \delta)\left\{\frac{1}{A\bar{c}}\sum_{j=1}^{NSTRIP} G_j\left[c^2 c_{m_j} - cc_{n_j}(\xi 14_j - XM)\right]2e_j \cos\gamma_j + \sum_{b=1}^{NB} g^{(b)}[C_M^{(b)} - C_Z^{(b)}(x_{LE}^{(b)} - XM)/\bar{c}]\right\} \tag{119}$$

$$C_N = (1 - \delta)\left\{\frac{1}{A\bar{c}}\sum_{j=1}^{NSTRIP} -G_j[c^2 c_{m_j} - cc_{n_j}(\xi 14_j - XM)]2e_j \sin\gamma_j + \sum_{b=1}^{NB} g^{(b)}[C_N^{(b)} - C_Y^{(b)}(x_{LE}^{(b)} - XM)/\bar{c}]\right\} \tag{120}$$

and

$$C_\ell = (1 - \delta)\frac{1}{2s}\left\{\frac{1}{A}\sum_{j=1}^{NSTRIP} G_j cc_{n_j}(y_j \cos\gamma_j + z_j \sin\gamma_j)2e_j + \sum_{b=1}^{NB} g^{(b)} C_Z^{(b)} y_c^{(b)} + \sum_{b=1}^{NB} g^{(b)} C_Y^{(b)} z_c^{(b)}\right\} \tag{121}$$

TABLE 4

TEST CASE OUTPUT LISTING

DATE
TIME

FIXED DATA DECK INPUT OD

INSTR 3

THE 4 ILLUSTRATIVE ANALYSIS CODES HAVE BEEN CALLED FOR IN THIS RUN

AEMI

DATE
TIME

NODE	FLX1(I)	FLY1(I)	FLZ1(I)
1	0.	.000000E+00	.000000E+00
2	.200000E+01	.000000E+00	.000000E+00
3	.400000E+00	.250000E+01	.000000E+00
4	.210000E+01	.250000E+01	.000000E+00
5	.600000E+00	.250000E+01	.000000E+00
6	.210000E+01	.250000E+01	.000000E+00
7	.120000E+01	.240000E+01	.120000E+01
8	.230000E+01	.240000E+01	.120000E+01
9	.100000E+00	.250000E+01	.100000E+00
10	.210000E+01	.250000E+01	.100000E+00
11	.600000E+00	0.	0.
12	.210000E+01	0.	0.
13	0.	-.250000E+01	-.500000E+00
14	.190000E+01	-.250000E+01	-.500000E+00

TABLE 4 CONTINUED

DATE
TIME

NODE	PHIN(I, 1)	PHIZ(I, 1)	PHIV(I, 1)
1	0.	0.	0.
2	.200000E+01	0.	0.
3	.400000E+00	0.	0.
4	.210000E+01	0.	0.
5	.563160E+00	0.	0.
6	.105000E+01	0.	0.
7	.111430E+01	0.	0.
8	.200000E+01	0.	0.
9	0.	0.	0.
10	0.	0.	0.
11	0.	0.	0.
12	0.	.200000E+01	0.
13	0.	.500000E+01	0.
14	0.	.150000E+01	0.

DATE
TIME

NODE	PHIN(I, 2)	PHIZ(I, 2)	PHIV(I, 2)
1	0.	0.	0.
2	0.	0.	0.
3	0.	0.	0.
4	0.	0.	0.
5	0.	0.	0.
6	0.	0.	0.
7	0.	0.	0.
8	0.	0.	0.
9	0.	0.	0.
10	.300000E+00	0.	0.
11	.150000E+01	0.	0.
12	0.	0.	0.
13	0.	0.	0.
14	0.	0.	.150000E+01

DATE
TIME

NODE	PHIX(I, 5)	PHIZ(I, 5)	PHIY(I, 5)
1	0.	0.	0.
2	0.	0.	0.
3	0.	0.	0.
4	0.	0.	0.
5	.232800E+00	0.	0.
6	.779900E+00	0.	0.
7	.905800E+00	0.	0.
8	.817000E+00	0.	0.
9	.500000E+00	0.	0.
10	.180000E+01	0.	0.
11	0.	0.	.200000E+01
12	0.	0.	.300000E+01
13	0.	0.	0.
14	0.	0.	.150000E+01

DATE
TIME

** ARRAY OF REDUCED FREQUENCIES **

.100000

REFERENCE CHORD	=	2.00000
REFERENCE SEMI-SPAN	=	1.00000
REFERENCE AREA	=	9.00000
MACH NUMBER	=	.85000
BETA	=	.52674
MOMENT AXIS	=	0.00000

IMAGE RADIUS = 2.00000*BODY RADIUS

NK	NSYM	NASYM	NGUST	NB	NBOX	NSBE	NSTRIP	MAXSTR	NP
1	2	1	13	2	12	13	6	6	3

NUMBER OF PANELS = 3
NUMBER OF BODIES = 2
NUMBER OF UNKNOWNS= 38

MACH	REFA	REFS	REFC	XM
.85E+00	.90E+01	.38E+01	.20E+01	0.

IPR1 = 0
IPR2 = 0
IPR3 = 0
NO. GUST ORIENTATIONS = 13

TABLE 4 CONTINUED

TABLE 4 CONTINUED

82

TABLE 4 CONTINUED

TABLE 4 CONTINUED

```
   ** PANEL NO.   3 INPUT VALUES **

X1 =     .000000  X2 =    2.100000  Y1 =    2.300000  Z1 =     .600000
X3 =    0.000000  X4 =    1.500000  Y2 =    2.300000  Z2 =    0.000000
NF =  2  NS =  1
GROUP NUMBER      =    3

        1  CHORDWISE DIVISIONS FOR PANEL  3
0.              .500000E+00     .100000E+01
        2  SPANWISE  DIVISIONS FOR PANEL  3
0.              .100000E+01


   ** SUMMARY OF PANEL DATA **

 PANEL    NF    NS  NR*ARRAY   DIHEDRAL
                                 ANGLE

     1     2     2         4     0.00000
     2     2     3        10    21.80141
     3     2     1        12   270.00003
```

TABLE 4 CONTINUED

** GEOMETRY ARRAYS FOR ALL PANELS **

PANEL NO.	STRIP NO.	BOX NO.	1/4 CHORD X	1/4 CHORD X-COORDINATES INBOARD	CENTER	OUTBOARD	BOX CHORD DELTA-X	1/4 CHORD SWEEP ANGLE
1	1	1	.84281	.75000	.37094	.49188	.94375	.34408
1	1	2	1.78656	1.25000	1.31469	1.37938	.94375	.18937
1	2	3	1.09306	.49188	.63969	.78750	.81875	.34408
1	2	4	1.86781	1.37938	1.45844	1.53750	.81875	.18937
2	3	5	1.26063	.78750	.92188	1.05625	.68750	.32114
2	3	6	1.95313	1.53750	1.60938	1.68125	.68750	.17611
2	4	7	1.42031	1.05625	1.12344	1.19063	.59375	.32114
2	4	8	2.01406	1.68125	1.71719	1.75313	.59375	.17611
2	5	9	1.52344	1.19063	1.25781	1.32500	.53125	.32114
2	5	10	2.05469	1.75313	1.78906	1.82500	.53125	.17611
3	6	11	.98250	.78750	.88750	.98750	.75000	5.49779
3	6	12	1.81250	1.53750	1.23750	.93750	.75000	5.49779

STRIP	Y	Z	DELTA-Y	DELTA-Z	E	CHORD	Y-L.E.
1	1.13750	.40000	.67500	0.00000	.33750	1.88750	.13500
2	1.88750	.40000	.82500	0.00000	.41250	1.63750	.43500
3	2.67500	.79000	.75000	.39000	.40389	1.37500	.75000
4	3.25750	.97500	.37500	.15000	.20194	1.18750	.97500
5	3.61250	1.12500	.37500	.15000	.20194	1.06250	1.12500
6	3.30000	.30000	0.00000	-.60000	.30000	1.50000	.30000

TABLE 4 CONTINUED

```
                    ** BODY NO.   1  INPUT VALUES **

      CENTER OF BODY COORDINATES    Y =      0.000000      Z =      0.000000
      AVERAGE HALF-WIDTH OF BODY    =        1.000000
      CROSS-SECTIONAL ASPECT RATIO =         1.000000
      NUMBER OF INTERFERENCE ELEMENTS ON BODY =    4
      NUMBER OF BLENDED BODY ELEMENTS =            9
      Z-AXIS INCIDENCE FLAG    =  2
      NT-FLAG =  1   NQ FLAG =  1

        5  XI-I ELEMENTS FOR BODY  1

 0.          .100000E+01     .200000E+01     .300000E+01

        5  RO-I  ELEMENTS FOR BODY  1

 .100000E+01     .100000E+01     .100000E+01     .100000E+01     .100000E+01

        4  THETA  ELEMENTS FOR BODY  1

 0.          .900000E+02     .180000E+03     .270000E+03

       10  XI-S ELEMENTS FOR BODY  1

-.200000E+01    -.140000E+01    -.140000E+01    -.100000E+01    0.          .100000E+01
 .200000E+01     .140000E+01     .140000E+01     .100000E+01

       10  RO-S  ELEMENTS FOR BODY  1

 0.          .650000E+00     .850000E+00     .100000E+01     .100000E+01     .100000E+01
 .100000E+01     .100000E+01     .850000E+00     0.
```

AD-A106 481 DOUGLAS AIRCRAFT CO LONG BEACH CA F/G 18/3
NUCLEAR BLAST RESPONSE COMPUTER PROGRAM, VOLUME II. DOUBLET-LAT--ETC(U)
AUG 81 J P GIESING, T P KALMAN, W P RODDEN DNA001-75-C-0216
UNCLASSIFIED AFWL-TR-81-32-VOL-2 NL

2 OF 3
AD A106481

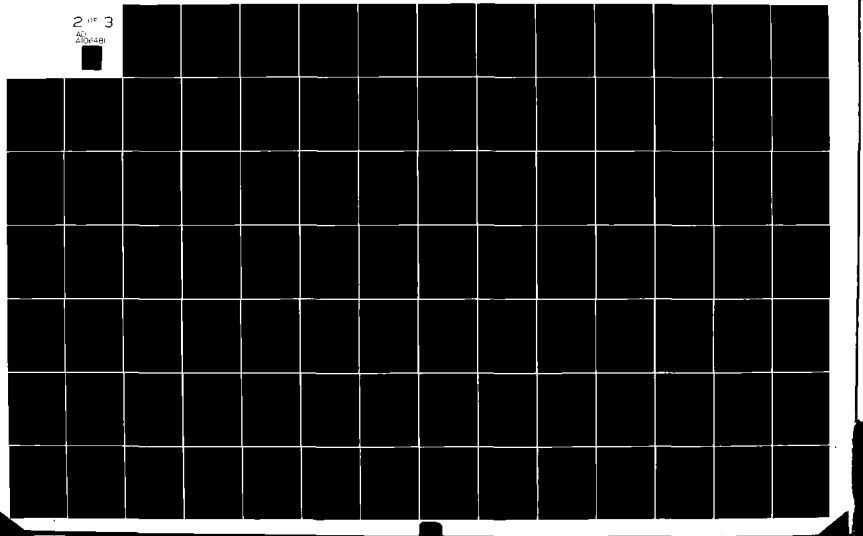

TABLE 4 CONTINUED

```
          ** BODY NO.   2  INPUT VALUES **

 CENTER OF BODY COORDINATES   Y =     2.500000     Z =     -.900000
 AVERAGE HALF-WIDTH OF BODY   =        .500000
 CROSS-SECTIONAL ASPECT RATIO =       1.000000
 NUMBER OF INTERFERENCE ELEMENTS ON BODY =   2
 NUMBER OF BLENDED BODY ELEMENTS =           4
 Z-V INTERPOLATION FLAG   =  2
 FI-FLAG =  0   WWG FLAG =  1

      3  XI=1 ELEMENTS FOR BODY  2

0.          .750000E+00     .150000E+01

      3  R=1  ELEMENTS FOR BODY  2

.500000E+00     .500000E+00     .500000E+00

      4  THETA  ELEMENTS FOR BODY  2

.450000E+02     .135000E+03     .225000E+03     .315000E+03

      5  XI=5 ELEMENTS FOR BODY  2

-.300000E+01    -.200000E+00    0.          .750000E+00     .150000E+01

      5  R=5  ELEMENTS FOR BODY  2

0.          .400000E+00     .500000E+00     .500000E+00     .500000E+00
```

HEADER DATA WRITTEN ON TAPE 19

NK	NSYM	NASYM	NGUST	NB	NBOX	NSBE	NSTRIP	MAXSTR	NP
1	2	1	13	2	12	13	6	6	3

MACH	REFA	REFS	REFC	XM
.85E+00	.90E+01	.38E+01	.20E+01	0.

TABLE 4 CONTINUED

** GEOMETRY ARRAYS FOR ALL BODIES **

INTERFERENCE BODY NUMBER	SEGMENT NUMBER	X=I	Y=I	Z=I	R=I	GAMMA
1	1	-.50000	0.00000	0.00000	1.00000	0.00000
1	2	.50000	0.00000	0.00000	1.00000	0.00000
1	3	1.50000	0.00000	0.00000	1.00000	0.00000
1	4	2.50000	0.00000	0.00000	1.00000	0.00000
2	5	.32500	2.30000	-.50000	.50000	0.00000
2	6	1.12500	2.30000	-.50000	.50000	0.00000

BLENDER BODY NUMBER	SEGMENT NUMBER	XTS1	XTS2	AO	AO-PRIME
1	1	-2.00000	-1.80000	.32500	1.25000
1	2	-1.80000	-1.40000	.80000	.75000
1	3	-1.40000	-1.00000	.97500	.12500
1	4	-1.00000	0.00000	1.00000	0.00000
1	5	0.00000	1.00000	1.00000	0.00000
1	6	1.00000	2.00000	1.00000	0.00000
1	7	2.00000	3.00000	1.00000	0.00000
1	8	3.00000	4.00000	.75000	-.50000
1	9	4.00000	5.00000	.25000	-.50000
2	10	-.40000	-.20000	.20000	2.00000
2	11	-.20000	0.00000	.45000	.50000
2	12	0.00000	.75000	.50000	0.00000
2	13	.75000	1.50000	.50000	0.00000

*** PRESSURES ***

KR = .1000

MODE NO 1

PANEL	STRIP	BOX	XLC	X	Y	Z	PRESSURES	
1	1	1	.12500	.37094	1.13750	.60000	9.559870	-.464436
1	1	2	.62500	1.31469	1.13750	.60000	2.983118	1.297246
1	2	3	.12500	.83969	1.88750	.60000	11.139581	-.453926
1	2	4	.62500	1.45844	1.88750	.60000	3.093743	1.429688
2	3	5	.12500	.92188	2.67500	.75000	8.358817	-.229856
2	3	6	.62500	1.60938	2.67500	.75000	2.795942	1.013496
2	4	7	.12500	1.12344	3.23750	.97500	8.370035	-.109012
2	4	8	.62500	1.71719	3.23750	.97500	2.883668	.457478
2	5	9	.12500	1.25781	3.61250	1.12500	8.888115	-.005793
2	5	10	.62500	1.74906	3.61250	1.12500	1.247547	.617041
1	6	11	.12500	.48750	2.30000	.50000	4.832781	-.194963
1	6	12	.62500	1.23750	2.30000	.50000	-.048498	.560486

MODE NO 5

PANEL	STRIP	BOX	XLC	X	Y	Z	PRESSURES	
1	1	1	.12500	.37094	1.13750	.60000	.910272	.048428
1	1	2	.62500	1.31469	1.13750	.60000	.345438	.230178
1	2	3	.12500	.83969	1.88750	.60000	-.177894	-.083261
1	2	4	.62500	1.45844	1.88750	.60000	.880502	.101041
2	3	5	.12500	.92188	2.67500	.75000	1.990016	.394316
2	3	6	.62500	1.60938	2.67500	.75000	.610781	.486028
2	4	7	.12500	1.12344	3.23750	.97500	3.805539	.357009
2	4	8	.62500	1.71719	3.23750	.97500	.515009	.388318
2	5	9	.12500	1.25781	3.61250	1.12500	2.800442	.287458
2	5	10	.62500	1.74906	3.61250	1.12500	.324129	.272483
1	6	11	.12500	.48750	2.30000	.50000	-4.314269	-.432466
1	6	12	.62500	1.23750	2.30000	.50000	-.639793	.608778

TABLE 4 CONTINUED

DEFINITION OF SYMBOLS

B = SEMI-SPAN
C.RAP = REFERENCE CHORD

L = BODY LENGTH
F.Z/Q = (VERTICAL FORCE)/(DYNAMIC PRESSURE)
F.Y/Q = (LATERAL FORCE)/(DYNAMIC PRESSURE)

SIGN CONVENTION

THE FOLLOWING TWO SIGN CONVENTIONS HOLD

(1) FORCES AND DEFLECTIONS POSITIVE DOWN ON HORIZONTAL SURFACES OR Z-BODIES AND POSITIVE OUTBOARD ON VERTICAL SURFACES OR Y-BODIES

(2) FORCES AND DEFLECTIONS POSITIVE UP ON HORIZONTAL SURFACES OR Z-BODIES AND POSITIVE INBOARD ON VERTICAL SURFACES OR Y-BODIES

TABLE 4 CONTINUED

TABLE 4 CONTINUED

MODE 1

STRIP	Y	Z	Y/S	LIFT COEFFICIENT REAL	LIFT COEFFICIENT IMAG.	MOMENT COEFFICIENT 1/4 CHORD OF STRIP REAL	MOMENT COEFFICIENT 1/4 CHORD OF STRIP IMAG.	CENTER OF PRESSURE REAL	CENTER OF PRESSURE IMAG.
1	1.1375	.6000	.2089	6.271294	.414495	.034132	-.272241	.2439	.8038
2	1.8875	.6000	.0687	7.111542	.487882	.116135	-.294037	.2319	.8576
3	2.6750	.7500	.7438	6.537179	.580270	-.001813	-.273040	.2503	.7726
4	3.2375	.4750	.8420	5.231162	.374029	.132098	-.167664	.2246	.6078
5	3.6125	1.1250	.8507	4.067841	.309435	.105118	-.114041	.2019	.6209
6	3.8000	.3000	.8063	2.391942	.182842	.111217	-.117314	.1199	.8915

STATION	SPANWISE COORD.	SPAN LOAD (CORCL*(CHORD)) REAL	SPAN LOAD (CORCL*(CHORD)) IMAG.
1	1.1375	.891856+01	.102086+00
2	1.8875	.592676+01	.398456+00
3	2.6750	.393486+01	.247826+00
4	3.2375	.210416+01	.222326+00
5	3.6125	.215576+01	.162376+00
6	3.8000	.179406+01	.113196+00

MODE 1

BODY ELEM.	Y	Z	X/L	RUNNING LOAD (VERTICAL) (DF=Z/Q) / DX REAL	IMAG.	RUNNING LOAD (LATERAL) (DF=Y/Q) / DX REAL	IMAG.
1	0.0000	0.0000	.0143	7.942983	-1.369642	.000000	.000000
2	0.0000	0.0000	.0571	5.730750	-.352003	.000000	.000000
3	0.0000	0.0000	.1143	3.594459	.132188	.000000	.000000
4	0.0000	0.0000	.2143	2.807923	.415978	.000000	.000000
5	0.0000	0.0000	.3571	4.815556	1.115698	.000000	.000000
6	0.0000	0.0001	.5000	2.218883	2.110379	.000000	.000000
7	0.0000	0.0000	.6429	-.063989	1.003885	.000000	.000000
8	0.0000	0.0000	.7857	-3.910423	-.520191	.000000	.000000
9	0.0000	0.0000	.9286	-1.805610	-.015215	.000000	.000000

TOTALS ON BODY 1

F=Z/Q =	1.061455	.414527	M=Z/Q =	.334267	-.017552
F=Y/Q =	-.000030	-.000000	M=Y/Q =	.000000	.000000

MODE 1

BODY ELEM.	Y	Z	X/L	RUNNING LOAD (VERTICAL) (DF=Z/Q) / DX REAL	IMAG.	RUNNING LOAD (LATERAL) (DF=Y/Q) / DX REAL	IMAG.
10	2.3000	-.5000	.0526	3.859531	-.058507	.060813	-.011573
11	2.3000	-.5000	.1579	2.311267	.075771	.451697	-.124254
12	2.3000	-.5000	.4079	-.120431	.285662	2.047048	-.137394
13	2.3000	-.5000	.8026	-1.295928	.504301	.731941	.223104

TOTALS ON BODY 2

F=Z/Q =	.019038	.040551	M=Z/Q =	.074282	-.028750
F=Y/Q =	.247418	.004124	M=Y/Q =	-.114883	-.009313

TABLE 4 CONTINUED

MODE 1

TOTALS ON LIFTING SURFACES

CZ	=	0,[illegible]	,417683	CY	=	0,000000	0,000000
CM	=	-2,883325	-,391749	CN	=	0,000000	0,000000
CRL	=	0,[illegible]	0,000000				

TOTALS ON ENTIRE AIRCRAFT

CZ	=	2,1[illegible]749	,933311	CY	=	0,000000	0,000000
CM	=	-1,111479	-,620455	CN	=	0,000000	0,000000
CRL	=	0,[illegible]000	0,000000				

TABLE 4 CONTINUED

MODE 1

STRIP	Y	Z	Y/S	LIFT COEFFICIENT		MOMENT COEFFICIENT 1/4 CHORD OF STRIP		CENTER OF PRESSURE	
				REAL	IMAG.	REAL	IMAG.	REAL	IMAG.
1	1,1375	,6000	,2093	,638854	,139502	-,011377	-,040106	,2678	,5375
2	1,8875	,6000	,4067	,151302	,008885	-,101213	-,020187	,9189	2,9677
3	2,6750	,7500	,7039	2,510408	,429168	,134856	-,062350	,1914	,3953
4	3,3375	,9750	,8520	2,060274	,372644	,124782	-,050497	,1875	,3455
5	3,8125	1,1250	,9503	1,544286	,280170	,114503	-,033099	,1768	,3041
6	2,3000	,5000	,4953	-2,478031	-,520617	-,149806	,087116	,1895	,4173

STATION	SPANWISE COORD.	SPAN LOAD REAL	(CnPL)/(CnBAR) IMAG.
1	1.1875	.803AAE+00	.131A9E+00
2	1.AA75	.123AAE+00	.7274AE-02
3	2.6750	.15815E+01	.29505E+00
4	3.2375	.12253E+01	.22127E+00
5	3.A125	.A51C3E+00	.1AAA4E+00
6	.3400	-.145A5E+01	-.3904AE+00

MODE 3

BODY PLANE	Y	Z	X/I	RUNNING LOAD (VERTICAL) (DF=Z/Q) / DX REAL	IMAG.	RUNNING LOAD (LATERAL) (DF=Y/Q) / DX REAL	IMAG.
1	0.0000	0.0000	.0143	-.000000	.000000	-7.955193	1.340842
2	0.0000	0.0000	.0571	-.000000	-.000000	-5.449005	.124474
3	0.0000	0.0000	.1143	-.000000	-.000000	-2.593401	-.738054
4	0.0000	0.0000	.2143	-.000000	-.000000	-.134992	-1.273444
5	0.0000	0.0000	.3571	-.000000	-.000000	.541497	-1.144481
6	0.0000	0.0000	.5000	-.000000	-.000000	.122769	-1.274744
7	0.0000	0.0000	.6429	-.000000	.000000	.652805	-1.238572
8	0.0000	0.0000	.7857	-.000000	.000000	4.009915	.400857
9	0.0000	0.0000	.9286	-.000000	-.000000	1.410578	.419897

TOTALS ON BODY 1

F=Z/Q =	-.000000	-.000000	M=Z/Q =	.000000	.000000
F=Y/Q =	.221619	-.409997	M=Y/Q =	-1.954502	.425961

TABLE 4 CONTINUED

MODE 3

BODY ELEM.	Y	Z	X/L	RUNNING LOAD (VERTICAL) (DF=Z/Q) / DX REAL	IMAG.	RUNNING LOAD (LATERAL) (DF=Y/Q) / DX REAL	IMAG.
10	2.3000	-.5000	.0526	-.005045	-.003848	-3.830957	.063853
11	2.3000	-.5000	.1579	-.046549	-.018924	-2.135536	-.090094
12	2.3000	-.5000	.4979	-.175231	-.026018	-1.014426	-.106791
13	2.3000	-.5000	.8026	-.245089	-.059056	-.388073	-.186942

TOTALS ON BODY 2

F=Z/Q =	-.336618	-.007551	M=Z/Q =	.021459	.004653
F=Y/Q =	-.209464	-.058483	M=Y/Q =	.068791	.034736

MODE 3

TOTALS ON LIFTING SURFACES

CZ	=	0.000000	0.000000	CY	=	-.843431	-.168138
CM	=	0.000000	0.000000	CN	=	.336820	.091743
CBL	=	.445870	.000045				

TOTALS ON ENTIRE AIRCRAFT

CZ	=	0.000000	0.000000	CY	=	-1.120740	-.695101
CM	=	0.000000	0.000000	CN	=	-1.358245	.153788
CBL	=	.580662	.047780				

TABLE 4 CONCLUDED

2. TYPICAL LOAD DISTRIBUTIONS

Schematics of typical loadings are presented in Figure 33 through 36 as an aid in the interpretation of the monitored output data. Specifically Figure 33 gives a typical chordwise loading for a wing in steady pitch and control surface deflection. For the pitch case a square root singularity exists at the leading edge. For the control surface rotation case an additional logarithmic singularity exists at the control surface leading edge.

Figure 34 presents a spanwise load distribution for; (a) a wing-fuselage combination and (b) a wing-pylon combination in steady pitch. The effect of the fuselage is to change the loading near the wing fuselage intersection. The extent to which this effect changes the wing load depends on the body diameter to wing span ratio. The pylon increases the inboard wing loading. The jump in wing loading, Δ, at the pylon location is equal to the pylon root loading.

Figure 35 presents a typical aerodynamic center location for a clean wing. For swept-back wings the a.c. moves aft near the root and forward near the tip. (The reverse is true for wings with forward sweep.) The effect of Mach Number is to move the a.c. further aft near the root and further forward near the wing tip with the cross over point near the wing tip.

Figure 36 presents the vertical running load, load per unit length, on a wing-fuselage combination. This loading can be thought of as the sum of two basic parts; a slender body type of loading and a lift carry through type. The slender body term changes most rapidly in regions where the body width or radius changes most rapidly. The wing lift carry-over term is largest in the area of the wing-fuselage intersection.

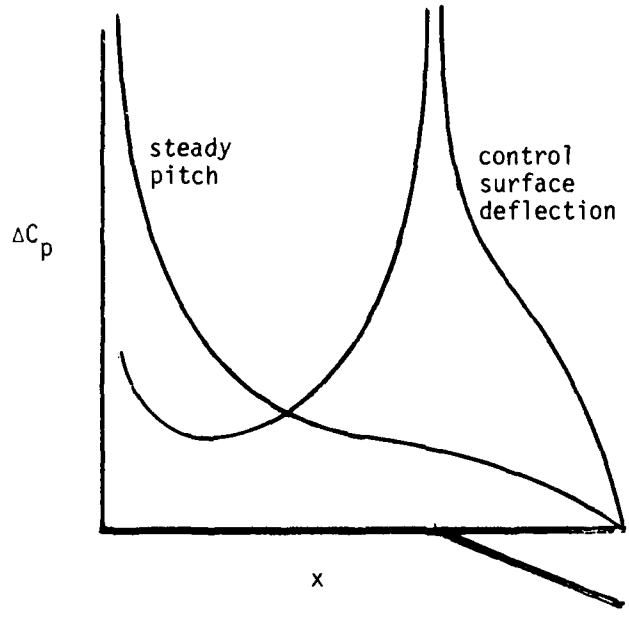

Figure 33 Typical Chordwise Loadings

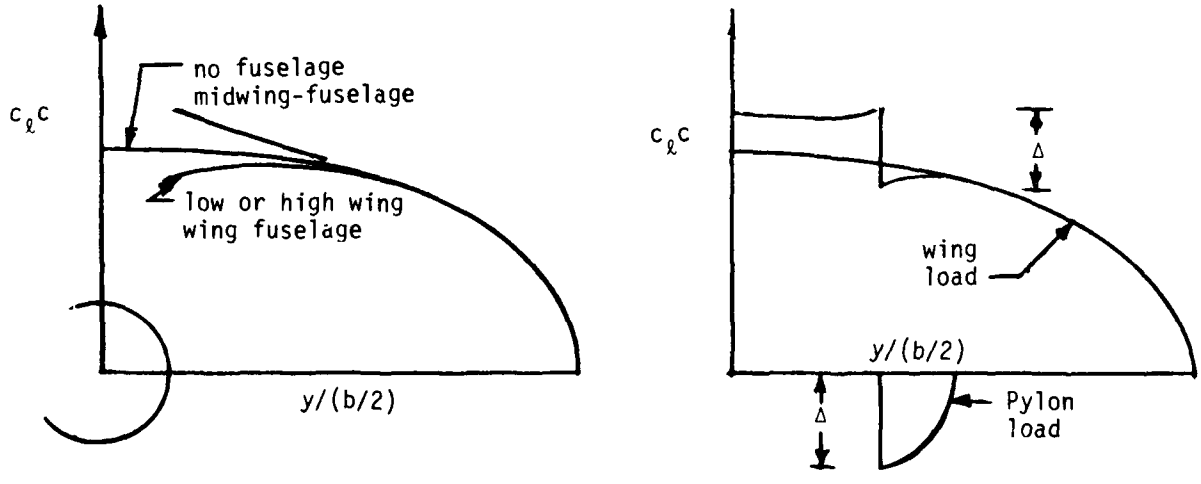

Figure 34 Typical Spanwise Load Distributions

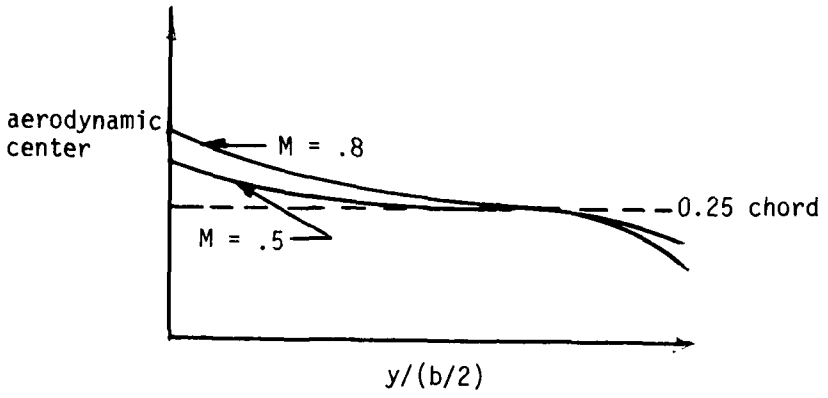

Figure 35 Typical Wing Aerodynamic Center Variation

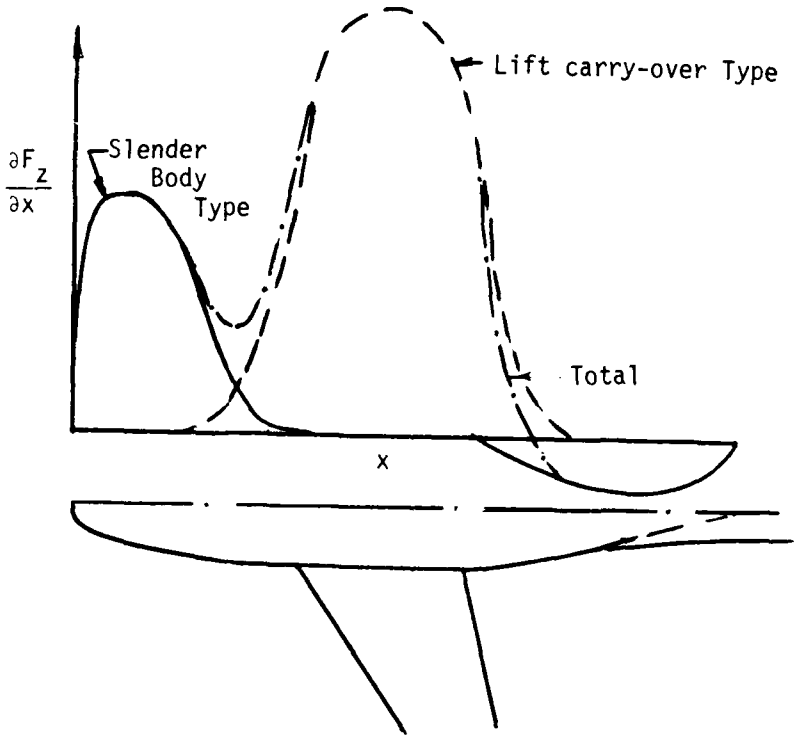

Figure 36 Typical Fuselage Lift Distribution

3. TROUBLE SHOOTING

In this subsection a series of problems are stated along with their possible cause. This list is not all inclusive but covers many common problem areas.

Problem: Dips in span loading near wing-fuselage intersections or in the middle of a wing or at pylon-wing intersections.

Possible Cause: Gaps or overlap between components or wing panels. Even a small gap between wing and fuselage interference tube can cause a significant dip in the loading there. The same holds true for wing-wing panels and wing-pylon panels.

Problem: Irregularities or waves in the chordwise pressure distribution.

Possible Cause: A discontinuous change in box size in the chordwise direction. Or in the case of a fold line of significant dihedral change (e.g., a wing-pylon intersection) the boxes do not line up in a chordwise direction on both sides of the fold line. Or there is an overlapping of boxes in the chordwise direction.

Problem: Large or unreasonable loads on surfaces.

Possible Cause: Surfaces may be overlapping. Or tail surface strips are not lined up with wing strips in the coplanar or nearly coplanar case. Or intersecting surfaces meeting at other than a strip edge. In general the problem may be that control points (3/4 chord of box) lie too close to singularities; either the bound type (1/4 chord of box) or the trailing type (lying on strip edges starting at the box and extending to downstream infinity).

Problem: The c_ℓ distribution has taken a jump where there is no pylon or intersecting surface.

Possible Cause: The local chord length has taken a similar jump. If intersecting surfaces are excluded then $c_\ell c$ is always continuous. Thus if c is discontinuous c_ℓ has the same discontinuity.

Problem: Large or unreasonable body loads.

Possible Cause: The flow field pickup points on the interference tube (given by θl_1, θl_2 ...) lie at or very near a lifting surface-body intersection. Or interference tubes of differing cross-sections are placed along the same longitudinal axis.

Problem: Sign of some or all of results is incorrect.

Possible Cause: The panel may be input upside down. That is, the dihedral of the panel may be different, by 180^o, from that which was intended. An example is a vertical tail input from the fuselage to tip has a positive normal in negative y-direction (dihedral = $+90^o$) whereas a pylon input from wing down to nacelle has a positive normal in the positive y-direction (dihedral = -90^o). Or modes may be input with incorrect signs.

Problem: Body has a loading even if it is not at angle of attack nor intersecting any lifting surface.

Possible Cause: There is no problem. All lifting surface elements generate some loading on all bodies even though not connected to that body.

Problem:	Tail surface has unreasonable loads.
Possible Cause	Tail surface lies within an interference tube. Only one interference tube is allowed on any one longitudinal axis, e.g., two interference tubes, one for the wing and one for the tail, can not be used for a single fuselage. Or tail strips do not line up with wing strips in the coplanar or nearly coplanar case.

SECTION VII

SUBROUTINE DESCRIPTION

1. INTRODUCTION

A large portion of the computer program being introduced into the VIBRA-6 system is documented in Reference 4 (Vol. II of Part II), and need not be repeated here. However new subroutines have been developed, old ones modified and some have had their argument lists changed to eliminate common blocks of data. Twenty-nine of the forty-six subroutines of the program have had some sort of change, and fourteen subroutines have been added.

No limits on dimension sizes have been assigned since a dynamic core feature is to be used for the entire VIBRA-6 system. The working array size will depend on the problem solved. Formulas dealing with the working array size are furnished in Volume I.

The listing of the program and subroutines is given in Volume III. Descriptions of each of the thirty-four modified and changed subroutines follow in alphabetic order.

2. DETAILED DESCRIPTION OF SUBROUTINES

2.1 SUBROUTINE AERO (MFIX1, MFIX2, NMSYM, NTOT, NOUT, NW, NEWBFZ, NEWBFY, NSTOT, CBSPAN, DCP, FZ, FY, CN, CM, SPLD, ISSTR, NSBEA, NBARAY, NCARAY, YB, ZB, XIS1, XIS2, CG, CS, EE, SG, YS, ZS, XIC, XIJ, DELX, COORD, CZB, CYB, CNB, CMB, CPR, CPI)

Functional Descirption

Subroutine AERO computes and prints the pressures and the aerodynamic derivatives for two fixed modes, MFIX1 and MFIX2. It is called once for each reduced frequency from subroutine SDLM.

Input Output Variables

MNEMONIC	DESCRIPTION
MFIX1	MFIX1 and MFIX2 are two mode numbers for which
MFIX2	aerodynamic parameters are calculated
NMSYM	The total number of symmetric modes
NTØT	The total number of unknowns
NØUT	Data set number of the system output data set
NW	Tape number containing the pressures for all points in all modes
NEWBFZ	Tape number containing the body element z-forces
NEWBFY	Tape number containing the body element y-forces
NSTOT	Maximum dimension of body force array or sectional lift coefficient array
CBSPAN	Reference length used in the calculation of span loads

MNEMONIC	DESCRIPTION
DCP	Complex array of pressures for all points (boxes) in one mode
FZ	Body element z-forces } in one mode
FY	Body element y-forces }
CN	Lift coefficients } for all strips in one mode
CM	Moment coefficients }
SPLD	Span loads
CZB	Total lift coefficients for bodies, z- and y- directions
CYB	
CNB	Total yawing } moment coefficients for bodies
CMB	Total pitching }
CPR	Centers of pressure (real - and imaginary parts) for lifting surface strips
CPI	

The following variables are described under Basic Variables in Section VII-3:

ISSTR, NSBEA, NBARAY, NCARAY, YB, ZB, XIS1, XIS2, CG, CS, EE, SG, YS, ZS, XIC, XIJ, DELX, COORD.

Calling Subroutine SDLM

2.2 SUBROUTINE BFSMAT(LENGTH, NE, NB, NP, NTP, NTOTAL, IO, IOA, FMACH, CBAR, KR, YB, ZB, YS, ZS, X, DELX, EE, XIC, SG, CG, AR, RIA, AO, XIS1, XIS2, AVR, NSARAY, NCARAY, NSBEA, NBEA1, NAS, NASB, BFS, BFSA, SCALER)

Functional Description

This subroutine is the basic calling routine that computes the $[FZ]^{(b)}$ and $[FY]^{(b)}$ matrices for both symmetric and antisymmetric conditions. These matrices are written on two tapes, in row order, alternating first a row of FZ, then a row of FY for symmetry is written on tape (scratch unit) IO, and similarly, a row of FZ, then a row of FY for antisymmetry is written on another tape, IOA.

Input Output Variables

MNEMONIC	DESCRIPTION
LENGTH	The total number of unknowns + the total number of z- and y-oriented slender body elements
NE	Ground effect flag
NB	Number of bodies
NP	Number of panels
NTP	Number of lifting surface boxes
NTØTAL	NTP + Total number of z- and y-oriented interference body elements
IØ	Tape number on which the BFS-matrix is written
IØA	Tape number on which the BFSA-matrix is written
FMACH	Mach Number
CBAR	Reference chord
KR	Reduced frequency
YB	Array of y-coordinates of bodies
ZB	Array of z-coordinates of bodies

MNEMONIC	DESCRIPTION
YS	Array of y-coordinates of lifting surface strips
ZS	Array of z-coordinates of lifting surface strips
X	Array of 3/4-chord locations of boxes and 1/2-chord for body elements
DELX	Array of lengths of panel boxes and body elements
EE	Array of the semiwidths of strips
XIC	Array of 1/4-chord locations of all boxes
SG	Array of the sines of the dihedral angles of strips
CG	Array of the cosines of the dihedral angles of strips
AR	Array of the cross-sectional aspect ratics of the bodies
RIA	Array of the radii of interference body elements
AO	Array of the slender body element radii
XIS1	Leading edge location of the slender body elements
XIS2	Trailing edge location of the slender body elements
AVR	Array of the average radii of all bodies
NSARAY	Array of the number of strips per panel
NCARAY	Array of the number of chordwise boxes per panel
NSBEA	Array of the number of slender body elements per body
NBEA1	Array of the number of interference body elements per body
NBEA2	z-y orientation flag array per bod, fixed as 2)
BFS	One row of the z- and y-forces in the BFS matrix (symmetry)
BFSA	One row of the z- and y-forces in the BFSA matrix (antisymmetry)
SCALER	Nondimensional image radius (input)

Calling Subroutine	SDLM
Called Subroutine	FWMW

2.3 SUBROUTINE CTLS (NEAASS, NDAS, ND, ELXI, ELYI, ELZI, XA, YA, ZA, XB, YB, ZB, XAR, YAR, ZAR, XBR, YBR, ZBR, XI, ETA, NTP6)

Functional Description

This subroutine computes the ξ, and η-coordinates of a generated node on the elastic axis of a control surface, for which no input-node exists, from an associated node (NDAS) of the associated elastic axis (NEAASS). (See Figure 14).

Input Output Variables

MNEMONIC	DESCRIPTION
NEAASS	Sequence number of the associated elastic axis (i.e., superpanel)
NDAS	Associated node number
ND	Generated node number for the current control surface elastic axis; numbering begins with ND = 1 for each control surface, ($1 \leq ND \leq NODASS$, where NODASS is card input)
ELXI, ELYI, ELZI	Arrays of the x-, y-, z-coordinates of all input nodes on all elastic axes
XA, YA, ZA / XB, YB, ZB	Coordinates of the {inboard / outboard} edge of elastic axis for control surface
XAR, YAR, ZAR / XBR, YBR, ZBR	Coordinate arrays of the {inboard / outboard} edges of all input elastic axes

MNEMONIC	DESCRIPTION
XI, ETA	ξ , η coordinate arrays of the generated nodes
NTP6	Reference number of the system output unit

Calling Subroutine NEWH

2.4 SUBROUTINE DOTP (NTPH, NTPDH, NTPH4, MASTH, MASTDH, MASTH4, IFNEWH, NSYM, NASYM, NODES, MODES, NB, IROW, PHIN, PHIZ, PHIY, COL, WORK)

Functional Description

This subroutine organizes the input/output arguments to subroutine ORGN for the computation steps of the $[\bar{H}]$ matrices for both symmetric and antisymmetric conditions for lifting surface panels as well as bodies.

Input Output Variables

MNEMONIC	DESCRIPTION
NTPH	Tape number containing the h arrays; output of subroutine SPLINE
NTPDH	Tape number containing the dh/dx arrays; output of subroutine SPLINE
NTPH4	Tape number containing the $h_{1/4c}$ arrays; output of subroutine SPLINE
MASTH, MASTDH, MASTH4	Output tapes containing the results of the dot products, $\{\bar{h}\}$, $\{d\bar{h}/dx\}$ and $\{\bar{h}_{1/4c}\}$ respectively
IFNEWH	Flag to select degrees of freedom; see subroutine SDLM
NSYM	The number of symmetric modes
NASYM	The number of antisymmetric modes
NODES	The number of nodes
MODES	The number of modes
NB	The number of bodies

MNEMONIC	DESCRIPTION
IROW	Maximum number of row elements in the work array
PHIN	Modal deflection matrix for panels
PHIZ	Modal deflection matrix for bodies in z-direction
PHIY	Modal deflection matrix for bodies in y-direction
COL	One column of the h, dh/dx or $h_{1/4c}$ matrices
WORK	Output of subroutine ORGN containing either of the matrices $[\bar{h}]$, $[\bar{dh}/dx]$ or $[\bar{h}_{1/4}]$ which are saved on the three tapes MASTH, MASTDH and MASTH4 respectively

Calling Subroutine SDLM

Called Subroutine ORGN

2.5 SUBROUTINE DPPS (K, KS, I, J1, J2, SGR, CGR, REFC, FMACH, YS, ZS, NBARAY, NCARAY, DT, DTA, YB, ZB, ARB, AVR, XLE, XTE, X, CG, EE, SG, XIC, DELX, XLAM, SCALER)

Functional Description

Subroutine DPPS prepares the variables necessary for the computation of one row of the DPP submatrix (for symmetry) and one row of the DPPA submatrix (for antisymmetry). The resulting two matrix rows are returned to subroutine GEND via the argument list in arrays DT and DTA respectively.

Input Output Variables

MNEMONIC	DESCRIPTION
K	Panel number in which the receiving point 'i' lies
KS	Strip number containing 'i'
I	Receiving point index
J1, J2	DO loop delimiters for the number of elements in one row of the submatrices
SGR, CGR	Sine and cosine of the receiving strip dihedral angle
DT	A row of the DPP submatrix
DTA	A row of the DPPA submatrix
SCALER	Nondimemsional image radius

The following variables are described under Basic Variables in Section VII, Part 3:

REFC, FMACH, YS, ZS, NBARAY, NCARAY, YB, ZB, ARB, AVR, XLE, XTE, X, CG, EE, SG, XIC, DELX, XLAM

Calling Subroutine	GEND
Called Subroutine	SUBP

2.6 SUBROUTINE DPZY(KB, IZ, I, J1, J2, IFIRST, ILAST, REFC, FMACH, YB, ZB, AVR, ARB, TH1A, TH2A, NT12, NBARAY, NCARAY, NZYKB, DPZ, DPY, DPZA, DPYA, XLE, XTE, X, CG, EE, SG, YS, ZS, XIC, DELX, XLAM, SCALER

Functional Description

Subroutine DPZY prepares the variables necessary for the computation of one row of either the DPZ or DPY submatrix (for symmetry), and one row of either the DPZA or DPYA submatrix (for antisymmetry) and calls subroutine SUBP in a double DO loop for each element of the row to perform the necessary summation around an interference body segment. The resulting matrix rows are returned to subroutine GEND via the argument list.

Input Output Variables

MNEMONIC	DESCRIPTION
KB	Body number in which the receiving point 'i' lies
IZ	Body element number of body KB in which 'i' lies
I	Receiving point index
J1, J2	DO loop delimiters for the number of elements in a row of the submatrices
IFIRST	Sequence number of the first element in body KB
ILAST	Sequence number of the last element in body KB
NZYKB	z-y flag of body KB
SCALER	Nondimensional image radius

The following variables are described under Basic Variables in Section VII-3:

REFC, FMACH, YB, ZB, AVR, ARB, TH1A, NT12, NBARAY, NCARAY, DPZ, DPY, DPZA, DPYA, XLE, XTE, X, CG, EE, SG, YS, ZD, XIC, DELX, XLAM.

Calling Subroutine	GEND
Called Subroutine	SUBP

2.7 SUBROUTINE DYPZ(KB, KS, LS, IZ, I, J1, J2, NYFLAG, FLND, FLNE, SGR, CGR, REFC, FMACH, KR, ARB, NBEA, LBO, LSO, JBO, DT, DTA, YB, ZB, RIA, X, YS, ZS, DELX)

Functional Description

Subroutine DYPZ prepares the variables necessary for the computation of one row of either the DYP, or the DYZ, or the DYY submatrix (for symmetry) and one row of either the DYPA, or the DYZA, or the DYYA submatrix (for antisymmetry). In either case it calls subroutine SUBB in a DO loop for each element of a row; latter is returned to subroutine GEND via the argument list.

Input Output Variables

MNEMONIC	DESCRIPTION
KB	Body number in which the receiving point 'i' lies
KS	Index of the receiving point y, z coordinates
LS	Index of the sending point y, z coordinates
IZ	Body element number in which 'i' lies
I	Receiving point index
J1, J2	DO loop delimiters for the number of elements in a row of the submatrices
NYFLAG	NYFLAG=0 for DYP, DYZ, DYPA and DYZA NYFLAG=1 for DYY and DYYA
FLND	Not used
FLNE	ϵ, ground effect flag
SGR, CGR	Sine and cosine of receiving point dihedral angle
LBO	Sequence number of first body with y orientation

MNEMONIC	DESCRIPTION
LSO	Index for the y, z coordinates of the first y-oriented body
JBO	Sending point index for first y-oriented body element
DT	A row of either of the submatrices DYP, DYZ or DYY
DTA	A row of either of the submatrices DYPA, DYZA or DYYA

The following variables are described under Basic Variables in Section VII-3:

REFC, *FMACH*, *KR*, *ARB*, *NBEA*, YB, ZB, *RIA*, X, YS, ZS, DELX

Calling Subroutine GEND

Called Subroutine SUBB

2.8 SUBROUTINE DZPY(KB, KS, LS, IZ, I, J1, J2, NYFLAG, FLND, FLNE, SGR, CGR, REFC, FMACH, KR, ARB, NBEA, DT, DTA, YB, ZB, RIA, X, YS, ZS, DELX)

Functional Description

Subroutine DZPY prepares the variables necessary for the computation of one row of either the DZP, or the DZZ or the DZY submatrix (for symmetry), and one row of either the DZPA, or the DZZA or the DZYA submatrix (for antisymmetry). In either case it calls subroutine SUBB in a double DO loop for each element of a row; latter is returned to subroutine GEND via the argument list.

Input Output Variables

MNEMONIC	DESCRIPTION
KB, KS	
LS	
IZ	
I	See Description given
J1, J2	in Section 2.6
NYFLAG	
FLND	
FLNE	
SGR, CGR	
DT	A row of either of the submatrices DZP, or DZZ, or DZY
DTA	A row of either of the submatrices DZPA, or DZZA, or DZYA

The following variables are described under Basic Variables in Section VII-3:

REFC, FMACH, KR, ARB, NBEA, YB, ZB, RIA, X, YS, ZS, DELX.

Calling Subroutine	GEND
Called Subroutine	SUBB

2.9 SUBROUTINE DZYMAT(D, DA, NFB, NLB, NTZYS, IDZDY, NTAPE, NTAP2, XP, BETA, IPRNT, NBEA, NSBE, NC, NS, AO, YB, ZB, AR, XIS1, XIS2, CG, SG, YP, ZP)

Functional Description

This subroutine sets up the argument list for the calculation of each row of the D_z and D_y matrices both in symmetry and antisymmetry and then calls subroutine ROWDYZ.

Input Output Variables

MNEMONIC	DESCRIPTION
D	Complex array containing a row of the D_z or D_y matrices in symmetry
DA	Complex array containing a row of the D_z or D_y matrices in antisymmetry
NFB	Number of the first body
NLB	Number of the last body
NTZYS	Number of slender body elements
IDZDY	Flag indicating whether the D_z, or the D_y matrix is calculated
NTAPE	Tape number (scratch unit) on which the output matrix rows, D, are saved
NTAP2	Tape number (scratch unit) on which the output matrix rows, DA, are saved
XP	x-coordinate of lifting surface box control points
BETA	$\beta = \sqrt{1 - M^2}$, M = Mach Number
IPRNT	Not used

The following variables are described under Basic Variables in Section VII-3:

NBEA, NSBE, NC, NS, AO, YB, ZB, AR, XIS1, XIS2, CG, SG, YP, ZP.

Calling Subroutine	SB
Called Subroutine	ROWDYZ

2.10 SUBROUTINE FWMW(NDX, NE, SGS, CGS, IRB, AO, ARB, XBLE, XBTE, YB, ZB, XS, YS, ZS, NAS, NASB, KR, BETA2, CBAR, AVR, FWZ, FWZA, FWY, FWYA, IF1, IPRNT, SCALER)

Functional Description

Given a unit pressure doublet,this subroutine calculates the effect of this doublet plus any contributions due to images, symmetry plane and ground effect on a given body both in symmetric and antisymmetric conditions.

Input Output Variables

MNEMONIC	DESCRIPTION
NDX	Not used
NE	Ground effect flag
SGS	Sine of sending point dihedral angle
CGS	Cosine of sending point dihedral angle
IRB	Number of the receiving body
AO	Radius of body element
ARB	Cross-sectional aspect ratio of body
XBLE	Leading edge location of slender body element
XBTE	Trailing edge location of slender body element
YB	Array of y-coordinates of bodies
ZB	Array of z-coordinates of bodies
XS	x-coordinate of sending point
YS	y-coordinate of sending point
ZS	z-coordinate of sending point

MNEMONIC	DESCRIPTION
NAS	Number of bodies
NASB	Array of body numbers
KR	Reduced frequency
BETA2	$\beta^2 = 1 - M^2$, M = Mach Number
CBAR	Reference chord
AVR	Array of the average radii of bodies
FWZ	Output z-forces in symmetry
FWZA	Output z-forces in antisymmetry
FWY	Output y-forces in symmetry
FWYA	Output y-forces in antisymmetry
IF1	Orientation flag of receiving body
IPRNT	Not used
SCALER	Nondimensional image radius

Calling Subroutine BFSMAT

Called Subroutine FZY2, SUBI

2.11 SUBROUTINE GEND(NPRINT, NTAPE, NTOT, IOPT, MASTDT, DT, DPZ, DPY, DTA, DPZA, DPYA, IFLA, NBEA, NT12, NBARAY, NCARAY, YB, ZB, ARB, AVR, RIA, XLE, XTE, TH1A, TH2A, X, CG, EE, SG, YS, ZS, XIC, YIN, ZIN, DELX, XLAM, SCALER)

Functional Description

Subroutine GEND generates the nine submatrices of the symmetric downwash factor matrix, [DT], and the nine submatrices of the antisymmetric downwash factor matrix, [DTA]. These two matrices are written on a utility tape in row order, one row of the DT matrix and one row of the DTA matrix as one record.

Input Output Variables

MNEMONIC	DESCRIPTION
NPRINT	Print flag for DT and DTA matrix rows; NPRINT = 0 for no print
NTAPE	Array of utility tape numbers
NTOT	Total number of unknowns
IOPT	Option flag for saving DT and DTA on output tape for future use, when IOPT = 1; IOPT = 0 otherwise
MASTDT	Output tape number on which the DT and DTA rows are saved when IOPT = 1
DT	Array containing one row of the DT matrix (symmetric downwash factors)
DPZ	Array containing one row of the DPZ submatrix
DPY	Array containing one row of the DPY submatrix
DTA	Array containing one row of the DTA matrix (antisymmetric downwash factors)

MNEMONIC	DESCRIPTION
DPZA	Array containing one row of the DPZA submatrix
DPYA	Array containing one row of the DPYA submatrix
SCALER	Nondimensional image radius

The following variables are described under Basic Variables in Section VII-3:

IFLA, NBEA, NT12, NBARAY, NCARAY, YB, ZB, ARB, AVR, RIA, XLE, XTE, TH1A, X, CG, EE, SG, YS, ZS, XIC, YIN, ZIN, DELX, XLAM.

Calling Subroutine SDLM

Called Subroutines DPPS, DPZY, DZYP, DYPZ

2.12 SUBROUTINE GENF (NMODES, NTOT, NTP, NB, YB, NSBETO, IPRINT, LINES, NTP6, NUTL1, NUTL2, NTPH, NTPH4, NTFORC, NTGF, MASTCP, MASTFZ, MASTFY, JKR, H, FMULT, NASYM, DELA, XIS1, XIS2, NSBEA FORCE, GF, WORK, NG)

FUNCTIONAL DESCRIPTION

This subroutine calculates element forces and generalized forces for all modes and gusts. The pressures ΔC_p are multiplied by the box area ΔA, to obtain the forces

$$[D\emptyset \vdots F_G] = \Delta A\ [\Delta C_p]$$

$D\emptyset$ represents the forces due to modes and F_G represents the forces due to gusts. This operation is done for lifting surfaces (panels), and bodies and for both symmetric and antisymmetric modes and gusts.

The generalized forces are calculated using these forces:

$$[\mathcal{C}\phi \vdots \mathcal{F}_G] = [H_{1/4}]^T\ [D\emptyset \vdots F_G]$$

Again this operation is repeated for lifting surfaces and bodies and symmetric and antisymmetric modes. The forces and generalized forces are written on tape.

Input Output Variables

MNEMONIC	DESCRIPTION
NMØDES	Array of mode numbers
NTØT	Maximum dimension of the force array
NTP	Number of lifting surface boxes
NB	Number of bodies
YB	Array of the y-coordinates of body centerlines

MNEMONIC	DESCRIPTION
NSBETO	Total number of slender body elements
IPRINT	Print flag
LINES	Maximum lines of print per page
NTP6	Data set number of the system output data set
NUTL1	Utility (scratch) tape number
NUTL2	Utility (scratch) tape number
NTPH	Tape number containing the [h] matrix
NTPH4	Tape number containing the $[h_{1/4c}]$ matrix
NTFORC	Tape number containing the output items of the aero module in the VIBRA-6 program (includes point forces and generalized forces)
NTGF	Tape number containing the generalized forces
MASTCP	Tape of pressures (on lifting surface boxes)
MASTFZ	Tape of z-body element forces
MASTFY	Tape of y-body element forces
JKR	Index of current reduced frequency
H	Array of deflections
FMULT	Array for temporary use
NASYM	Number of antisymmetric modes
DELA	Array of lifting surface areas
XIS1	Leading edge location of slender body elements
XIS2	Trailing edge location of slender body elements
NSBEA	Array of the number of slender body elements per body
FORCE	One column of the point force matrix
GF	One column of the generalized force matrix

MNEMONIC	DESCRIPTION
WØRK	Complex work array

Calling Subroutine SDLM

2.13 SUBROUTINE GEOM (DELA, IFLA, NBEA, NTI2, NAS, NASB, ISSTR, NSSTR, NSBEA, NBARAY, NCARAY, NSARAY, AO, YB, ZB, ARB, AVR, AOP, RIA, XLE, XTE, THIA, XIS1, XIS2, X, CG, CS, EE, SG, YS, ZS, XIC, XIJ, YIN, ZIN, DELX, XLAM, COORD, NTAERO, TH, TAU, XII, RI, XIS, RS, GMA, DYS, DZS, GMAR, XI1, XI2, ETA1, ETA2, ZETA1, ZETA2, XC, ETA, ZETA, ETAS, ZETAS, IHD, TEMP, ITEMP)

Functional Description

Subroutine GEOM calculates the geometry array elements for all lifting surface panels and all interference body and slender body elements. The basic geometry arrays are saved in core and are used throughout the program. Those coordinate arrays that are required subsequent to the aero module of VIBRA-6, are saved on the output tape NTAERO.

Input Output Variables

MNEMONIC	DESCRIPTION
NTAERO	Output tape number containing the coordinate arrays for the case
TH	Fractional chordwise divisions for panel
TAU	Fractional spanwise divisions for panel
XII	X-coordinates of the interference body element endpoints
RI	Radii of the interference body element endpoints
XIS	X-coordinates of the slender body element endpoints
RS	Radii of the slender body element endpoints

MNEMONIC	DESCRIPTION
GMA	Dihedral angles for all panels
DYS, DZS	Δy, Δz of panel strips
GMAR	Array of dihedral angles for all strips
XI1, XI2	Inboard, outboard x-coordinates of the 1/4-chord location of all lifting surface boxes
ETA1, ETA2	Inboard, outboard y-coordinates of all lifting surface boxes; also, y-coordinates of all slender body elements (centerline)
ZETA1, ZETA2	Inboard, outboard z-coordinates of all lifting surface boxes; also, z-coordinates of all slender body elements (centerline)
XC	X-coordinates of lifting surface box corners
ETA	Y-coordinates of lifting surface box centerlines
ZETA	Z-coordinates of lifting surface box centerlines
ETAS	Y-coordinates of slender body element centerlines
ZETAS	Z-coordinates of slender body element centerlines
IHD, TEMP, ITEMP	Temporary storage for selected constants and geometry arrays of a case

The following variables are described under Basic Variables in Section VII-3:

DELA, IFLA, NBEA, NT12, NAS, NASB, ISSTR, NSSTR, NSBEA, NBARAY, NCARAY NSARAY, AO, YB, ZB, ARB, AVR, AOP, RIA, XLE, XTE, TH1A, XIS1, XIS2, X, CG, CS, EE, SG, YS, ZS, XIC, XIJ, YIN, ZIN, DELX, XLAM, COORD.

Calling Subroutine SDLM

Called Subroutine GRUP

2.14 SUBROUTINE GRUP(NS, J2, IOLD, IGRUP, MAXSSTR, ISSTR, NSSTR, COORD)

Functional Description

This subroutine calculates the superstrip number of each strip on all lifting surface panels and saves these in an array to be used in subroutine AERØ for the span load calculations. Input/output to this subroutine is via the argument list.

Input Output Variables

MNEMONIC	DESCRIPTION
NS	Number of strips in panel
J2	Strip number of last strip in panel
IOLD	Group number of preceding panel; IØLD=0 for the first panel
IGRUP	Group number of current panel
MAXSTR	Number of superstrips
ISSTR	Superstrip number of each strip
NSSTR	Number of strips per superstrip
COORD	Spanwise coordinate of strips

Calling Subroutine GEOM

2.15 SUBROUTINE GUST (NWT, NWTA, NTOT, NBOX, NB, NBARAY, NCARAY, NBEA, FMACH, KR, CBAR, X, YS, ZS, SG, CG, CR, NG, IPRINT, LINES, NOUT, WGS, WGA, COL, NDW, NMT, NASYM)

Functional Description

This subroutine computes the gust boundary conditions for thirteen symmetric, and thirteen antisymmetric modes according to the equations described in Section II. (See Figure 5).

Input Output Variables

MNEMONIC	DESCRIPTION
NWT	Tape number on which the symmetric gust boundary conditions are saved
NWTA	Tape number on which the antisymmetric gust boundary conditions are saved
NTOT	Number of unknowns
NBOX	Number of boxes (elements) on lifting surfaces
NB	Number of bodies
NBARAY	$nba_p = \sum_{i=1}^{p} (nc_i)(ns_i)$, where p = panel number nc_i = number of chordwise boxes ns_i = number of spanwise strips } in panel i
NCARAY	nc = number of chordwise boxes per panel
NBEA	Number of interfence body elements per body
FMACH	Mach Number

MNEMONIC	DESCRIPTION
KR	Reduced frequency
CBAR	Reference chord
X	3/4-chord x-coordinates of all lifting surface boxes and 1/2-chord x-coordinates of body elements
YS	y-coordinates of strip centerlines and
ZS	z-coordinates of body axes
SG	sine of dihedral angles of strips
CG	cosine of dihedral angles of strips
CR	Array of the direction cosines for the gust boundary conditions
NG	Number of gusts
IPRINT	Print flag
LINES	Maximum lines of print per page
NOUT	Data set number of the system output data set
WGS	One column of the symmetric gust boundary conditions
WGA	One column of the antisymmetric gust boundary conditions
COL	Array for temporary use
NDW	Tape number containing the incremental normalwash ΔW due to slender bodies
NMT	Total number of symmetric and antisymmetric modes
NASYM	Number of antisymmetric modes

Calling Subroutine SDLM

2.17 SUBROUTINE MATMUL(NW, NPSTAP, NBFM, NEWBFZ, NEWBFY, NWORK, NTSBE, NSBETO, LENGTH, NTOT, NMODE, NMODEB, IPRINT, KR, DT, RDT, WORK, RWORK)

Functional Description

Subroutine MATMUL computes the z- and y-forces on all slender body elements and for all modes using the output matrix of subroutine BFSMAT, the solution matrix obtained by subroutine SOLVIT and the $C_{pz}\Delta A$, $C_{py}\Delta A$ columns obtained by subroutine MUZYC. These arrays are input from utility (scratch) tapes. As the matrix multiplication is performed, the resulting body forces are saved in column order on two utility tapes: z-forces on tape NEWBFZ, y-forces on tape NEWBFY.

Input Output Variables

MNEMONIC	DESCRIPTION
NW	Tape number containing the solution matrix (output of SOLVIT)
NPSTAP	Tape number containing the $C_{pz}\Delta A$ and $C_{py}\Delta A$ arrays
NBFM	Tape number containing the output matrix of subroutine BFSMAT
NEWBFZ	Tape number containing the output z-forces
NEWBFY	Tape number containing the output y-forces
NWORK	Dimension of the work array WORK
NTSBE	Length of the $C_{pz}\Delta A$, $C_{py}\Delta A$ arrays
NSBETO	Total number of slender body elements

2.16 SUBROUTINE HATS (XA, YA, XO, YO, LMBDA, X14C, X34C, Y, H14C, H34C, HP, IHAT, IFPRLL, I1I2, NTH, SCOEF, THB)

Functional Description

This subroutine computes elements of the $h_{1/4C}$-, $h_{3/4C}$- and h'- matrix columns for lifting surface boxes in one section of a superpanel. The matrix SCOEF calculated in subroutine SPLN can be used to determine a function f_τ at any value of τ_i.

$$\left\{f(\tau_i)\right\} = \left[\text{SPLINE}_j^{(n)}\right] \left\{C_n\right\}$$

$$= \left[\text{SPLINE}_j^{(n)}\right] \left[\text{SCOEF}\right] \left\{\text{PHI}\right\}$$

$$= [H] \left\{\text{PHI}\right\}$$

This subroutine outputs [H] at the 1/4- and 3/4-chord points of each box of a superpanel. Also output is the derivative of [H] at the 3/4-chord points of the boxes. Notice that $\left[\text{SPLINE}_j^{(n)}\right]$ is different from $\left[\text{SPLINE}_i^{(n)}\right]$. The former is for the nodal points i = 1, 2··· and the latter is for the interpolated points j = 1, 2··· .

Input Output Variables

MNEMONIC	DESCRIPTION
XA, YA	Inboard edge coordinates of elastic beam
XO, YO	Reference coordinates of current section
LMBDA	Λ = sweep angle of elastic beam
X14C	X-coordinate array of the 1/4-chord locations of all lifting surface boxes
X34C	X-coordinate array of the 3/4-chord locations of all lifting surface boxes

MNEMONIC	DESCRIPTION
Y	"Spanwise" coordinate array of all lifting surface boxes.
H14C H34C HP	Array containing a column of the $\begin{Bmatrix} h_{1/4C} \\ h_{3/4C} \\ h' \end{Bmatrix}$ matrix
IHAT	Flag to select h-, α-, or θ-calculations; IHAT = 1 for h, 2 for α, 3 for θ
IFPRLL	Flag to indicate sections of parallel cutting lines when IFPRLL = 1; IFPRLL = 0 otherwise
NPAIR	The number of I1, I2 pairs in the current section of a superpanel.
I1I2	Array of the 'first-, last-box number pairs'
NTH	NTH = NODES+2 = the number of spline coefficients for the current superpanel
SCOEF	Array of spline coefficients for the current superpanels
THB	Array containing the θB_j values for the current superpanel

Calling Subroutine NEWH

MNEMONIC	DESCRIPTION
LENGTH	Column dimension of the output matrix of subroutine BFSMAT
NTOT	Number of unknowns
NMODE	Number of modes
NMODEB	Number of modes on bodies only
IPRINT	Print flag for body element forces ; IPRINT = 0 for no print
KR	Reduced frequency
DT	Temporary complex work array
RDT	Temporary real array equivalent to DT
WORK	Complex work array
RWORK	Temporary real array equivalent to WORK

Calling Subroutine SDLM

2.18 SUBROUTINE MUZYC (H, DHDX, K, NTZY, NFBODY, NLBODY, NSBE, KR, CBAR, AO, AOP, XIS1, XIS2, AR, NTPH, NTPDH, UZY, CPZY, UZYA, CPZYA, NR, FMACH, YB, ZB, CR, NG, H, DHDX)

Functional Description

Subroutine MUZYC calculates the axial doublet strengths and loading for slender bodies both in symmetric and antisymmetric conditions.

Input Output Variables

MNEMONIC	DESCRIPTION
H	Array containing a column of the h-matrix
DHDX	Array containing a column of the dh/dx-matrix
K	Flag for types of mode; K = 2 for z-direction K = 3 for y-direction
NFBODY	Number of first body
NLBODY	Number of last body
NSBE	Array of the number of slender body elements per body
KR	Reduced frequency
CBAR	Reference chord
AO	Array of the slender body element half widths (radii)
AOP	x-derivative of the AO array
XIS1	Leading edge location of the slender body elements
XIS2	Trailing edge location of the slender body elements
AR	Array of the cross-sectional aspect ratios of bodies
NTPH	Tape number (scratch unit) containing the h matrices
NTPDH	Tape number (scratch unit) containing the dh/dx matrices
UZY	A column of the μ_z or μ_y array

MNEMONIC	DESCRIPTION
CPZY	A column of the $C_{pz}\Delta A$ or $C_{py}\Delta A$ array
UZYA	A column of the μ_z or μ_y array for antisymmetric gust
CPZYA	A column of the $C_{pz}\Delta A$ or $C_{py}\Delta A$ array for anti-symmetric gust
NR	Flag for gust calculations
CR	Array of the direction cosines for gust calculations
NG	Number of gusts
FMACH, YB, ZB	See Section VI-3
H, DHDX	Arrays of the h and dh/dx matrices

Calling Subroutine SB

2.19 SUBROUTINE NEWH (NTP5, NTP6, NTAPE, MASTH4, MASTH, MASTDH, NTOT, NYSM, NASYM, NROW, MODES, NBARAY, NP, NCARAY, YS, ZS, Y, X14C, X34C, H34C, HP NODE, XI, ETA, ELXI, ELYI, ELZI, HCOL, PHI, THB, IFP, IPAIR, I1I2, SWORK, WORK, NUDETO, NDOFTO, PHIT, MDOF, NODES)

FUNCTIONAL DESCRIPTION

Subroutine NEWH is the working-main of the h-, α-, θ-calculation subroutines for lifting surcace panels only. It reads card input for all superpanels and calls subroutine SPLN for the calculation of the spline coefficients; it also calls subroutine HATS which calculates the slopes and deflections at all aerodynamic elements due to a unit deflection of each degree of freedom at each node, taken one at a time. That is, HATS produces deflection and slope influence coefficient matrices [H], $[H_{1/4c}]$, [dH/dx]. These influence coefficient matrices are used along with the modal matrix [PHI], in NEWH, to produce the slopes and deflections, [h], $[h_{1/4c}]$, [dh/dx] due to the modes

$$[h] = [H] [PHI]$$

$$[h_{1/4c}] = [H_{1/4c}] [PHI]$$

$$[dh/dx] = [dH/dx] [PHI]$$

Also in NEWH the [PHI] matrix is extracted from the general modal matrix [PHIT]. The [PHIT] matrix contains up to eight degrees of freedom per lifting surface superpanel node, i.e., h, α, θ, f, ℓ, ψ, β, ζ where as [PHI] contains only the up to three values, i.e. h α θ. Also special procedures place the control surface or tab degrees of

freedom, β or δ, into the α degrees of freedom for a control surface superpanel.

The slopes used above are taken at the 3/4-chord point of each box. The deflections are taken at the same point, [h], and also at the 1/4-chord point $[h_{1/4c}]$. These matrices are output on three tapes; [h] is on MASTH, [dh/dx] is on MASTDH and $[h_{1/4c}]$ is on MASTH4 :

Input Output Variables

MNEMONIC	DESCRIPTION
NTP5, NTP6	Reference number of the system input/output data sets (NTP5 = 5, NTP6 = 6 on IBM 370)
NTAPE	Direct access unit on which the h, α, θ columns are stored (temporarily)
MASTH4	Tape number containing the $h_{1/4c}$-columns
MASTH	Tape number containing the $h_{3/4c}$-columns
MASTDH	Tape number containing the dh/dx-columns
NTOT	Total number of lifting surface boxes
NSYM, NASYM	Total number of {symmetric, antisymmetric} modes
MODES	MODES = NSYM + NASYM
NBARAY	$nb_i = \sum_{k=1}^{i} nc_k\, ns_k$, i = 1, NP, where NP = number of panels; nc_k = number of chordwise boxes, ns_k = number of spanwise strips } in panel k
NCARAY	Array of the number of chordwise boxes per panel

MNEMONIC	DESCRIPTION
YS, ZS	Arrays of the y- and z-coordinates per strip
Y	Array of the y-coordinates of all boxes
X14C	Array of the 1/4-chord x-coordinates of all boxes
X34C	Array of the 3/4-chord x-coordinates of all boxes
H14C H34C	Array containing a column of the $\begin{Bmatrix} h_{1/4c} \\ h_{3/4c} \end{Bmatrix}$ matrix
HP	Array containing a column of the dh/dx-(i.e.h') matrix
NODE	Array containing the input node-numbers for any one superpanel
XI, ETA	ξ-, η-arrays (x-and "spanwise" coordinates) of all nodes in any one superpanel
ELXI ELYI ELZI	Arrays $\begin{Bmatrix} \xi \\ \eta \\ \zeta \end{Bmatrix}$ of all nodes for the case
HCOL	Array for the temporary storage of any one of the h (or h') arrays
PHI	Modal matrix
THB	Array containing the θB-column (see subroutine SPLN)
IFP	Array containing the "parallel-flags" of all sections of a superpanel

MNEMONIC	DESCRIPTION
IPAIR	Array containing the number of "first, last" box-pairs in a section for all sections of a superpanel
III2	Array containing the first, last box numbers for all sections and all superpanels
SWORK	Work array
WORK	An NROW by NROW work array
NODETO	Total number of modes
NDOFTO	Total number of degrees of freedom
PHIT	The general modal matrix
MDOF	Maximum number of degrees of freedom per node
NODES	Number of nodes on all superpanels

Calling Subroutine	SDLM
Called Subroutines	ATAN3, CTLS, HATS, SPLN, ZEROUT

2.20 SUBROUTINE ORGN(NTAPE, MASTAP, NSYM, NASYM, NODES, MODES, IROW, COL, PHI, WORK)

Functional Description

Subroutine SPLINE has calculated an interpolation matrix for unit deflections at nodal points taken one at a time, i.e., an interpolation influence coefficient matrix. To obtain the deflection for a set of modes, $[\phi]$, a matrix multiplication must be done.

$[\bar{H}_{1/4}] = [h_{1/4}][\phi]$, $[\bar{H}_{3/4}] = [h_{3/4}][\phi]$, $[d\bar{H}/dx] = [dh/dx][\phi]$

These multiplications must be done for both symmetric and antisymmetric matrices and for lifting surfaces and bodies. Subroutine ORGN performs these matrix multiplications.

Input Output Variables

MNEMONIC	DESCRIPTION
NTAPE	Input tape containing one of the matrices [H]
MASTAP	Output tape containing one of the matrices $[\bar{H}]$
NSYM	Number of symmetric modes
NASYM	Number of antisymmetric modes
NØDES	Number of nodes
MØDES	Total number of modes
IROW	Maximum number of row elements in the [H] matrices
COL	Array for the temporary storage of one column of the [H] matrices
PHI	One column of the modal deflection matrices [PHI]
WORK	Work array containing one of the $[\bar{H}]$ matrices

Calling Subroutine

DOTP

2.21 SUBROUTINE PISTON (NB, NBOX, NSBETO, KR, CBAR, FMACH, NTPH, NTPDH, NTPH4, MASTCP MASTFZ, MASTFY, NEWTPH, NBARAY, NCARAY, NSBEA, YB, ZB, AO, AOP, XIS1, XIS2, CG, SG, EE, YS, ZS, H, DHDX, HP, XC, JRUN, IPRINT, DCP, DCPS, DCPA, DFQ, DFQS, DFQA, IPOINT, NR, CR)

Functional Description

This subroutine is called from subroutine SDLM only if the input item NKP is different from zero. In this case subroutine PISTON is called once for each reduced frequency in the array for which piston theory calculations are specified. It computes pressures on lifting surface boxes, and body z-, y-forces, for all modes and all gusts. The pressure columns are saved on tape MASTCP, while the body z-forces (y-forces) are saved on tape MASTFZ (MASTFY). An input IPOINT, tells whether "average" or "point" pressures and forces are calculated for the blast onset flows. (See Section II.4 for details).

The equations implemented in this subroutine are as follows. Equation (61) is used for lifting surface elements and equation (80) for body elements, for the case of motion dependent forces. Equation (64) and (70) are used for lifting surface elements and equation (84) is used for body elements, for the case of blast gust dependent forces.

Input Output Variables

MNEMONIC	DESCRIPTION
NB	Number of bodies
NBOX	Total number of lifting surface boxes
NSBETO	Total number of slender body elements

MNEMONIC	DESCRIPTION
KR	Reduced frequency
CBAR	Reference chord
FMACH	Mach number
NTPH, NTPDH, NTPH4	Tape number containing {h arrays; dh/dx arrays; $h_{1/4c}$ arrays}
MASTCP	Tape number on which the pressures on lifting surface boxes are saved
MASTFZ, MASTFY	Tape number on which the body {z-forces are saved; y-forces are saved}
NEWTPH	Tape number on which the $h_{1/2c}$ -arrays
H	Array containing a column of the [h] matrix
DHDX	Array containing a column of the [dh/dx] matrix
HP	Array containing a column of the [h'] matrix
XC	A four-dimensional array containing the x-coordinates of the four corners of all lifting surface boxes.
JRUN	Sequence number of the current frequency for which piston theory is used ($1 \leq JRUN \leq NKP$)
IPRINT	Detail print flag; IPRINT > 1 prints all pressures and body element forces
DCP, DCPS	Complex array containing a column of the pressures (ΔCp) on lifting surface boxes due to either a mode or a symmetric gust column.

MNEMONIC	DESCRIPTION
DCPA	Complex array containing a column of the pressures (ΔCp) on lifting surface boxes due to an antisymmetric gust column
DFQ, DFQS,	Complex array containing a column of either the z- or the y-body forces due to a mode, or the z-body forces due to a symmetric gust column.
DFQA	Complex array containing a column of the z-body forces due to an antisymmetric gust column.1 Note that y-bosy forces due to gust columns are stored (temporarily) in arrays DCPS and DCPA
IPOINT	Flag to select point pressures when IPOINT $\neq$ 0
NR, NG	Number of gust columns
CR	The 3 X 20 array containing the gust direction cosines

The following variables are described under Basic Variables in Section VII-3:

NBARAY, NCARAY, NSBEA, YB, ZB, AO, AOP, XIS1, XIS2, CG, SG, EE, YS, ZS.

Calling Subroutine SDLM

2.22 SUBROUTINE ROWDYZ(NFB, NLB, ROW, NTZYS, D, DA, DX, DY, DZ, IRB, BETA, IDZDY, NTAPE, NTAP2, SGR, CGR, IPRNT, NT12, NSBE, AO, YB, ZB, AR, XIS1, XIS2)

Functional Description

This subroutine performs the logic required to set up the argument list for subroutine DZY for the purpose of calculating a row of the D_z or D_y matrix both for symmetric and antisymmetric conditions .

Input Output Variables

MNEMONIC	DESCRIPTION
NFB	First body number
NLB	Last body number
ROW	Row number of the D_z or D_y matrix being calculated
NTZYS	Number of columns to be calculated
D	A row of the D_z or D_y matrix for symmetry
DA	A row of the D_z or D_y matrix for antisymmetry
DX	x-coordinate } of the receiving point
DY	y-coordinate } of the receiving point
DZ	z-coordinate } of the receiving point
BETA	$\beta = \sqrt{1 - M^2}$, M = Mach Number
IDZDY	Flag required for subroutine FLLD
NTAPE	Tape number (scratch unit) on which rows of the symmetric matrix D are saved
NTAP2	Tape number (scratch unit) on which rows of the antisymmetric matrix DA are saved
SGR	Sine } of the receiving point dihedral angle
CGR	Cosine } of the receiving point dihedral angle
IPRNT	Print flag

The following variables are described under Basic Variables in Section VII-3:

NT12, NSBE, AO, YB, ZB, AR, XIS1, XIS2.

Calling Subroutine	DZYMAT
Called Subroutine	DZY

2.23 SUBROUTINE RWREC(IFLAG, NTAPE, A, NCWORD, NUMBR, NEWTAP)

Functional Description

This subroutine reads and/or writes unformatted complex records A of dimension NCWORD on tape according to three options defined by the flag IFLAG.

Input Output Variables

MNEMONIC	DESCRIPTION
IFLAG	Option flag; IFLAG = 0, write A on NTAPE, IFLAG = 1, read A from NTAPE, IFLAG = 2, copy A from NTAPE onto NEWTAP, 'NUMBR' of times
NTAPE	Input/output unit number to use
A	Complex array to be read and/or written
NCWORD	Length of array A
NUMBR	Number of arrays to copy from NTAPE onto NEWTAP when IFLAG = 2; NUMBR = 0 otherwise
NEWTAP	Output unit, when IFLAG = 2; NEWTAP = 0 otherwise

Calling Subroutines

BFSMAT, GENF, MATMUL, SB, SDLM

2.24 SUBROUTINE SB (NM, NSYM, NASYM, NTP6, NTPH, NTPDH, IPRINT, WORK, DW, CPZYA, UZYA, NBEA, NSBE, NC, NS, AO, YB, ZB, AR, AOP, XIS1, XIS2, X, CG, SG, YP, ZP, CR, NG)

Functional Description

Subroutine SB calculates the normalwash at lifting surface boxes and interference body elements due to slender body elements both for symmetric and antisymmetric conditions.

Input Output Variables

MNEMONIC	DESCRIPTION
NM	Total number of modes for bodies
NSYM	Number of symmetric modes
NASYM	Number of antisymmetric modes
NTP6	Data set number of the system output data set
NTPH	Tape number (scratch unit) containing the h matrices
NTPDH	Tape number (scratch unit) containing the dh/dx matrices
IPRINT	Print flag
DW	Array containing a column of the incremental normalwash matrix, [ΔW]
CPZYA	Array containing a column of the[C_{pz} Δ A], or [C_{py} Δ A] matrices
UZYA	Array containing a column of the [M_z] or [M_y] matrices
WORK	Complex work array

MNEMONIC	DESCRIPTION
CR	Array of the direction cosines for gust calculations
NG	Number of gusts

The following variables are described under Basic Variables in Section VII-3:

NBEA, NSBE, NC, NS, AO, YB, ZB, AR, AOP, XIS1, XIS2, X, CG, SG, YP, ZP.

Calling Subroutine: SDLM

Called Subroutines: DUMULT, DZYMAT, MUZYC, READD, RWREC

2.25 SUBROUTINE SDLM (ELXI, ELYI, ELXI, PHIN, PHIZ, PHIY, NODES, NSYM, NASYM, MFIX1, MFIX2, IFNEWH, MDOF, PHI, NAS, NASB, NBARAY, NCARAY, NSARAY, ISSTR, NSSTR, IFLA, NBEA, NT12, NSBEA, YB, ZB, ARB, AVR, XLE, XTE, RIA, TH1A, AO, AOP, XIS1, XIS2, CG, CS, EE, SG, YS, ZS, XIJ, YIN, ZIN, COORD, X, XIC, DELX, XLAM, H, DHDX, DELA, DT, DTA, RHS, XC)

Functional Description

Subroutine SDLM is essentially the main program of the entire aero program segment of VIBRA-6. It first calls the subroutines that generate the basic geometry arrays and deflections, then the rest of the subroutines are called in an overall DO loop on all reduced frequencies.

Input Output Variables

MNEMONIC	DESCRIPTION
ELXI	x-coordinate)
ELYI	y-coordinate } array of the modes
ELZI	z-coordinate)
PHIN	Modal deflection matrix for all nodes on panels
PHIZ	Modal deflection matrix for all nodes on bodies in z-direction
PHIY	Modal deflection matrix for all nodes on bodies in y-direction
NODES	Maximum number of nodes
NSYM	Number of symmetric modes
NASYM	Number of antisymmetric modes

MNEMONIC	DESCRIPTION
MFIX1	Two mode numbers for which aerodynamic
MFIX2	parameters are calculated
IFNEWH	Flag to select degrees of freedom; IFNEWH = 0 for h- alone, IFNEWH ≠ 0 for use of available sectional data
MDOF	The number of degrees of freedom in the sectional data (ϕ - matrix)
PHI	The total modal deflection matrix, [ϕ]
H	Real array for a column of the h matrix
DHDX	Real array for a column of the dh/dx matrix
DT	Complex array for a row of the DT matrix
DTA	Complex array for a row of the DTA matrix
RHS	Complex array for temporary use
XC	X-coordinates of lifting surface box corners

The following variables are described under Basic Variables in Section VII-3:

NAS, NASB, NBARAY, NCARAY, NSARAY, ISSTR, NSSTR, IFLA, NT12, NSBEA, YB, ZB, ARB, AVR, XLE, XTE, RIA, TH1A, AO, AOP, XIS1, XIS2, CG, CS, EE, SG, YS, ZS, XIJ, YIN, ZIN, COORD, X, XIC, DELX, XLAM, DELA.

Calling Subroutine	CSDLM
Called Subroutines	GEOM, SPLINE, DOTP, GEND, BFSMAT, SB, WANDWT, GUST, RHSIDE, SOLVIT, MATMUL, GENF, AERO, RWREC, HEADNG, NEWH, PISTON, ZEROUT

MNEMONIC	DESCRIPTION
I1	Index of first element in the coordinate arrays
I2	Index of last element in the coordinate arrays
NXQ	Number of nodes
LMAX	Maximum dimension of the coordinate arrays
X1L	3/4-chord } x-coordinates of panel boxes
X2L	1/4-chord }
X3L	x-coordinates of body element endpoints
YL	y-coordinates of panel boxes
XP	The extracted x-coordinate array for the current superbody/superpanel
YP	The extracted y-coordinate array for the current superpanel; YP = 0 for superbodies
H	One column of the [h] matrix
DHDX	One column of the [dh/dx] matrix
ISP	Not used
NSBP	Not used
NBCUM	$nba_i = \sum_{b=1}^{i} (NSBE_b + 1)$ for all bodies, i = 1, NB
NPCUM	$npa_i = \sum_{p=1}^{i} (nc_p)(ns_p)$ for all panels, i = 1, NP

where nc_p = the number of chordwise boxes in panel p

ns_p = the number of spanwise strips in panel p

2.26 SUBROUTINE SORT(IF1, IF2, NSUP, INSUP, I1, I2, NXQ,
LMAX, X1L, X2L, X3L, YL, XP, YP, H, DHDX,
ISP, NSBP, NBCUM, NPCUM, NTPH, NTPDH,
NTPSH, KPRINT, NTP6, KCUM1, KCUM2, KCUM3,
NTOT, ISORT, NODE, SUPRH, SUPRDH)

Functional Description

Subroutine SORT has a dual role: it extracts the coordinates of all points in the current superbody/superpanel when it is called from subroutine SPLINE with the flag ISORT set to 1, while on the second call, when ISØRT=2, it expands the h and dh/dx columns, generated by subroutine SPL2 for one superbody/superpanel, into full h and dh/dx columns and saves these on the output tape NTPSH.

Input Output Variables

MNEMONIC	DESCRIPTION
IF1	Flag to select either surface spline (IF1 = 0) or linear spline (IF1 = 1)
IF2	Flag to choose 1/4-chord x-coordinates for superpanels, when IF2 = 1. IF2 = 0 means that 3/4-chord x-coordinates are used for superpanels, and body element endpoints for superbodies.
NSUP	Number of bodies/panels in superbody/superpanel
INSUP	Array of bodies/panels in superbody/superpanel.

MNEMONIC	DESCRIPTION
NTPH	Tape number containing the h columns for a superbody/superpanel
NTPDH	Tape number containing the dh/dx columns for a superbody/superpanel
NTPSH	Tape number containing the expanded (full) h and dh/dx arrays
KPRINT	KPRINT = 1 prints the h and dh/dx arrays; KPRINT = 0 no print
NTP6	The data set number of the system output data set
KCUM1	Column number of the h-arrays
KCUM2	Column number of the dh/dx-arrays
KCUM3	Column number of the h-arrays for 1/4-chord x-coordinates
NTOT	Length (dimension) of the expanded h and dh/dx arrays
ISORT	Flag that selects one of the two segments in subroutine SORT; ISORT = 1 branches to segment 1, the coordinate-extractor, ISORT = 2 branches to segment 2, the h- and dh/dx-expander
SUPRH	Array containing a column of the [h] matrices
SUPRDH	Array containing a column of the [dh/dx] matrices
NODE	Array of node numbers

Calling Subroutine SPLINE

2.27 SUBROUTINE SPLINE (MASTH, MASTDH, MASTH4, NMODEB, NMODE, ELXI, ELYI, ELZI, WORK NSBEA, NBARAY, NCARAY, NSARAY, XIS1, XIS2, X, CG, SG, YS, ZS, XIC, PHI, PHIZ, PHIY, MDOF, NØDES, NMØDES, NDOFB , IFNEWH, XIJ, NBCUM, INSUP, NODE, XIQ, ETAQ, CSG, X3L, YL, XP , YP, H, DHDX)

Functional Description

The four subroutines SPLINE, SORT, SPL1, SPL2, constitute a surface spline interpolation procedure based on the method of Harder and Desmarais (Reference 9). The equations used in this procedure are documented in Section II.3. A set of interpolation functions are used whose coefficients are found in SPL1. The slopes, dh/dx, and deflections, h, are then determined at specified points (XP, YP) in SPL2 using these functions and coefficients. Subroutine SPLINE organizes the arguments for the three called subroutines SORT, SPL1 and SPL2. It also saves the final h and dh/dx matrices on tapes for all body nodes (if any), then for all panel nodes.

Input Output Variables

MNEMONIC	DESCRIPTION
MASTH	Tape number containing the [h] matrices for bodies and panels
MASTDH	Tape number containing the [dh/dx] matrices for bodies and panels
MASTH4	Tape number containing the $[h_{1/4c}]$ matrix for panels
NMODEB	Number of columns in the [h] matrix for bodies
NMODE	Number of columns in the [h] matrix for panels

MNEMONIC	DESCRIPTION
ELXI	x-coordinate
ELYI	y-coordinate } array of the nodes
ELZI	z-coordinate
WORK	Work array
PHI	The total modal deflection matrix, $[\phi]$
PHIZ	Modal deflection matrix for all nodes on bodies in z-direction
PHIY	Modal deflection matrix for all nodes on bodies in y-direction
MDOF	The number of degrees of freedom in the ϕ matrix
NODES	The total number of nodes
NMODES	The total number of modes
NDOFB	The number of degrees of freedom for body bays
IFNEWH	Flag to select degrees of freedom; see subroutine SDLM
NBCUM	$nb_i = \sum_{j=1}^{i} (nsbe_j+1)$, i = 1, NB where $nsbe_j$ is the number of slender body elements in body j
INSUP	Array of the body-numbers/panel-numbers in the current superbody/superpanel
NODE	Array of node numbers in the current superbody/superpanel
XIQ	x-coordinate array of the nodal points in the current superbody/superpanel

MNEMONIC	DESCRIPTION
ETAQ	y-coordinate array of the nodal points in the current superbody/superpanel
CSG	Cosines of the modified dihedral angles of strips
X3L	Array of the slender body element end points in the current superbody
YL	y-coordinate array of all elements in the current superbody
XP, YP	x, y-coordinates of all lifting surface boxes in the current superpanel
H	A column of the h matrix
DHDX	A column of the dh/dx matrix

The following variables are described under Basic Variables in Section VII-3:

NSBEA, NBARAY, NCARAY, NSARAY, XIS1, XIS2, X, CG, SG, YS, ZS, XIC, XIJ.

Calling Subroutine SDLM

Called Subroutines SORT, SPL1 and SPL2

2.28 SUBROUTINE SPLN (SPLINE, SCOEF, THB, XI, ETA, XA, YA, XB, YB, NODES, NDIM, IPRINT, NTP6)

Functional Description

This subroutine calculates the coefficients to be used in HATS for interpolation of h, α and θ along the elastic axis (along τ). Influence coefficient type of modes are used. That is coefficients are calculated for unit deflections of the variable to be interpolated, one node at a time. The unit deflection matrix [T] is given by equation (89) and includes a linear extrapolation to the elastic axis end point. The one dimensional version of the Harder and Desmaris spline curve used is:

$$f(\tau) = C_1 + C_2\tau + \sum_{n=3}^{N} C_n (\tau-\tau_n)^2 \ln (\tau-\tau_n)^2$$

The coefficients C_n can be determined if $f(\tau)$ is known at N + 2 points,

i.e., τ_i, i = 1, 2 N + 2

or, $\{f(\tau_i)\} = [\text{SPLINE}\ {}^{(n)}_{i}]\ \{C_n\}$

But, $\{f\} = [T]\ \{PHI\}$

$$\{C_n\} = [\text{SPLINE}]^{-1}\ [T]\ \{PHI\}$$

$$\{C_n\} = [\text{SCOEF}]\ \{PHI\}$$

The subroutine outputs [SCOEF] to be used later in HATS.

Input Output Variables

MNEMONIC	DESCRIPTION
SPLINE	The NDIM by NDIM matrix [SPLINE]
SCØEF	The NDIM by NØDES matrix of spline coefficients
THB	Array containing the θ B_j values for a superpanel
XI, ETA	The ξ- η- arrays for a superpanel

MNEMONIC	DESCRIPTION
XA, YA	Inboard } coordinates of elastic beam
XB, YB	Outboard }
NØDES	Number of nodes in the current superpanel
NDIM	NDIM = NØDES + 4
IPRINT	Print flag; IPRINT = 2 prints the [SPLINE] and [SCØEF] matrices
NTP6	Reference number of the system output data set

Calling Subroutine NEWH

Called Subroutine MIS1

SUBROUTINE SPL1(IF1, NXQ, LMAX, NTP1, NTP6, XIQ, ETAQ, RHS, XKD, IXCON, IYCON, NMAX)

Functional Description

Equations 36 and 39 are solved in this subroutine. Consider these equations together:

$$\begin{Bmatrix} 0 \\ \Delta \end{Bmatrix} = [KD] \begin{Bmatrix} a \\ F \end{Bmatrix}$$

where

$$[KD] = \begin{bmatrix} B & P_k^T \\ P_k & R_{k\ell} \end{bmatrix}$$

This set of equations is solved using unit solutions:

$$\begin{Bmatrix} 0 \\ \Delta \end{Bmatrix} = \begin{bmatrix} 0 \\ I \end{bmatrix} \{\Delta\}$$

$$\begin{Bmatrix} a \\ F \end{Bmatrix} = [CMAT] \{\Delta\}$$

Placing these in the first equation gives:

$$\begin{bmatrix} 0 \\ I \end{bmatrix} = [KD] [CMAT]$$

This subroutine solves for CMAT. Using the relation between $\begin{Bmatrix} a \\ F \end{Bmatrix}$ and $\{\Delta\}$ shows that

$$[CMAT] = \begin{bmatrix} I_{a_\Delta} \\ I_{F_\Delta} \end{bmatrix}$$

See equations 41b and 42c.

Input Output Variables

IF1	Flag to select either surface spline (IF1 = 0) or linear spline (IF1 = 1)
NXQ	Number of nodes in the current superbody/superpanel

MNEMONIC	DESCRIPTION
LMAX	Not used
NTP1	Utility (scratch) tape number
NTP6	The data set number of the system output data set
XIQ	x-coordinates of the nodal points
ETAQ	y-coordinates of the nodal points
RHS	Matrix of a set of unit deflections for which the matrix equation is solved by subroutine MIS1
XKD	Influence coefficient matrix
IXCON	Constant flags for superbodies; IXCON = 1, x=constant; IXCON=0 otherwise;
IYCON	IYCON = 1, y=constant; IYCON=0 otherwise
NMAX	The row- and column-dimensions of the square matrices RHS and XKD

Calling Subroutine	SPLINE
Called Subroutine	MIS1

2.30 SUBROUTINE SPL2(IF1, IF2, NXQ, LMAX, NTP2, NTP3, NTP6, KPRINT, NTPH, NTPDH, I2, XP, YP, XIQ, ETAQ, XKF, DKFDX, CMAT, SUM, NMAX)

Functional Description

This subroutine finds {h} and {dh/dx} at the points to be interpolated knowing the coefficients [CMAT] determined in subroutine SPL1. This subroutine calculates $[I_{jk}]$ and $[\partial I_{jk}/\partial x_j]$ (see Eqs. (47) and (48), as follows:

$$[I_{jk}] = [KF]\,[CMAT]$$

$$\left[\frac{\partial I_{jk}}{\partial x}\right] = [DKFDX]\,[CMAT]$$

where

$$[KF] = [P_j\ R_{j\ell}]$$

$$[DKFDX] = [\partial P_j/\partial x\ \ \partial R_{j\ell}/\partial x]$$

Input Output Variables

MNEMONIC	DESCRIPTION
IF1	Flag to select either surface spline (IF1 = 0) or linear spline (IF1 = 1)
IF2	IF2 = 1 bypasses the dh/dx calculations when the 1/4-chord x-coordinates are used for panel boxes; IF2 = 0 otherwise
LMAX	Maximum dimension of the aero coordinate arrays XP, YP for the current superpanel
NTP2	Utility (scratch) tape number
NTP3	Utility (scratch) tape number
NTP6	The data set number of the system output data set

MNEMONIC	DESCRIPTION
KPRINT	Print flag; KPRINT = 1, print the h and dh/dx columns, KPRINT = 0, no print
NTPH	Tape number containing the h columns
NTPDH	Tape number containing the dh/dx columns
I2	Index of the last element in the XP, YP arrays
XP	x-coordinate } array of the aero points in the current superpanel/superbody
YP	y-coordinate }
XIQ	x-coordinate } array of the nodal points in the current superpanel/superbody
ETAQ	y-coordinate }
XKF	The KF-matrix
DKFDX	The DKDF-matrix
CMAT	Matrix of the set of coefficients calculated in subroutine SPL1
SUM	Result of the matrix multiplication, i.e., one of the matrices [h] or [dh/dx]
NMAX	Column dimension of the matrix SUM; Row and column dimension of the matrix CMAT

Calling Subroutine SPLINE

2.31 SUBROUTINE SUBB(KB, KS, I, J, JZ, JB, LB, LS, NDY, NYFL, FLND, FLNE, PI, EPS, SGR, CGR, SGS, CGS, AR, SL, CL, TL, FL, BETA, SUM, YB, ZB, RIA, X, YS, ZS, DELX)

Functional Description

Subroutine SUBB computes the downwash factor matrix elements for all receiving points, and all sending points on interference bodies, one element at a time, both for symmetric conditions and for antisymmetric conditions. The results of the calculations are returned to the calling routine in the array SUM via the argument list.

Input Output Variables

MNEMONIC	DESCRIPTION
KB	Index of receiving body. 0 when receiving point is on panel
KS	Strip number in which receiving point lies
I	Receiving point index (row number of DT matrix)
J	Sending point index (column number of DT matrix)
JZ	Not used
JB	Sending body element number
LB	Sending body number
LS	Index of sending element y- and z-coordinates
NDY	Body flag; NDY = 1 for sending points in y-oriented bodies, NDY = 0 otherwise
NYFL	NYFL = 0 for DYP and DYZ elements, NYFL = 1 for DYY elements
FLND	Not used
FLNE	Ground effect flag
PI	π = 3.14159

MNEMONIC	DESCRIPTION
EPS	$\varepsilon = 0.00001$
SGR	Sine of receiving point dihedral angle
CGR	Cosine of receiving point dihedral angle
SGS	Sine of sending point dihedral angle
CGS	Cosine of sending point dihedral angle
AR	Cross-sectional aspect ratio of receiving body
SL	$\sin\lambda = 0$
CL	$\cos\lambda = 1$
TL	$\tan\lambda = 0$
FL	Reference chord
BETA	$\beta = \sqrt{1 - M^2}$, where M = Mach Number
SUM	One element of the DT matrix, and one element of the DTA matrix, for sending points on an interference body

The following variables are described under Basic Variables in Section VII-3: YB, ZB, RIA, X, YS, ZS, DELX.

Calling Subroutines	DZPY, DYPZ
Called Subroutine	DZY

2.32 SUBROUTINE SUBP(I, L, LS, J, IO, IR, NBXS, NCPNB, SGR, CGR, YREC, ZREC, SUM, NCARAY, YB, ZB, ARB, AVR, XLE, XTE, X, CG, EE, SG, YS, ZS, XIC, DELX, XLAM, SCALER)

Functional Description

Subroutine SUBP computes the downwash factor elements, DP_{ij}, for symmetric conditions, and DPA_{ij} for antisymmetric conditions, for all receiving points i on panels and interference body elements, and sending points j on panels, one element at a time. The results of the calculations are returned to the calling routine in the array SUM via the argument list.

Input Output Variables

MNEMONIC	DESCRIPTION
I	Receiving point index
L	Panel number } in which the sending point lies
LS	Strip number }
J	Column number of DP matrix
IO	Chordwise box number that corresponds to sending point j
IR	Sending point index
NBXS	The number of boxes on the panel in which the sending point lies plus the total number of boxes of the preceding panels
NCPNB	The number of boxes in the first strip of the panel in which the sending point lies plus the total number of boxes of the preceding panels
SGR	sine } of the dihedral angle of the receiving strip
CGR	cosine }

MNEMONIC	DESCRIPTION
YREC	y-coordinate } of receiving points
ZREC	z-coordinate }
SUM	One element of the DP matrix and one element of the DPA matrix
SCALER	Nondimensional image radius

The following variables are described under Basic Variables in Section VII-3:

NCARAY, YB, ZB, ARB, AVR, XLE, XTE, X, CG, EE, SG, YS, ZS, XIC, DELX, XLAM :

Calling Subroutines	DPPS, DPZY
Called Subroutines	SNPDF, INCRO, SUBI

2.33 SUBROUTINE WANDWT(IPRINT, LINES, NOUT, NTOT, NBOX, NB, NDW, NTAPH, NTPDH, NWT, NWTA, REFC, KR, H, DHDX, W, DW, COL)

Functional Description

This subroutine calculates the complex downwash boundary conditions, W, on the lifting surfaces due to lifting surface motion, and combines these with the normalwash, ΔW, due to the slender bodies. Both symmetric and antisymmetric motions are considered. The normalwash matrix for symmetry, WT, is saved on tape NWT, the one for antisymmetry, WTA, is saved on tape NWTA.

Input Output Variables

MNEMONIC	DESCRIPTION
IPRINT	Print flag
LINES	Maximum number of lines per page
NOUT	Data set number of the system output data set
NTOT	Number of unknowns
NBOX	Number of lifting surface boxes
NB	Number of bodies
NDW	Tape number containing the ΔW matrix
NTAPH	Tape number containing the h matrix
NTPDH	Tape number containing the dh/dx matrix
NWT	Tape number on which the WT matrix (normalwash columns for symmetry) is written
NWTA	Tape number on which the WTA matrix (normalwash columns for antisymmetry) is written
REFC	Reference chord
KR	Reduced frequency

MNEMONIC	DESCRIPTION
H	A column of the h matrix
DHDX	A column of the dh/dx matrix
W	A column of the W matrix
DW	A column of the ΔW matrix
COL	Complex array for temporary storage

Calling Subroutine SDLM

2.34 SUBROUTINE ZEROUT(WORK, LENGTH, LOOP, ITAPE)

Functional Description

This subroutine initializes the complex array WORK of dimension LENGTH to zeroes. Also, this array of zeroes in WORK may be written on tape ITAPE 'LOOP' times whenever the arguments LOOP and ITAPE have non-zero values.

Input Output Variables

MNEMONIC	DESCRIPTION
WORK	Complex work array
LENGTH	Length of array WORK
LOOP	The number of zero arrays to be written on the output unit ITAPE
ITAPE	Output unit number

Calling Subroutine	GENF, SB, SDLM

3. BASIC VARIABLES

The following variables are used throughout the aerodynamics module of program VIBRA-6.

MNEMONIC	DESCRIPTION
NB	Number of bodies
ND	ND = 0
NE	ε, ground effect flag
NP	Number of panels
NBY	Number of y-oriented bodies
NBZ	Number of z-oriented bodies
NTO	NTO = NTP + NTZ + NTY (see below)
NTP	Total number of lifting surface boxes
NTY	Number of y-oriented interference body elements
NTZ	Number of z-oriented interference body elements
NTYS	Number of y-oriented slender body elements
NTZS	Number of z-oriented slender body elements
MAXGR	Number of components (groups of panels)
MAXSTR	Number of superstrips on all panels
NSBETO	Total number of slender body elements
NSTRIP	Number of lifting surface strips
KR	Reduced frequency
XM	Moment axis
REFA	Reference area; usually area of both wings
REFC	Reference chord

MNEMONIC	DESCRIPTION
REFS	Reference semispan
FMACH	Mach Number
LINES	Maximum number of print lines per page
NAS	Number of associated bodies per panel
NASB	Associated body numbers for all panels
NBARAY	$nba_i = \sum_{j=1}^{i} nc_j\, ns_j$, $i = 1, NP$ (see below)
NCARAY, NC	nc_i = number of chordwise boxes per panel, $i = 1, NP$
NSARAY, NS	ns_i = number of spanwise strips per panel, $i = 1, NP$
ISSTR	Superstrip number of each strip
NSSTR	Number of strips per superstrip
IFLA	Sequence numbers of the first and last body element per body
NBEA	Number of interference body elements per body and their z-y orientation flags
NT12	Number of μ-points (on interference body elements) per body
NSBEA, NSBE	Number of slender body elements per body
YB	y-coordinate array of body centerlines
ZB	z-coordinate array of body centerlines
ARB	Cross-sectional aspect ratio per body
AVR	Average characteristic half-width per body
XLE	Leading edge x-coordinate per body

MNEMONIC	DESCRIPTION
XTE	Trailing edge x-coordinate per body
RIA	Body interference element radii
TH1A	Array of the TH1-values (angular orientation) for all bodies
TH2A	Zero array
AO	Slender body element half-widths (y-direction); radii for circular cross sections
AOP	x-derivative of the AO values for all slender body elements
XIS1	Leading edge x-coordinates of slender body elements
XIS2	Trailing edge x-coordinates of slender body elements
CG	Cosine of the dihedral angles of all strips
CS	Chord-length of strips
EE	Half-width of strips
SG	Sine of the dihedral angles of all strips
YS	y-coordinate of strip centerlines and body elements
ZS	z-coordinate of strip centerlines and body elements
XIJ	x-coordinate of leading edge of strip centerlines
YIN	y-coordinate of inboard edge of panel
ZIN	z-coordinate of inboard edge of panel
COORD	Spanwise coordinate of strips
X	3/4-chord x-coordinates of all lifting surface bodies and interference body element midpoints
XIC	1/4-chord x-coordinates of all lifting surface boxes

MNEMONIC	DESCRIPTION
DELX	Average chord-lengths of all lifting surface boxes and interference body element lengths
XLAM	Tangent of the sweep angle of the 1/4-chord line (bound vortex) of all lifting surface boxes
DELA	Lifting surface box areas

REFERENCES

1. Hobbs, N. P., Zartarian, G., and Walsh, J. P., A Digital Computer Program for Calculating the Blast Response of Aircraft to Nuclear Explosions, Air Force Weapons Laboratory, Report No. AFWL-TR-70-140, Vol. I, April 1971.

2. Albano, E., and Rodden, W. P., "A Doublet-Lattice Method for Calculating Lift Distributions on Oscillating Surfaces in Subsonic Flows," AIAA J., Vol. 7, No. 2, pp. 279-285, and No. 11, p. 2192, 1969.

3. Giesing, J. P., Kalman, T. P., and Rodden, W. P., Subsonic Unsteady Aerodynamics for General Configurations; Part I - Direct Application of the Nonplanar Doublet-Lattice Method, Air Force Flight Dynamics Laboratory, Report No. AFFDL-TR-71-5, Part I, November 1971.

4. Giesing, J. P., Kalman, T. P., and Rodden, W. P., Subsonic Unsteady Aerodynamics for General Configurations; Part II - Application of the Doublet-Lattice Method and the Method of Images to Lifting-Surface/ Body Interference, Air Force Flight Dynamics Laboratory, Report No. AFFDL-TR-71-5, Part II, April 1972.

5. Giesing, J. P., Kalman, T. P., and Rodden, W. P., "Subsonic Steady and Oscillatory Aerodynamics for Multiple Interfering Wings and Bodies," J. Aircraft, Vol. 9, No. 10, pp. 693-702, 1972.

6. Giesing, J. P., Rodden, W. P., and Stahl, B., "Sears Function and Lifting Surface Theory for Harmonic Gust Fields", J. Aircraft, Vol. 7, No. 3, pp. 252-255, 1970.

7. Zartarian, G., Application of the Doublet-Lattice Method for Determination of Blast Loads on Lifting Surfaces at Subsonic Speeds, Air Force Weapons Laboratory, Report No. AFWL-TR-72-207, January 1973.

8. Ashley, H., and Zartarian, G., "Piston Theory - A new Aerodynamic Tool for the Aeroelastician", J. Aero. Sci., Vol. 23, No. 12, pp. 1109-1118, 1956.

9. Harder, R.L., and Desmarais, R.N., "Interpolation Using Surface Splines", J. Aircr., Vol. 9, No. 2, pp. 189-191, 1972.

10. Miles, J.W., The Potential Theory of Unsteady Supersonic Flow, Cambridge: At the University Press, 1959.

11. Giesing, J.P., and Kalman, T.P., Aerodynamic Loads on Advanced Fighter Aircraft, Air Force Flight Dynamics Laboratory, Report No. AFFDL-TR-73-45, October 1973.

12. Lomax, H., Heaslet, M.A., and Sluder, L., "The Indicial Lift and Pitching Moment for a Sinking or Pitching Two-Dimensional Wing Flying at Subsonic or Supersonic Speeds", *NACA TN 2403, July 1951.*

13. Drischler, J.A., and Diederich, F.W., "Lift and Moment Responses to Penetration of Sharp - Edged Traveling Gusts, with Application to Penetration of Weak Blast Waves", NACA TN 3956, May 1957.

14. Goodman, T.R., and Sargent, T.P., "Some Evidence Justifying the Representation of Blasts as Traveling Gusts", J. Aero. Sci., Vol. 26, No. 9, p. 608, 1959.

APPENDIX A

THE BLAST ONSET PRESSURE FIELD

The analyses of References 13 and 14 show that the loads induced by the diffraction of a blast wave about a thin airfoil are equivalent to those obtained when only the travelling gust part of the problem is considered. Quoting Reference 14, "It is the purpose of this note to show that when a blast wave of any magnitude is represented by a travelling gust and the impulse is computed using apparent-mass concepts, the result is equivalent to accounting for diffraction of the blast wave". The article then shows that the apparent-mass concept (acoustic theory) lies within 10% of the correct value for blast waves ranging in strength from acoustic (weak) to infinitely strong.

The above conclusion can be understood more clearly if basic acousitc theory is considered. First, it should be stated that the gust or velocity field and the overpressure field are just different aspects of the blast wave and are not independent. The velocity field can be obtained from the pressure field and vice versa. Acoustic problems are solved, in general, as follows. The incoming wave creates an onset flow at the aircraft surface. This onset flow is not really fundamentally different from any other onset flow field, e.g., a flow at an angle of attack. A disturbance flow must be generated at the surface so that the sum of the two (i.e., the onset and disturbance flow) produces streamlines that pass around the body and thus

---

13. Drischler, J.A., and Diederich, F.W., "*Lift and Moment Responses to Penetration of Sharp - Edged Traveling Gusts, with Application to Penetration of Weak Blast Waves*", NACA TN 3956, May 1957.

14. Goodman, T.R., and Sargent,T.P., "*Some Evidence Justifying the Representation of Blasts as Traveling Gusts*", J.Aero. Sci., Vol. 26, No. 9, p. 608, 1959.

satisfy the body boundary condition of no flow through the body surface. The final pressure field is then obtained by adding the pressure fields from the onset and disturbance flows. For a lifting surface the disturbance pressure takes a jump across the surface at all times, whereas the onset flow does not. The difference in pressure across the surface of the onset flow depends on the thickness of the surface and the gradient of the pressure field.

The conclusion reached in Reference 14 is that the onset pressure field does not affect the surface to any noticeable degree and that the disturbance pressure field (called added-mass effect) contains all of the lifting effect. It is postulated that the reason for this conclusion depends on the fact that a "thin" airfoil was the surface considered. To be completely accurate the lift induced by the onset pressure field should be added, however small it may be.

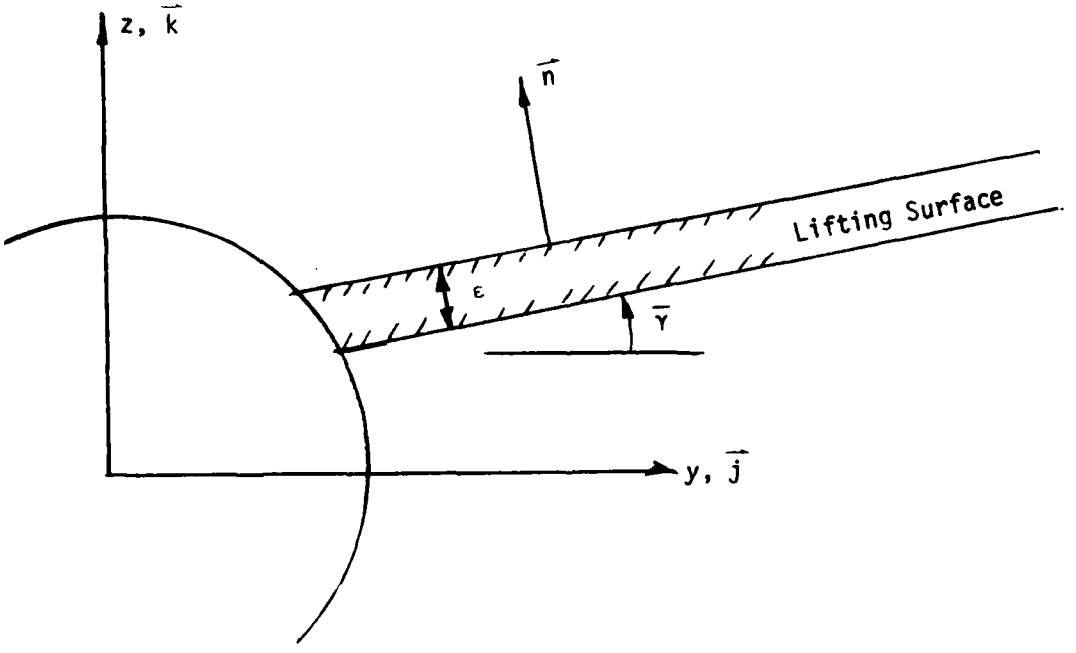

Figure A 1 Wing Geometrical Variables

Consider Figure 37. The jump in pressure across the surface is given in terms of the pressure gradient normal to the surface $\partial P/\partial n$ and the surface thickness ε as follows:

$$\Delta C_p = \frac{\varepsilon}{q} \frac{\partial P}{\partial n}$$

$$= \frac{\varepsilon}{q} \frac{\partial P}{\partial \ell} \left(\frac{\partial \ell}{\partial z} \cos\bar{\gamma} - \frac{\partial \ell}{\partial y} \sin\bar{\gamma} \right)$$

In the frequency domain the overpressure is given by:

$$P = P_o \exp\left(-i2kR\ell/\bar{c}\right)$$

where

$$R = M_\infty/(1 + M_\infty \cos\alpha)$$

$$\ell = x \cos\alpha + y \cos\beta + z \cos\gamma$$

and

$$\frac{\partial \ell}{\partial z} = \cos\gamma; \quad \frac{\partial \ell}{\partial y} = \cos\beta$$

and $\cos\alpha$, $\cos\beta$ and $\cos\gamma$ are the direction cosines of the blast orientation. The final result for ΔC_p is then,

$$\Delta C_p = - \varepsilon \frac{P_o}{q} \frac{i2kR}{\bar{c}} \left(\cos\gamma \cos\bar{\gamma} - \cos\beta \sin\bar{\gamma}\right) \exp\left(-i2kR\ell/\bar{c}\right)$$

The surface loading due to the onset pressure field is proportional to ε, the surface thickness, and is therefore usually small for conventional aircraft wings. Even though it is small, however, it should be retained in the analysis.

The loading across a fuselage may now be considered. Let $\partial F/\partial x$

AD-A106 481 DOUGLAS AIRCRAFT CO LONG BEACH CA F/G 18/3
NUCLEAR BLAST RESPONSE COMPUTER PROGRAM, VOLUME II, DOUBLET-LAT--ETC(U)
AUG 81 J P GIESING, T P KALMAN, W P RODDEN DNA001-75-C-0216
UNCLASSIFIED AFWL-TR-81-32-VOL-2 NL

be the force (normalized by dynamic pressure) on a fuselage cross section in the direction of motion of the blast wave. This force is the result of integrating the onset pressure field around a circle and is given by:

$$\frac{\partial F}{\partial x} = \frac{1}{q} \int_0^{2\pi} p \, (\vec{n} \cdot \underset{\sim}{\vec{k}}) \, a \, d\theta$$

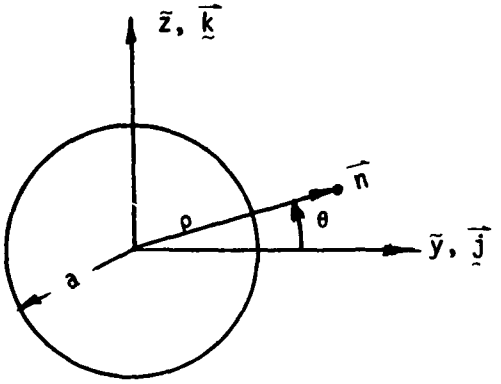

Figure A-2 Body Geometrical Variables

where, in Figure 38, $\tilde{z}$ is in the direction of the blast and $\tilde{y}$ is parallel to the blast wave front centered on the body axis. The quantities of interest in the integral are:

$$\vec{n} \cdot \underset{\sim}{\vec{k}} = (\underset{\sim}{\vec{j}} \cos\theta + \underset{\sim}{\vec{k}} \sin\theta) \cdot \underset{\sim}{\vec{k}} = \sin\theta$$

$$p = p_0 \exp(-i2kR\ell/\bar{c})$$

$$\bar{\ell} = x \cos\alpha + Y_c \cos\beta + Z_c \cos\gamma$$

$$\ell = z \cos\tilde{\alpha} + \bar{\ell}$$

where

$$\cos\tilde{\gamma} = \sqrt{\cos^2\beta + \cos^2\gamma}$$

and $\tilde{z} = a \sin\theta$. The quantities Y_c, Z_c are the coordinates of the fuselage center in aircraft coordinates. Then $\frac{\partial F}{\partial x}$ becomes

$$\frac{\partial F}{\partial x} = a \frac{P_o}{q} \exp(-i2kR\bar{\ell}/\bar{c}) \int_0^{2\pi} e^{\frac{-i2kRa \cos\tilde{\gamma} \sin\theta}{\bar{c}}} \sin\theta \, d\theta$$

or, upon noting that $\sin(\theta + \pi) = -\sin\theta$, one obtains:

$$\frac{\partial F}{\partial x} = -a \frac{P_o}{q} \exp(-i2kR\bar{\ell}/\bar{c}) \int_0^{\pi} 2i \sin\theta \sin\left(\frac{2kRa \cos\tilde{\gamma} \sin\theta}{\bar{c}}\right) d\theta$$

The integral can be expressed as a Bessel function since

$$\frac{d J_n(X)}{d X} = -\frac{1}{\pi} \int_0^{\pi} \sin(X \sin\theta - n\theta) \sin\theta \, d\theta$$

Thus, if $n = 0$ and $X = 2kRa \cos\bar{\gamma}/\bar{c}$, then $\frac{\partial F}{\partial x}$ becomes:

$$\frac{\partial F}{\partial x} = a \frac{P_o}{q} \exp(-i2kR\bar{\ell}/\bar{c}) \, 2\pi i \frac{dJ_0(X)}{dX}$$

and after differentiating the Bessel function, the final result is:

$$\frac{\partial F}{\partial x} = -a \frac{P_o}{q} \, 2\pi i \, J_1(2kRa \cos\bar{\gamma}/\bar{c}) \exp(-i2kR\bar{\ell}/\bar{c})$$

The force per unit length in the $\bar{y}$ direction (parallel to the blast front) is zero since the pressure does not vary in that direction. Thus, the force per unit length in any direction can be obtained. Specifically, the running loads in the z- and y-directions are:

$$\frac{\partial F_z}{\partial x} = \frac{\partial F}{\partial x} \frac{\cos\gamma}{\cos\tilde{\gamma}}$$

$$\frac{\partial F_y}{\partial x} = \frac{\partial F}{\partial x} \frac{\cos\beta}{\cos\tilde{\gamma}}$$

Currently, the aerodynamics module calculates only loadings due to the "disturbance flow". This module can be modified to produce "onset

flow" loadings as well. The "onset flow" loadings would be passed to the frequency response and unit gust load modules and unit solutions generated in the same fashion as presently done for the "disturbance flow". These solutions would then pass to the blast and time response modules for multiplication with the Fourier transforms of the gust velocity and onset pressure time histories. The inverse transform summation of the two resulting frequency response solutions would then yield the time history of the loads and responses to the total loading.

SYMBOLS

A	Reference area (full area)
a	Body radius
AR	Aspect ratio of body cross-section (=height/width)
b	Wing span
c	Local chord length
$\bar{c}$	Reference chord length
C_ℓ	Rolling moment coefficient (Rolling Moment)/$\bar{q}$Ab
C_M	Pitching moment coefficient (Pitching Moment)/$\bar{q}A\bar{c}$
C_y	Lateral force coefficient (Lateral Force)/$\bar{q}$A
C_z	Vertical force coefficient (Vertical Force)/$\bar{q}$A
DLM	Doublet-Lattice Method
e	Strip semi width
$\frac{\partial F_y}{\partial x}$, $\frac{\partial F_z}{\partial x}$	Running load (normalized by $\bar{q}$) on bodies in y and z directions
f	Frequency in HZ or cps. $f = \frac{\omega}{2\pi}$
$G(\xi)$	Gust particle velocity profile as a function of distance of penetration, ξ
G_o	Fourier transform of $G(\xi)$
G	Symmetry factor for lifting surfaces that lie in the symmetry plane
g	Symmetry factor for bodies that lie in the symmetry plane, also gust frequency response
h,α,θ	Modal deflections at a modal point. h; deflection normal to lifting surface. α,θ; angular deflections pitch and bending in elastic axis coordinates

$\vec{i},\vec{j},\vec{k}$	Unit vectors in the x, y and z directions
I_{jk}	Spline interpolation matrix whose elements relate the deflection of point j due to the deflection at point k
$\alpha I_{jk}/\alpha x$	Slope of spline interpolation matrix
$J_n(P),Y_n(P)$	Bessel functions
k_r	Reduced frequency, $\omega\bar{c}/2U$
ℓ	Distance from blast to point on aircraft measured in a line parallel to the blast direction of travel
M or M_∞	Free Stream Mach number
$\tilde{M}$	Added mass of body cross section
$\vec{n}$	Unit vector normal to lifting surface
p	$2k_r M_\infty a/\bar{c}$
PT	Piston Theory
q	Generalized modal coordinates
$\bar{q}$	Dynamic pressure, $\frac{1}{2}\rho U^2$
s	Semispan, b/2
t	Time
U or U_∞	Freestream velocity, or aircraft velocity
$\bar{V}_g$	Velocity vector of gust wave front
$\bar{v}_g$	Unit vector in direction of $\bar{V}_g$
w	Normalwash on lifting surface
x,y,z	Right-handed coordinates fixed in aircraft
x_a,y_a,z_a	Right-handed coordinates fixed at blast origin
α,β,γ	Direction cosines of the blast wave velocity when it hits the aircraft in aircraft coordinates; $\bar{\gamma}$ is also dihedral of panel

ΔP	Difference of upper and lower lifting surface pressures
ΔC_p	Coefficient form of ΔP
θ	Fraction of local chord
$\theta 1$	Angular position on body surface
Λ	Elastic axis sweep
λ	Wave length = $2\pi V_g/\omega$
$[\phi]$	Modal matrix
τ	Distance along elastic axis, also $\tau = 2k_r R/\bar{c}$
$\bar{\tau}$	$\Delta x\ k_r\ R \cos\alpha/\bar{c}$
ω	Frequency, rad/sec

END

DATE
FILMED

12-81

DTIC